University of Nevada, Reno

Detection and Analysis of Spatiotemporal Changes in Great Basin Groundwater Dependent Vegetation Vigor

A thesis submitted in partial fulfillment of the requirements for the degree of Master of Science in Hydrology

By:

Guy T. Smith

Dr. Greg Pohll/Thesis Advisor

December, 2016

THE GRADUATE SCHOOL

We recommend that the thesis
prepared under our supervision by

GUY SMITH

Entitled

Detection and Analysis of Spatiotemporal Changes in Great Basin Groundwater Dependent Vegetation Vigor

be accepted in partial fulfillment of the
requirements for the degree of

MASTER OF SCIENCE

Greg Pohll, Advisor

Justin Huntington, Committee Member

Peter Weisberg, Graduate School Representative

David W. Zeh, Ph.D., Dean, Graduate School

December, 2016

Abstract

Throughout much of the arid Western United States, groundwater-dependent ecosystems (GDEs; those in which the flora necessarily rely on surface expressions of groundwater) represent hotspots of biodiversity, providing pockets of rich mesic habitat in an otherwise arid landscape. Yet, despite their integral ecological role, little is known about the long term dynamic spatiotemporal response of GDEs in arid lands to both disturbance and climatic variability. Climate change and anthropogenic groundwater abstraction have combined to drastically alter the hydrologic regime throughout regions of the Great Basin. As such, anthropogenically induced or exacerbated hydrologic disturbance have placed springs, wetlands, phreatophytic flats and a slew of additional Great Basin GDEs under intense environmental stress. Given the ecological and economic value of the many ecosystem services these unique environments perform, improving understanding of their spatiotemporal dynamics such that resource managers may simultaneously meet the needs of both humans and nature, is of the utmost importance.

Remotely sensed vegetation indices (VI) are commonly used proxies for estimating vegetation vigor and net primary productivity across many terrestrial ecosystems, though limitations in data availability and computing power have historically confined these analyses both spatially and temporally. In this work, however, spatiotemporally vast analyses of GDE vegetation vigor change through space and time were conducted using Google's Earth Engine (EE) cloud computing and environmental monitoring platform. This platform allows for the streamlining of computationally intense environmental analyses, and to access pre-processed Landsat archive and gridded meteorological data, effectively overcoming the temporal and spatial constraints previously posed by limited economic resources and computing power. Results of Landsat derived GDE vegetation vigor and associated environmental variable time series' and trend analyses illustrate the existence of a strong and highly significant coupling

between depth to groundwater (DT_G) and GDE vegetation vigor. Further, it was found that the presence of groundwater-vegetation feedbacks renders these systems highly prone to irreversible transitions to alternative, often barren or xerophytic, ecohydrological states, should a given GDE become decoupled from shallow groundwater resources as a result of surpassing species and tissue specific soil moisture threshold values.

Table of Contents

Table of Figures

1.0 Introduction

Water stored beneath the Earth's surface as groundwater represents the largest reservoir of liquid freshwater on our planet, comprising a staggering 96% of the precious resource (Shiklomanov, 2003). Across the Great Basin section of the Basin and Range physiographic province, where average annual precipitation reaches a mere 15-35 cm year^{-1}, groundwater represents the principal, if not sole, source of water (Nichols, 2000; Devitt et al., 2011). Throughout this region, rapid groundwater abstraction combined with population growth, climate change and extended periods of drought have placed increasing pressure on subterranean water resources in recent years (Nichols, 1994; 2000; Cooper et al., 2006; Deacon et al., 2007; Devitt et al., 2011; Devitt & Bird, 2015).

In arid and semiarid regions worldwide, and particularly so in endorheic regions like the Great Basin, the presence of shallow aquifers facilitate groundwater dependant ecosystems (GDEs) like springs, rivers, lakes and phreatophytic meadows. These ecologically invaluable communities support greater vegetation densities (Manning, 1999; Maitre et al., 1999; Elmore et al., 2003; Naumburg, 2005; Cooper et al., 2006; Patten et al., 2007; etc.), and increased biodiversity (Manning, 1999; Elmore et al., 2003; Ridolfi et al., 2007; Kløve et al., 2011), relative to areas with deeper water tables, through the continued provision of water in a region critically limited by this natural commodity. Though GDEs come in many shapes and sizes, they are unified by their necessary dependence upon subterranean water in order to maintain their present structure and function (Eamus et al., 2006; 2015; Eamus & Froend, 2006; Froend & Sommer, 2010; Kløve et al., 2011).

GDEs can be broadly divided into three types, as first suggested by Eamus et al. (2006b). Type I GDEs are those which rely on subsurface expressions of groundwater resources. Or, in other words, are those ecosystems that exist entirely within the subsurface aquifer (e.g. submerged cave systems, aquifer dwelling microbes etc.). Type II GDEs are

ecosystems which depend on surface expressions of groundwater. Lakes, ponds, rivers, streams and any other systems that exist as a consequence of surface expressions of subsurface water fall into this category. Finally, type III GDEs exist on the surface, with their access to groundwater facilitated by a form of vegetation known as a phreatophyte (Eamus et al., 2006; 2015; Eamus & Froend, 2006).

A phreatophyte is a plant--most commonly a tree, shrub or grass--that is characterized by long roots, penetrating deep into the soil in order to reach for the upper portion of the watertable (Gatewood et al. 1950; Robinson, 1970; Nichols,1993; 1994; 2000). A more functional definition proposed by Naumburg et al. (2005) states that phreatophytes grow where precipitation alone provides an inadequate quantity of water for their long-term survival, and thus phreatophytes require groundwater. These species act as ecosystem engineers, influencing groundwater levels across their range such that conditions are optimized for their existence and propagation. Phreatophytes may be classified as either obligate or facultative depending on their level of groundwater dependence, though implicit in the definition of GDEs is the caveat that without groundwater, the structure and function of the ecosystem in question would be compromised.

Though phreatophytes common to the Great Basin boast relatively meager groundwater evapotranspiration (ET_G) rates and are commonly found in densities of 20% total cover or less (Nichols, 2000), their simple spatial breadth renders these ecosystem engineers crucial components of regional water budgets (Nichols, 1993; 1994; 2000; Devitt et al., 2011; Beamer et al., 2013). Greasewood (*Sarcobatus vermiculatus*), the dominant phreatophyte of the Great Basin (Nichols, 1993; 1994), occupies an area of at least 4.8 million hectares in western North America (Shreve, 1942). Given their vast distribution and continuous water access, an improved understanding of these dynamic ecosystems and their interactions with the water table is paramount to a water managers ability to close basin budgets, and provide accurate estimates of the volume of groundwater potentially available for human use.

Throughout the multitude of closed and semi-closed hydrographic basins comprising the Nevada portion of the Great Basin, a water budget must be realized, with a perennial yield volume specified for potential “beneficial” human uses. Perennial yield, as defined by the Nevada Division of Water Resources (NDWR)--the agency tasked with regulating water resources throughout Nevada--is “the maximum amount of groundwater that can be salvaged each year over the long term without depleting the groundwater reservoir” (Horton, 2008). It is, therefore, often the case that water managers responsible for basins in which shallow aquifers facilitate a significant volume of annual GDE ET_G, define the basin's perennial yield as being a majority, if not all of, this evapotranspired volume (Nichols, 1993, 1994, 2001; Elmore et al,. 2003).

Not surprisingly, regions with shallow groundwater (< 5m) commonly support greater vegetation densities than areas in which the underlying water is deeper (Nichols, 1994; 2000; Manning, 1999; Elmore et al., 2003; Naumburg et al., 2005; Patten et al., 2008; Eamus et al., 2015). When left solely to natural devices, this combination of dense and diverse vegetation and consistent access to water can create a mesic microclimate (e.g. from Maitre et al. (1999) a 7℃ temperature decrease and a 14% relative humidity increase) which attracts a large variety of wildlife, resulting in a biologically rich and diverse environment (Manning, 1999; Elmore et al., 2003; Ridolfi et al., 2007; Kløve et al., 2011; Eamus et al., 2015). Nowhere is this particular richness more pronounced than in the so often water limited arid and semi-arid environments of the world, in which GDEs commonly act as biologically rich “island” ecosystems, surrounded by water-limited, xerophyte-dominated, low productivity desert ecosystems (Patten et al., 2008; Eamus et al., 2015).

Somewhat remarkably, these unique species are not only able to themselves consistently access groundwater, but through a process known as hydraulic redistribution (i.e. hydraulic lift) can actually transport groundwater from as much as 18 meters deep (Robinson, 1958; Nichols, 1994, 2000; Cooper et al., 2006) to shallow soil horizons, wherein it may be

utilized by associated, non-phreatophytic vegetation assemblages (Naumburg et al., 2005; Steinwand et al., 2006; Asbjornsen et al., 2011; Orellana et al., 2012). These vegetative ecosystem engineers are therefore crucial to the survival of the entire associated assemblage of flora and fauna, as without their provision of deep subterranean water many of these species would likely not exist where hydrologic redistribution allows them to.

In addition to the biodiversity they promote through the provision of critical habitat for a number of federally listed threatened and endangered species, (Deacon et al., 2007; Patten et al, 2007; Huntington et al., 2016) GDEs in the Great Basin, stimulated by their consistent water access, perform a number of ecosystem services. These ecosystem services include but are not limited to, dust prevention (Patten et al., 2008; Elmore et al., 2008), groundwater purification and desalinization (Murray et al., 2006; Patten, 2008), nutrient cycling (Murray et al., 2006) and the sequestration of atmospheric CO_2 (Chapin III, 2000; Murray et al., 2006). In light of the provision of these services, balancing human water abstraction needs with those of GDE vegetation is necessary not only for the continued integrity of the ecosystems themselves, but also for ensuring the crucial ecosystem services which they perform are not threatened by our own gluttony for water.

GDEs represent a crucial yet poorly understood aspect of our natural environment (Kløve et al., 2011). Given the criticality of the ecosystem services that GDEs provide, as well as the scarcity of the crucial mesic habitat that they represent, ensuring their continued ecological integrity represents a fundamental aspect of any successful water resource management strategy. In light of this, the potential impacts of natural climatic variability both independent of, and in combination with, anthropogenic groundwater abstraction are important considerations for water resource managers throughout the Great Basin and arid Western United States.

In recent years, the short-term ecological response of GDE communities to perturbations of their historic hydrologic and climatic regimes has received increasing attention. Naumburg et

al. (2005) provided a thorough review on the impacts of both declining and rising water tables on GDE vegetation, as well as a a pair of conceptual models describing the dynamic relationship between GDEs and depth to groundwater (DT_G). They conclude that, despite the remarkable ability of phreatophytes to engineer environmental conditions that are suitable for their continued survival, excessive disturbance can result in a dramatic threshold response. Should the rate of water table drawdown exceed a given species maximum root growth rate, or surpass a maximum rooting depth, water stress, canopy dieback and even catastrophic shifts in ecosystem structure and function, may be experienced (Naumburg et al., 2005; Ridolfi et al., 2006, 2007; Froend & Sommer, 2010; Asbjornsen et al., 2012; Eamus et al., 2015). Ultimately, this scenario may lead to increases in temperature, dust generation and groundwater salinization (Patten et al., 2007), and decreases in carbon sequestration as well as community resilience, thereby leaving the door open to hysteretic community succession (Ridolfi & Laio, 2006; Cooper et al., 2006; Elmore et al., 2008; Froend & Sommer, 2010; Asbjorsen et al., 2011; Eamus, 2006a; Eamus et al., 2015).

There exist a plethora of examples in recent literature of anthropogenically exacerbated groundwater drawdown leading to a threshold response, one that almost certainly would not have been realized if the system were influenced by natural processes alone (Cooper et al., 2006; Ridolfi et al., 2006; Froend & Sommer, 2010; Eamus, 2015). In fact, anthropogenic alteration of subsurface hydrologic flows is considered to be one of, if not the single, greatest threats to the integrity of GDEs worldwide (Eamus et al., 2006a, 2015; Münch & Conrad, 2007) as well as specifically within the Great Basin physiographic region (Patten, 2007; Pritchett & Manning, 2012).

What is not clear, however, are the key groundwater factor(s) and specific threshold values which determine whether a gradual or threshold response will be exhibited by a given GDE. Moreover, though a number of both spatially and temporally limited studies have aimed to address these uncertainties, only one of these considered the long term (30+ year) behavior of

GDE communities (Froend & Sommer, 2010), and even this lone temporally vast study was limited in its spatial coverage by manual vegetation sampling techniques. Consequently, an improved understanding of how both climate and anthropogenic perturbations of hydrologic regime affect the vigor and resilience of GDEs at spatiotemporal scales relevant to resource managers, is needed in order to improve regional groundwater models and budgets, ecosystem assessments, adaptive management frameworks, and the identification and designation of protected areas (Eamus & Froend, 2006; Froend & Sommer, 2010; Kløve et al., 2011; Huntington et al., 2016).

Historically, the absence of long-term, large-scale observations has constrained GDE analyses, and precluded the possibility of scientifically informed management decisions on the basin scale (Nichols, 2000; Huntington et al., 2016). More recently, however, decades of remotely sensed observations from the Landsat archive have proven effective in filling this data gap. The longevity and frequent return interval of the observations in the lineage Landsat's Thematic Mapper (TM), Enhanced Thematic Mapper Plus (ETM+), and Operational Land Imager (OLI), combine to provide an unparalleled 30+ year record of GDE vegetation vigor, that would not otherwise be attainable (Huntington et al., 2016). Vegetation indices, like the Enhanced Vegetation Index (EVI), derived from these remote sensing platforms have further proven the utility of Landsat observations through the successful identification, assessment and monitoring of GDEs changes relative to changing climate and hydrology (Elmore et al., 2000; 2003; 2006a; 2006b; Eamus et al., 2006; Groeneveld, 2008; Yang et al., 2011; Pritchett and Manning, 2012; Barron et al., 2012; Nguyen et al., 2014; Homer et al, 2015; Huntington et al., 2016). Moreover, despite significant changes in bandwidths between synonymous channels across Landsat sensors, Huntington et al. (2016) found vegetation indices (VIs) originating from different Landsat platforms to be highly comparable, and the differences negligible enough to allow for seamless analysis over the entire archive.

Thanks to the freely accessible nature of the landsat archive, land and resource managers may now utilize this decades long dataset in order to ascertain invaluable information about the dynamic structure and function of GDEs throughout the Great Basin and arid and semi-arid Western United States. This vast quantity of data represents a tremendous improvement in the availability of pertinent data to resource managers throughout these regions relative to classic field and energy balance approaches. That being said, however, the sheer volume of data contained within the Landsat archive, presents a new array of challenges, including limitations in data storage and computational efficiency (Huntington et al., 2016). Fortunately, both of these potential limitations can be easily addressed by parallelized cloud computing within Google's Earth Engine (EE), a powerful new planetary-scale platform for environmental data and analysis. In order to effectively quantify GDE changes relative to changing climate and hydrology, the effects of natural variability must be isolated from anthropogenic impacts.

2.0 Objective

The objectives of this work are to: 1) Identify patterns of GDE vegetation vigor change through space and time using an EVI slope map derived from an ordinary least squares (OLS) regression of 32-year historical enhanced vegetation index datasets, computed on Google's earth Engine using observations from sensors of the Landsat TM, ETM+, and OLI lineage, and 2) determine the extent to which spatiotemporal patterns in observed GDE above ground net primary productivity (ANPP), as represented by 32-year historical EVI datasets, may be explained by changes in annual precipitation, summer precipitation, summer theoretical water deficit (TWD) and groundwater levels.

3.0 Study Areas

Study sites were selected primarily for their vegetative cover characteristic of Nevada's endemic phreatophytic flora, and their proximity to one or more USGS or Nevada State

Engineer's office hydrograph locations of sufficient return sampling interval (1+ sample/year). All sites selected fall within the Great Basin section of the Basin and Range physiographic province as defined by Fenneman (1928, 1932), a vast stretch of land that covers the majority of Nevada, and portions of Utah, California, Oregon, Idaho and Arizona.

The Great Basin, made of 260 smaller closed and interconnected basins, collectively represents the largest endorheic basin in North America (Harrill et al., 1988). Generally, these basins contain a highly permeable basin-fill aquifer, a deeper underlying semi-permeable fractured carbonate regional aquifer, and finally relatively impermeable basement rock which effectively confines the aquifer system to the two above levels. This basement rock typically rises up to form the regions north-south oriented mountain ranges, and as such these topographic divides often define hydrographic boundaries, as well. Flow systems in these basins can be restricted to a single basin, or be comprised of multiple hydrologically connected basins (Eaton, 1982; Harrill & Prudic, 1983; Harrill et al., 1988; Patten et al., 2008).

Most closed or semi-closed basins and valleys of the Great Basin have a central playa underlain--at least in the absence of anthropogenic influence--by a shallow (< 2.5m) water table (Nichols, 1994; 2000). The margins of playa are populated by halophytic vegetation of the salt desert community, which is typically found growing in areas with a DT_G of about 2.5m or less, though it has been observed at depths up to 3.6 m (Blaney et al., 1993). Saltgrass (*Distichlis spicata* var*. stricta*), the dominant species in this margin community, is commonly found in association with lower densities of pickleweed (*Allenrolfea occidentalis*), and saltsage (*Atriplex tridentata*).

Just up-gradient of the playa margins beyond the salt desert community typically exists the greasewood-shadscale community. Greasewood (*Sarcobatus vermiculatis*) is widespread across the lower portions of alluvial fans and desert valleys throughout the Great Basin, and represents the dominant species in the shadscale-greasewood community (Robinson, 1958; Robertson, 1983; Nichols; 2000). Though greasewood may occasionally be found growing in

monotonic stands (generally in areas of hypersaline or alkali groundwater, an environment in which greasewoods tolerance gives it a competitive advantage), it is most often found associated with shadscale (*Atriplex confertifolia*) and with smaller proportions of saltbrush (*Atriplex canescens*), spiny hopsage (*Grayia spinosa*) and winterfat (*Certoides lanata*) (Robinson, 1958; Nichols, 1994; 2000). Where soils are less saline rabbitbrush (*Chrycothammus nauseosus*) and big sagebrush (*Artemisia tridentata*) may also occupy roles within this community. The various shrubs comprising the greasewood-shadscale type III GDE community typically require 1 m or more of unsaturated soil (White, 1932), and are therefore most commonly found in areas with water table depths of 1.5-11 m (Nichols, 2000), but have been observed growing with water table depths of almost 20 m (Robinson, 1958).

Specific study locations were selected to represent a range of GDEs and environmental conditions within the Great Basin important for three scenarios: 1) Baseline assessment of GDE vegetation with respect to climate and DT_G, 2) relatively constant and continuous changes in DT_G, and, 3) variable and discontinuous changes in DT_G (Figure 1).

3.1 Baseline assessment of GDE vegetation

Located in eastern Nevada near the Utah-Nevada border, Spring Valley (Figure 2) is one of several basins which the Southern Nevada Water Authority (SNWA) has proposed as a site for major groundwater development and export to Las Vegas. This large scale groundwater development project aims to decrease the Las Vegas area's dependence on surface waters from the over-allocated Colorado River through the conveyance of up to 1.91 $x10^8$ cubic meters per year (m^3 $year^{-1}$). State and federal laws as well as a stipulated agreement reached between SNWA and federal agencies require a thorough review of the potential environmental impacts resulting from such development, including detailed hydrologic and biological assessments and monitoring (Southern Nevada Water Authority, 2011).

Spring Valley covers an area of roughly 4,302 km^2, and boasts an impressive perennial yield of $1.04x10^8$ m^3 $year^{-1}$ (NDWR, 2016b). DT_G throughout the valley floor of Spring Valley

ranges from 2 to 10 m below land surface, and annual precipitation ranges from 16 to 29 cm (Moreo et al., 2007). Natural groundwater discharge in Spring Valley occurs primarily in type II (Springs, groundwater fed ponds, ephemeral wetlands, etc.) and type III GDEs, as evaporation from soil and open water, and phreatophyte transpiration, respectively. The greasewood dominated community analyzed in this study lies about halfway along the basin's valley floor gradient, in a location likely to be impacted by groundwater development due to its proximity both up and down-gradient to proposed pumping well locations (Rush & Kamzi, 1965). Observations and analysis of the long-term annual-to-decadal variability of the relatively unperturbed GDEs occupying the Spring valley study site hold the potential to provide valuable insights into the natural long-term functionality of Great Basin type III GDEs, as well as their resilience to disturbance and succession resulting from natural variability alone.

3.2 Groundwater level change

Throughout the Great Basin, the combination of meager annual precipitation totals and minimal surface water storage preclude the use of surface and rain waters alone, for irrigation. Instead growers must pump groundwater in order to irrigate their agricultural land. This trend applies to municipalities as well, with large communities across the arid and semi-arid Western United States like Las Vegas, Reno, Salt Lake City, and many others, relying on an ever increasing proportion of groundwater to meet water demands (Thiros, 2003; Deacon et al., 2007). Additional consumptive uses of groundwater in the region include large scale mining operations, with both lithium brine mining and the dewatering of large pit and underground mines being common practices to the Great Basin's many deep and saturated alluvial fill aquifers.

Inevitably, though, as it was put by Theis (1940) "all water discharged by wells is balanced by a loss of water somewhere". Groundwater pumping for municipal use, agricultural irrigation, mining activities, and a multitude of additional uses often times results in the lowering of local water tables. This occurs due to the fact that the water lost to pumping, is at first derived

from storage within the aquifer being pumped (Theis, 1940). The ultimate consequence of this anthropogenic perturbation of change in aquifer storage is the lowering of the phreatic surface (i.e. water table) and subsequent reduction in groundwater discharge via reduced phreatophyte evapotranspiration (ET) and vegetation vigor (Bredehoeft et al., 1982; Bredehoeft, 2002; Nichols 1994: 2000: Elmore et al., 2006; Naumburg et al., 2005; Cooper et al., 2006; Patten et al., 2008; Groeneveld, 2008; Huntington et al., 2016).

3.2.1 Constant and continuous groundwater level change

Fish Lake Valley straddles the Nevada-California border (Figure 3), lying predominantly in Esmeralda County, Nevada, and extending into portions of both Mono and Inyo Counties, California. Between the two states the semi-closed basin covers an area of roughly 2,616 km^2, and has an estimated perennial yield of $3.70x10^7$ m^3 $year^{-1}$(Loeltz & Eakin, 1953; Rush, 1973; CA DWR bulletin 118, 2004; NSE summary, 2016). Fish Lake Valley receives between 10 to 50 cm of annual precipitation, and is characterized by DT_G values varying from in excess of 100 m deep in upper portions of some alluvial fans, to less than 2 m below land surface near the Valley's playa and principle areas of groundwater ET_G (Rush, 1973). Saltgrass dominated meadow communities were reported to have DT_G values in the range of 0 to 3.5 m below land surface, and combined with playa surfaces cover roughly 93.5 km^2 of valley floor. The various spatially prevalent greasewood dominated communities cover an extent of 200 km^2, with DT_G values beneath these type III GDEs ranging from 3 to 15 m below land surface (both saltgrass and greasewood ranges represent pre-disturbance values) (Rush, 1973). Irrigated agriculture has expanded throughout the valley since the completion of the 1973 reconnaissance report, with NDWR approved groundwater abstraction permits for irrigation growing from roughly $1.36x10^7$ m^3 $year^{-1}$ in 1973 to more than $6.17x10^7$ m^3 $year^{-1}$ in 2016 ($2.47x10^7$ m^3 $year^{-1}$ more than the basin's perennial yield) (Rush, 1973; NDWR, 2016e). An apparent consequence of the anthropogenically modified hydrologic conditions found within Fish Lake Valley has been the

continuous and relatively constant decline of groundwater levels throughout the basin since approximately 1970.

San Emidio Desert is a relatively small hydrographic basin of only 790 km^2 (Figure 4) that lies split between Washoe and Pershing Counties, Nevada, approximately 160 km North-Northeast of Reno, Nevada (NDWR, 2016d). The semi-closed basin ranges in elevation from roughly 1,190 m above mean sea level (AMSL) at its lowest point, to nearly 2,500 m AMSL atop Tohakum Peak. Annual precipitation totals range from less than 13 cm $year^{-1}$ to as much as greater than 50 cm $year^{-1}$, with the greatest values found in the highest elevations (Glancy & Rush, 1968; NDWR, 2016d). Depth to groundwater historically ranged from as great as 80+ m in the upper portions of alluvial fans, to within 1 m of the playa surface in the lower reaches of the drainage. In the absence of anthropogenic hydrologic perturbation, groundwater movement in San Emidio Desert is generally towards the North, in the direction of the Black Rock Desert (Glancy & Rush, 1968). Greasewood dominated type III GDEs with DT_G ranging from 6 m to as much as 19 m cover 60.7 km^2 of valley floor, with an additional 12.1 km^2 of mixed greasewood and salt desert community occupying playa margins, underline by DT_G ranging between 1.5 m to 6 m. Finally relatively bare playa covers roughly 24.3 km^3 of San Emidio Desert, and is underlain by rather shallow DT_G (0.6 - 2.5 m). Despite its small size and relative isolation, San Emidio Desert has a decades long history of agriculture and mining activities, with perhaps the most notable of these being the Wind Mountain Gold and Silver Mine located along the basins eastern edge. Basin groundwater allocations in 2016 totaled more than $9.25x10^6$ m^3 $year^{-1}$, well exceeding the basin's modest perennial yield of $5.67x10^6$ m^3 $year^{-1}$ (NSE ruling 3569, 1988; NDWR, 2016d).

3.2.2 Variable and discontinuous groundwater level change

Boulder Flat hydrographic area (Figure 5) is a 1,409 km^2 drainage located in the middle portion of the Humboldt River basin between Battle Mountain and Carlin, Nevada (Huntington et al., 2014; NDWR, 2016a). Boulder Flat and four other adjacent hydrographic basins function as

a single extensive groundwater flow system, with precipitation representing the sole recharge mechanism, and ET_G, as well as both surface and subsurface flows through the Humboldt corridor representing the conglomerate basins sinks. (Plume & Ponce, 1999; Huntington et al. , 2014). Precipitation throughout Boulder Flat ranges between 20-51 cm $year^{-1}$, with a mean of 28.75 cm annually (Berger, 2000). Several mining operations are located in Boulder Flat, including Newmont Genesis, Carlin, and Leeville mines, and Barrick Goldstrike mines (Huntington et al., 2014). Infiltration of excess water from mine dewatering operations has caused valley floor groundwater levels to rise from anywhere between 1.5 to 6 m over an area of 50 km^2 across Boulder Flat. This water, discharged from injection wells, rapid infiltration basins (RIBs), and through infiltration of irrigation water both from fields and the storage reservoir, has created shallow groundwater conditions throughout the lower reaches of the basin, characterized by resulting significant rises in ET_G (Plume, 2005; Zhan et al., 2011; Huntington et al., 2014). Greasewood represents the dominant form of type III GDE vegetation in Boulder Flat, and is intermixed with smaller amounts of rabbitbrush, saltgrass and facultatively dependent sagebrush, as well as some regions of riparian vegetation (Huntington et al., 2014).

Smith Valley (Figure 6), one of several independent hydrographic basins comprising the Walker River Flow System, lies approximately 60 km east of the obtuse angle of the California-Nevada border. The vast majority of the roughly elliptical 982 km^2 basin falls within Lyon County, Nevada, with a small area along the basin's western edge falling into Douglas County (Loeltz & Eakin, 1953; NDWR, 2016c). Precipitation in Smith Valley ranges between 10-50 cm $year^{-1}$, with the valley floor receiving a mean of 19.1 cm $year^{-1}$ (Loeltz & Eakin, 1953; Rush & Schroer, 1975). Despite being a portion of the Walker River Flow System, Smith Valley actually functions more or less as two hydrographic basins separated by a groundwater divide. The first is comprised the southernmost two thirds of the Basin, and functions as a bonafide portion of the river system. In this region, flow in generally towards the River from both the North and the

South (Rush & Schroer, 1975). The second portion, with which this study is concerned, functions instead as a hydrographically closed basin, its terminus the ephemeral Artesia Lake. The aforementioned groundwater divide represents the Southern border, and rising hydrophobic rock formations underlying the surrounding mountain ranges closing the Western, Northern and Eastern edges (Rush & Schroer, 1975). Throughout both regions, the highest reaches of alluvial fans reveal depths to groundwater in excess of 65 m, but the majority of the valley was historically characterized by DT_G levels under 15 m. The Artesia lake area (all study locations) fall within areas delineated in 1972 as being within 3 m of land surface. Discharge in the Southern region is dominated by surface and groundwater flows through the Walker River Corridor. In the Northern portion, however, ET_G from 52.6 km^2 of playa and phreatophytic vegetation surrounding Artesia Lake dominates the discharge component of water budgets (Rush & Schroer, 1975). Past studies and an August 2016 field visit suggest greasewood is the dominant form of GDE vegetation throughout much of the Artesia Lake area (DT_G 1.5 - 15 m), with smaller regions of concentrated saltgrass occurring where DT_G is between 0 and 2 m below land surface. Smith Valley's perennial groundwater allocation of roughly $6.78x10^7$ m^3 $year^{-1}$ well exceeds the basin perennial yield of $2.10x10^7$ m^3 $year^{-1}$, and in fact comes close to the Walker River system-wide perennial yield of $7.65x10^7$ m^3 $year^{-1}$ (NDWR, 2016c).

4.0 Methods

Estimates of GDE vegetation vigor through both space and time were realized by calculating VI's from remotely sensed imagery contained within the Landsat archive. Using Google's Earth Engine Cloud Computing Platform in order to both vastly improve processing time, and to take advantage of the pre-georegistered and radiometrically corrected archive of Landsat images provided on Google's servers, EVI was calculated over the the spatial extent of hydrographic study basins, over the length of the entire Landsat record. An ordinary least squares regression of pixelwise EVI values through time was then performed and the resulting

EVI slope map used to guide spatial averaging of EVI and environmental variables for further focused time series analysis of GDE vegetation vigor with respect to climate and hydrology.

4.1 Data preparation for GDE assessments

Landsat remote sensing observations have repeatedly demonstrated ecosystem monitoring utility (see introduction), and are increasingly being used in long-term GDE evaluations (Elmore et al., 2000; 2003; 2006a; 2006b; Eamus et al., 2006; Groeneveld et al., 2007; Groeneveld, 2008; Yang et al., 2011; Pritchett & Manning, 2012; Barron et al., 2014; Nguyen et al., 2014; Homer et al, 2015; Huntington et al., 2016) Total canopy chlorophyll content has been found to explain more than 92% of ANPP variation (Gitelson et al., 2014), and remotely sensed VI's track chlorophyll content with a high degree of accuracy (Gitelson & Merzlyak, 1997), particularly in arid environments where canopies rarely overlap. Therefore, the values of the VIs derived from the landsat archive are representative of the ANPP and thus vegetation vigor, of GDE vegetation through both space and time.

This study considered scenes acquired by multiple sensors in the Landsat lineage. Specifically, Thematic Mapper scenes obtained between between January 11st, 1984 and May 5th, 2012, Enhanced Thematic Mapper Plus scenes from January 1st, 1999 to August 16th, 2016, and Operational Land Imager scenes obtained from April 11th, 2013 to August 17th, 2016, were considered. This wide range of images was further refined to unobscured scenes depicting the extent of a given study site falling between Julian day 182 and 273 (July 1st-September 30th, non-leap year) for any given year. The analyses performed were limited to scenes falling between these two dates for any given year in order to more easily differentiate between GDE and non-GDE areas geospatially, as their phenotypic expressions differ from surrounding xerophytic vegetation to the greatest degree, during this period (Huntington et al., 2016).

There exists a growing record of the use of summer specific VIs as proxies for annual phreatophyte ET within the Great Basin (Nichols et al., 2000; Groenveld et al., 2007; Smith et

al., 2007; Beamer et al., 2013; Garcia et al., 2014; Huntington Et al., 2016). The late summer period represents the time of peak GDE groundwater usage for that year, as most any other water resources that may be available to GDE vegetation have long since been spent (Groenveld et al., 2007; Huntington et al., 2016). It is postulated, therefore, that any impacts related to the availability of groundwater as a hydrological resource for GDE vegetation will be most apparent during the time of year that this resource would, in the absence of any impacts, be principally called upon.

Following this temporal filtering, images were combined into a single, multi-temporal image stack. Next, the enhanced vegetation index was calculated by equation 1 (below), and added to the image stack as a new 'band'

$$EVI = \frac{(NIR-RED)}{(\mathrm{NIR}+C_1*\mathrm{RED}-\mathrm{C}_2*\mathrm{BLUE}-\mathrm{L})} \quad (1)$$

where C1, C2, and L are coefficients, to correct for aerosol resistance. NIR, RED and BLUE are for Landsat bands 4, 3, 1, and 5, 4, 2, for Landsat 4-7, and Landsat 8, respectively. The stack of images for a given study basin was then annually consolidated in order to create a single image representative of GDE vegetation vigor for the mid to late summer target period. Every image within the target period r was considered, and median EVI values were selected on a pixel-wise basis, and aggregated into a single scene. Median values were used rather than the mean of all qualified scenes due to the limited number of scenes in some years leaving the mean highly vulnerable to outliers. Fmask software was used in order to perform an automated identification and masking of clouds, cloud shadows, and snow covered areas in order to minimize the possibility or errors arising due to unsatisfactory conditions for the remote sensing of GDE vegetation (Zhu & Woodcock, 2012; 2014; Zhu et al., 2015).

In addition to VI derived estimates of GDE vegetation vigor through space and time, hydrographs from any groundwater monitoring wells in proximity to the vegetation in question is annually averaged and examined for relationships between DT_G and GDE vegetation vigor (i.e.

EVI). DT_G data derived from NDWR and USGS groundwater level data bases were constrained by the requirement of a minimum of one DT_G data point per calendar year spanned by the record, though these entries need not be evenly spaced in time. For years in which multiple measurements fell, a single DT_G value was realized by taking the average of all values within the year. Conversely, for years missing DT_G data, an estimate was realized by linear interpolation of the two most temporally proximal entries in the record. The location, datasource, temporal span and number of data points for each hydrograph considered in this analysis can be found in Appendix E.

In a manner similar to that of the EVI, annually aggregated time series of both total water year (October 1st - September 30th) and summer (June 15th-September 30th) precipitation (PPT), as well as summer (June 15th-September 30th) theoretical water deficit (TWD) over the same spatial extents, were be obtained from the University of Idaho Gridded Surface Meteorological Dataset (GRIDMET). University of Idaho GRIDMET data covers the entirety of the coterminous United States with a 4 km spatial resolution, and daily temporal resolution, providing unparalleled high-resolution surface meteorological data for Landscape-scale analyses (Abatzoglou, 2012). Unlike EVI, where median values were considered such that the small sample size provided was not skewed by outliers resulting from partially obscured, or otherwise dubious images, the sum of environmental variables over given periods of time were considered. For this study, TWD is defined as being the cumulative difference between reference evapotranspiration (ET_O) and PPT over a given period of time. TWD can be calculated by equation 2, below:

$$TWD = \sum PPT - \sum ET_O \quad (2)$$

Where PPT is the cumulative sum of precipitation, and ET_O is the sum of daily Penman-Monteith reference evapotranspiration values, throughout a given period. TWD, though not a complete water balance, was included to approximate the climatic water deficit (CWD) of a

given study location. The CWD approach provides an ecologically functional descriptor of climatic influences that limit plant distributions (Stephenson, 1990, 1998; Dilts et al., 2015). While practical constraints precluded the calculation of a full water balance necessary to realize CWD, TWD provides a 'cheap' functional approximation that serves the purposes of this work well.

4.2 Slope Map

In order to preliminarily identify regions of potentially disturbed GDE vegetation, a map of EVI slope based on annual mid-late summer median EVI values from 1985-2010 (i.e. 25 data points) was created for each study basin considered. Ordinary least squares (OLS) regression was performed via Google's EE cloud computing platform to derive per-pixel annual EVI slope estimates. The resulting geospatial representation of the annual rate of changes in GDE vegetation vigor was used to identify and describe patterns of spatiotemporal change of phreatophytic communities throughout the study basins.

The EVI calculation and regression performed in this step was, unlike subsequent portions of the analyses described herein, performed on data from sensors of the Landsat TM, ETM+, and OLI lineage that was radiometrically corrected following the method put forth by Chandler et al. (2009) *only to* top-of-atmosphere reflectance. The absence of correction to at-surface reflectance renders the data considered in the slope map, at best, rough. Nonetheless, as this step served primarily to identify spatial regions of GDE impact for subsequent, quantitative analyses, errors arising from incomplete radiometric correction are assumed to be negligible.

4.3 GDE time series analysis

The seasonal and historical temporal constraints described in the above data preparation section were applied to the lineage of Landsat scenes retrieved from the archive for these time series analyses, as well. Unlike the data used in the creation of the EVI Slope Maps, however, the 2,150 unique Landsat scenes that were collected over the 5 study basins in order

to create 16 individual spatially averaged EVI time series considered in this study, were radiometrically and atmospherically corrected to *at-surface-reflectance*. This correction was achieved through the completion of steps outlined by both Tasumi et al. (2008) and Trezza and Allen (2013). Implementation of the Tasumi/Trezza method was accomplished using Google's EE to access both geospatially distributed, near-surface hourly vapor pressure data from the North American Land Data Assimilation System (NLDAS) (Mitchell et al., 2004) to estimate precipitable water and atmospheric transmittance (Tasumi et al., 2008), and the 30m National Elevation Dataset (NED) in order to estimate geospatially distributed atmospheric pressure (ASCE-EWRI, 2005). Following the retrieval and estimation of these prerequisite variables, scenes were individually corrected to at-surface-reflectance, also within Google's EE.

Next, preceding the application of the Fmask algorithm to scenes selected from the Landsat archive, Landsat quicklooks were downloaded and manually examined. This manual examination was carried out in order to identify scenes where the presence of clouds throughout much of the scenes extent may have previously disqualified the scene from further analysis despite GDEs of interest (typically a small spatial area relative to the geospatial coverage of individual Landsat scenes) remaining unobscured. The converse, and albeit less common, scenario where the majority of the scene remains unobscured yet the GDE of interest is partially or completely covered, is also captured by this step. Fmask was then applied to the remaining scenes in order to automatically identify and mask any regions of cloud, cloud shadow, or snow cover which might have slipped through the manual filtering process. Finally, scenes in which more than 30% of a given polygons spatial area were masked were eliminated, such that they wouldn't impact spatially averaged time series results.

Once the relative insignificance of polygon size impacts had been established (see results), the aforementioned EVI slope maps were used in conjunction with a multitude of geospatial datasets to guide the drawing of polygons. Between 1-3 regions over which impacts to GDE vegetation vigor were considered, were drawn manually for each study basin, such that

their extent was comprised only of spatial areas being described as GDEs in one or more of the multitude of reports or datasets described below. Following this functional division, the pixel-wise values of EVI and the environmental variables discussed in the data preparation section, through time were averaged on an annual, region-wise basis. In other words, the EVI and environmental signals of all of the pixels within a given region of common impact were spatially averaged into a single value representative of that region's value, for a given year.

EVI Slope Maps described above were used in concert with a USGS published phreatophyte geospatial extent dataset (Mathie et al., 2008), Google Earth's derived digital elevation model, and both a multitude of historic NSE and USGS Reconnaissance Reports and Bulletins, and recent peer reviewed works, manually delineate various regions comprised solely or predominantly of GDE vegetation, for further quantitative impact analysis. Spring Valley served as the control for this study, and the lone polygon considered there (SPV) was drawn such that its entirety was comprised of GDE vegetation as reported by both Rush & Kamzi (1965) and Moreo et al. (2007). Fish Lake Valley's three polygons (FLV1, FLV2 and FLV3) were drawn such that they were comprised only of GDE regions designated by both Loeltz & Eakin (1953) and Rush (1973). One polygon was drawn for San Emidio Desert (SE), its spatial extent lies entirely within GDE communities described by Glancy (1968). The single polygon drawn for Boulder Flat (BF) was guided by relatively recent reports from Berger (2000) and Huntington et al. (2014). In Smith Valley, the other variable impact basin considered, the two polygons (SMV1 and SMV2) were drawn within GDE areas as designated by both Loeltz & Eakin (1953) and Rush & Schroer (1975).

In order to detect and quantify the significance of changes in EVI and the other environmental and hydrologic variables considered, the nonparametric Mann-Kendall test for trend and Sen's estimate of slope were calculated for each time series considered in these analyses. These trend tests were carried out using the MAKESENS Excel template application (Salmi et al., 2002), and are detailed in the results section.

Next, to in order to attribute any changes in detected GDE vegetation vigor (i.e. EVI) to the proper environmental forcing, a number of correlation coefficients were calculated, with GDE EVI as the dependent variable, and DT_G, summer and water year precipitation and summer TWD, respectively, as the independent variables. Pearson's correlation coefficient is a commonplace measure of the association between two continuous variables. Implicit in its calculation are the assumptions that the data are linearly related, normally distributed and homoscedastic. Spearman correlation is simply a rank-based version or the Pearson coefficient, without the assumptions of normality or linearity. Finally Kendall's tau correlation coefficient quantifies the numbers of both concordant and discordant data pairs and measures the discrepancy between these (Chok, 2010). Each of these measures of correlation returns a value between -1 and 1 indicative of both the strength and nature (direct or inverse) of the relationship between the two series considered, as well as a p-value detailing the likelihood these observations are the result of simple chance. Cohen's (1988) conventions were used to interpret the effect size of correlation coefficients returned (e.g. 0.10-0.29, small effect, 0.30-0.49 moderate effect, 0.50 and above, large effect).

Finally, relationships between annual GDE vegetation vigor and both atmospheric and climatic feedbacks are further evaluated by plotting median annual EVI and reference evapotranspiration (ET_O) on primary and secondary y-axes, respectively, both against annual water year PPT on the x-axis (Figure 9). EVI and ET_O were grouped based on observation year, with 1984-1999 representing the "early" period, and 2000-2015 representing the "late", for each study polygon. This functional division was carried out to more clearly illustrate any changes in the climate-atmosphere-vegetation relationship that might have occurred over the course of the 32-year record. The resulting figure illustration is somewhat synonymous to the classic complementary relationship between ET and ET_O in arid environments (Brutsaert & Stricker, 1979; Hobbins et al., 2004; Huntington et al., 2011; Jaksa et al., 2013), as EVI is exceptionally

closely correlated with Great Basin GDE ET (Beamer et al., 2013), and the use of summer VIs as proxies for annual phreatophyte ET is well established within the Great Basin.

5.0 Results

5.1 Polygon area influence

To assess the influence the magnitude of a given polygon's area has on the resulting time series', five overlapping polygons of increasing size were drawn in Fish Lake Valley, and their resulting time series analyzed for trend and covariance. The results of this initial analysis (described in detail in Appendix A) suggest that the influence of polygon size on the resulting time series' is overall, insignificant. That being said, smaller polygons tended to be more prone to drastic swings, while the largest polygons lost some degree of temporal specificity, returning generally more gradual EVI curves, overall. Following the establishment of the relative insignificance of polygon size on the resulting time series', polygons were drawn to isolate regions of common impact for hydrologic and environmental influence analysis.

5.2 Baseline assessment of vegetation and climate

The long-term variability of vegetation vigor, depth to groundwater and climate for Spring Valley are illustrated in Figures 7 and 8 by plotting EVI with DT_G and water year PPT, over time. Results of the nonparametric Mann-Kendall trend test failed to identify trends of any significance in EVI, summer precipitation, water year precipitation or summer theoretical water deficit, and therefore Sen's estimates of slope will not be reported for these variables. The lone trend of significance identified by the Mann-Kendall tests on control site time series was an exceptionally slow change in the depth to groundwater. DT_G was found to be increasing at a rate of 0.02 m $year^{-1}$ ($p > 0.01$), with a Mann-Kendall test statistic (Z) of 3.10.

In the absence of large scale anthropogenic hydrologic alteration, the vegetation vigor of the GDE observed in SPV was found to covary most closely with water year precipitation. Strong and highly significant ($p > 2x10^{-5}$) Pearson's and Spearman's correlation coefficients of

0.73 and 0.72, respectively, were observed between EVI and water year PPT throughout the 32-year time series analyzed. Much less significant ($p > 0.05$), moderate strength Pearson's correlation coefficients were observed between EVI and both summer TWD (0.41) and summer PPT (0.38). Specific p-values, as well as correlation coefficients unreported due to their insignificance may be found in appendix C.

Figure 9 illustrates clearly that Spring Valley, in the absence of anthropogenic hydrologic disturbance, has maintained a relatively stationary climate-atmosphere-vegetation relationship through time. Throughout the course of the 32-year record, as water year PPT increases, EVI increases and ET_O decreases.

These results are consistent with past observations of the complementary relationship in the Great Basin (Huntington et al., 2011; 2016; Beamer et al., 2013), as well as surface energy balance theory. In water limited environments where energy is relatively uniform in space, energy that would have resulted in ET with adequate water, instead results in sensible heat production and subsequent increases in air temperature, vapor pressure deficit and, ultimately, ET_O (Brutsaert and Stricker, 1979). The results presented here illustrate clearly the complementary relationship and drying scenario described above, and confirm the relative lack of impact experienced by GDEs in Spring Valley, to date.

5.3 Constant and continuous groundwater level change

Annual groundwater levels, water year PPT and median summer EVI for Fish Lake Valley polygons 1-3 is illustrated in Figures 10-17. Throughout Fish Lake Valley groundwater levels have steadily decreased since the 1970s due to groundwater abstraction, primarily for the valley's plentitude of irrigated agricultural lands. Mann-Kendall trend test results indicate highly significant ($1x10^{-3} > p$) positive and negative trends for depth to groundwater and summer median GDE EVI, respectively, for FLV1, FLV2 and FLV3. The rate of increase in depth to groundwater was found to be 0.15, 0.54, and 0.27, meters per year, and median summer EVI decreased at rates of $-6.42x10^{-3}$, $-6.0x10^{-4}$, and $-1.04x10^{-3}$, $year^{-1}$ for polygons 1, 2 and 3,

respectively. No trends of any significance were observed for water year PPT, summer PPT, or summer TWD, across all three Fish Lake Valley polygons. Specific values of Mann-Kendall test statistics and additional information regarding Mann-Kendall trend and Sen's slope estimates may be found in appendix D.

Though a number of statistically significant correlations were identified between EVI and the environmental variables considered for each of the three polygons in Fish Lake Valley, across the board the strongest and most statistically significant relationships identified were between EVI and DT_G. Polygons 1, 2 and 3 boasted impressively significant ($2x10^{-6} > p$) and strong, negative Pearson correlation coefficients of -0.91, -0.75 and -0.74, respectively. Spearman's correlation coefficients between the two variables across all three polygons were slightly less significant, ($2x10^{-5} > p$), though similarly negative and strong (-0.88, -0.68 and -0.81 for FLV1, FLV2 and FLV3, respectively).

The EVI time series of polygon 1 was observed to have no statistically significant correlations with any environmental variable other than DT_G. In polygon 3, beyond EVI and DT_G, a lone significant ($0.05 > p$), moderately strong, positive Spearman correlation coefficient of 0.40 was observed between EVI and water year PPT. Polygon 2's EVI time series was found to have significant ($0.05 > p$), positive Pearson's correlation coefficients of 0.38 for summer PPT and 0.36 for water year PPT, as well as a somewhat more significant ($0.005 > p$) and strong Spearman correlation of 0.53 between EVI and water year precipitation.

A closer examination of Figure 13 reveals polygon 2's EVI rather closely tracking changes in DT_G for the period of 1984-1999, and the apparent cessation of this relationship around the year 2000. Dividing the correlation analysis of polygon 2 into both and early (1984-1999) and late (2000-2015) periods confirms these qualitative observations. A significant ($4x10^{-4} > p$) and quite strong negative Pearson's correlation coefficient of -0.78 exists between EVI and DT_G for the early period, while water year PPT shows no correlation with EVI over the same period. Conversely, for the late period, the Spearman's correlation coefficient between EVI and

water year PPT is significant ($5x10^{-3} > p$) and strong, whereas no statistically appreciable correlation exists between EVI and DT_G, over this period.

Figures 12, 15 and 18 show the complementary relationship between ET and ET_O for Fish Lake Valley polygons 1, 2 and 3--similar to the complimentary Spring Valley figure (Figure 9), described in detail in section 5.1. These figures, as well, are divided into both an early and late period in order to more clearly illustrate changes in the climate-atmosphere-vegetation relationship over time. Figure 12 shows a transition from an inverse, to a direct, relationship between water year PPT and EVI, indicating a shift towards greater water sensitivity in this ecosystem. Figures 15 and 18 (associated with Polygons 2 and 3, respectively) show similar increases in ecosystem sensitivity to water year PPT, though both of these ecosystems began with almost no relationship, rather than an inverse one, with water year PPT.

San Emidio Desert Polygon annual summer median EVI values, in combination with water year PPT and $DT_{G,}$ are illustrated in Figures 19 and 21. Kendall-Mann trend tests performed on the various time series associated with SE returned a number of significant trends, with water year PPT remaining the sole insignificantly changed environmental variable. EVI and DT_G were observed to be decreasing ($0.001 > p$) at rates of $1.18x10^{-3}$ $year^{-1}$, and 0.1 m $year^{-1}$ DTG, respectively. Summer PPT ($0.1 > p$) and TWD ($0.05 > p$) were also found to be decreasing at respective rates of -0.34 and -0.99 mm $year^{-1}$. Specific values of Mann-Kendall test statistics, Sen's slope intercept estimates and more for San Emidio Desert Polygon 1 may be found in appendix D.

SE's median summer EVI time series was found to be highly significantly and quite strongly correlated with changes in $DT_{G,}$ in a negative manner. SE's Pearson's correlation coefficient ($1x10^{-6} > p$) of -0.76, and its somewhat less significant ($1x10^{-4} > p$) and strong Spearman's correlation coefficient of -0.65, both suggest rather unequivocally that DT_G is the most influential environmental variable on GDE ANPP, considered here. Moreover, neither

Pearson's nor Spearman's correlation coefficients between all of the remaining environmental variables and median summer EVI returned values of even minimal significance ($0.1 > p$).

Figure 21 illustrates the complementary relationship between ET (as EVI) and ET_O for the lone San Emidio Desert polygon. Qualitative examination of this figure reveals nearly identical slopes of the two best fit lines, indicating the dynamic nature of the relationship between EVI and water year PPT has changed very little throughout the course of the study. That being said, however, it would appear as if vegetation vigor has been universally decreased, perhaps indicating the community has experienced increased stress in the more recent period from 1999-2015.

5.4 Variable and discontinuous groundwater level change

The long-term vegetation vigor of the GDEs in Boulder Flat's lone polygon with respect to climate and hydrology is illustrated in Figures 22 and 23 by plotting polygon-wide spatial averages of summer median EVI over time with DT_G and water year precipitation, occupying secondary y-axes. A Mann-Kendall trend test and Sen's slope estimate performed on the polygons 32-year long record of median EVI values revealed a statistically significant ($0.001 > p$) trend of EVI decreasing at a rate of 4.56×10^{-3} $year^{-1}$. A similar trend analysis of the 31-year DT_G record returned a statistically significant ($0.001 > p$) trend of increase in the depth to groundwater of 0.15 m $year^{-1}$. Mann-Kendall trend tests did not, however, return any statistically significant ($0.1 > p$) trends when performed on BF's summer PPT, TWD and water year PPT, time series. Therefore Sen's slope estimates for these series will not be reported. Additional information and statistics regarding both Sen's slope estimates and Mann-Kendall trend tests on BF may be found in appendix D.

The vegetation vigor of the GDEs observed in BF was found to covary most closely and significantly with depth to groundwater, even despite sudden, large scale anthropogenic hydrologic alteration resulting from mining operations up-gradient from the study polygon. Strong, negative and highly significant Pearson's ($p > 1 \times 10^{-11}$) and Spearman's ($p > 1 \times 10^{-5}$)

correlation coefficients of -0.91 and -0.71, respectively, were observed between EVI and depth to groundwater throughout the 31-year time series analyzed. Though both Mann-Kendall trend tests and Sen's slope estimates were completed for all remaining variables, no trends of any significance were observed for water year PPT, summer PPT, or summer TWD. Specific correlation coefficient p-values as well as correlation coefficients unreported due to their insignificance may be found in appendix C.

Figure 24 illustrates the complementary relationship shared by ET and ET_O throughout the study polygon considered for Boulder Flat from 1984-2015, and specifically how that relationship changes through time. Boulder Flat's EVI time series was distinctly lower and significantly more precipitation dependent, prior to mine dewatering activities. This dewatering appears to have resulted in significant volumes of groundwater infiltration down-gradient of an irrigation reservoir and the subsequent induction of large swaths of GDEs in areas previously indescribable as such. The consistent availability of groundwater to GDEs resulting from the presence of a large volume of continuously infiltrating water results in the practical indifference of GDEs in this polygon to water year precipitation totals.

Figures 25 and 26 and illustrate 32-year records of spatially averaged summer median EVI paired respectively with water year PPT, and DT_G, for Smith Valley polygon 1, as do Figures 28 and 29 for Smith Valley polygon 2. The Mann-Kendall trend test, when performed on the two EVI time series, returned significant trends of declining EVI, with SMV1 declining at a rate of -2.82×10^{-3} ($0.001 > p$), and SMV2 characterized by a rate of EVI decline of 2.0×10^{-3} $year^{-1}$ ($0.05 > p$). Mann-Kendall trend test on both SMV1 and SMV2's depth to groundwater time series' revealed statistically significant ($0.001 > p$) increases in DT_G, with DT_G increasing at a rate of 0.42 m $year^{-1}$, and 0.45 m $year^{-1}$, for polygons 1 and 2, respectively. Trend tests applied to both SMV1 and SMV2's water year PPT, summer PPT and summer TWD time series' revealed no trends of significance ($0.05 > p$), and therefore Sen's estimates of slope will not be reported for these 6 series. Mann-Kendall test statistics (Z), Sen's slope and intercept

estimates, and additional information are available for all time Smith Valley series considered in this work in appendix D.

Though multiple statistically significant correlations were observed between EVI time series of the two Smith Valley study polygons and the environmental variables considered for these polygons, once again, the strongest and most statistically significant relationships identified were between EVI and DT_G. Polygon 1's EVI-DT_G relationship was characterized by strong, negative, highly significant Pearson's ($5x10^{-5} > p$) and Spearman's ($5x10^{-7} > p$) correlation coefficients, which returned values of -0.66 and -0.78, respectively. Additionally, SMV1's EVI and water year PPT time series', as well as its EVI and summer TWD series', were found to be characterized by moderately strong, positive, statistically significant ($0.05 > p$) Pearson's and Spearman's correlation coefficients of, 0.37 and 0.32, respectively. In a manner similar to that of SMV1, SMV2's EVI-DT_G relationship returned strong, negative, statistically significant Pearson's ($5x10^{-4} > p$) and Spearman's ($0.001 > p$) correlation coefficients of -0.59, and -0.58. Polygon 2 was also found to have somewhat less significant, strong, positive Pearson's ($5x10^{-4} > p$) and Spearman's ($5x10^{-3} > p$) correlation coefficients of 0.59 and 0.50. Summer precipitation was not correlated with EVI through time in a statistically significant ($0.05 > p$) manner, for either polygon 1 or 2. Similarly, polygon 2's EVI was not correlated in a significant manner ($0.05 > p$) with summer TWD.

The multiple cycles of impact and recovery experienced throughout the 32-year period of observation for Smith Valley preclude the simple division of the complementary figures (Figures 27 and 30, for SMV1 and SMV2, respectively) into two simple periods of pre-impact and post-impact as was done for all previous study sites. Moreover, due to Smith Valley's long and rich agrarian history, and specifically the irrigation ditches that have conveyed Walker River water to fields throughout the valley since the 1860s, the complementary figures for polygons 1 and 2 respond to precipitation differently than do GDEs not confounded by this system. This results in a significant correlation between EVI and water year PPT across both polygons during both

periods of time considered, though only as a consequence of anthropogenic activity (see section 6, below).

6.0 Discussion

6.1 Baseline assessment of vegetation and climate

The EVI time series for the baseline assessment study polygon, Spring Valley 1, was found to have no significant Mann-Kendall trend throughout the period considered. Trends of significance were identified in neither the summer, nor the water year PPT time series, though the strongest ($R = 0.73$) and most significant ($5x10^{-5} > p$) correlation between any two time series was observed between the water year PPT time series and Spring Valley Polygon 1's EVI time series. Though somewhat weak correlations were observed between EVI and both summer TWD and summer PPT time series', the strength and significance of these relationships pale in comparison to the aforementioned EVI-water year PPT association. Additionally, Spring Valley polygon 1's DT_G time series revealed groundwater levels decreasing in a highly significant manner, though no significant correlation was observed between this series and the polygon-wide EVI time series. The meager rate of phreatic decline of 2 cm $year^{-1}$ is the likely culprit of the lack of an observed relationship between the DT_G and EVI time series, for this particular polygon. Together, these results suggest that, in the absence of pronounced anthropogenic hydrologic disturbance resulting in changes to the depth of the phreatic surface of a given basin, water year PPT acts as the primary factor controlling GDE vegetation vigor, considered in this study.

The strength of the observed vegetation vigor-PPT relationship is likely, in part, a consequence of phreatophytes ability to switch between shallow soil moisture and groundwater, preferentially using the former when available (Naumburg et al., 2005; Steinwand et al., 2006; McLendon et al., 2008; Devitt & Bird, 2015). Though the EVI time series clearly responds to highs in annual PPT, groundwater appears to support a rather more constant minimum EVI

value throughout the series (Figure 8). The lack of a significant relationship (0.05 > p) between DT_G and EVI is interpreted to be a consequence of the Spring Valley's relatively unchanged watertable depths, which were found to be increasing in depth at a meager rate of 2 cm $year^{-1}$ (Figure 7), throughout the study period.

Shallow groundwater throughout valley floors of the Great Basin is derived primarily from mountain block recharge associated with snowmelt (Thomas et al., 1996; Hershey et al., 2007). Therefore water year precipitation is a primary constraint on the natural variability of basin-wide interannual trends in DT_G. In the absence of anthropogenic perturbation of the hydrologic cycle, water influxes to hydrographic areas throughout the Great Basin are limited to only interbasin flow and precipitation. It follows, therefore, that in the absence of human perturbation resulting in transient aquifer conditions, water year PPT is representative of aquifer recharge, and will be proportional to aquifer discharge through the course of a given water year. Viewed in this context, the observed strong correlation between Spring Valley EVI and water year PPT may simply be explained as the combined consequence of interannual variations in local aquifer recharge, and the preferential use of shallow soil moisture by phreatophytes, when available.

Paleoclimatic reconstructions indicate the Great Basin has experienced multiple extended (> 100 year) droughts in the past two millennia (Mensing et al., 2004; 2008). Nonetheless, these same packrat midden and pollen core records clearly illustrate that throughout periods of drought the relative abundance of phreatophytic species either remained unchanged or increased (Elmore et al., 2003; Mensing et al., 2004; 2008). The abundance of GDE pollen in these times of sparse precipitation indicates that GDE vegetation is particularly resilient to extended drought.

GDE vegetation's resilience to drought is so pronounced, palaeoclimatologists even use a sagebrush / saltbush + greasewood (non-phreatophyte / phreatophyte) pollen ratio as measure of available moisture (Byrne et al., 1979; Wigand, 1987; Mensing, 2001; Mensing et al, 2004; 2008). During periods of minimal precipitation, deep rooted phreatophytes are not only

able to preferentially switch between water sources, but also can achieve exceptionally rapid root growth rates in order to “keep up” with water tables falling at natural rates (Naumburg et al., 2005; Canham et al., 2011), up to community specific maximum rooting depths (i.e. extinction depth). These unique adaptations impart upon phreatophytic species a competitive advantage over xeric floral assemblages throughout periods of sparse or irregular precipitation (Mensing, 2001; Mensing et al., 2004).

Though GDEs are well adapted to extended drought, their resilience is rooted in their ability to consistently access groundwater; a remarkable trait resulting from rapid, but not limitless root growth rates. In reality, while other forms of Great Basin vegetation are well adapted to intense water stress, with some xeric shrubs boasting impressive xylem cavitation tolerances up to -12.0 MPa, Great Basin phreatophytes are actually rather sensitive to drops in water potential (Hacke et al., 2000; Naumburg et al., 2005). That is to say, while they are adept at securing water sources, phreatophytes are rather poorly evolved in terms of their ability to withstand direct water stress, with Rabbitbrush experiencing extensive xylem cavitation at pressures lower than -2.0 MPa, and Greasewood likely following suit at soil water potentials of roughly -4.0MPa (Donovan et al., 1996; Hacke et al., 2000). Therefore, despite their impressive resilience toward natural disturbances, Great Basin GDE vegetation is highly susceptible to acute water table drawdown events resulting from abstraction alone, or in combination with natural fluctuations in DT_G.

6.2 Groundwater level change and GDE vegetation vigor

For each of the polygons considered where anthropogenic groundwater abstraction was the suspected culprit of observed groundwater elevation change, rather strong and highly significant ($0.001 > p$) Mann-Kendall trends were observed in DT_G for all seven well hydrographs associated with impacted sites, as well as in all seven of the polygon’s spatially averaged median summer EVI time series. These trends were characterized by Sen’s slope estimates ranging from 0.08 to -0.54 m $year^{-1}$ and -6.00×10^{-4} - to 4.56×10^{-3} (dimensionless $year^{-}$

^{1}) for DT_G and EVI, respectively. Across these same seven polygons, four individual summer TWD and summer PPT time series returned Mann-Kendall trend tests of significance (0.05 > p). Despite these statistically meaningful trends, however, the absence of significant (0.01 > p) correlation coefficients between EVI, summer TWD and summer PPT across any of the study polygons considered, demonstrates, rather unequivocally, the lack of influence these environmental variables have on GDE vegetation vigor in anthropogenically impacted basins.

In addition to each of the seven impacted polygons being found to have rather pronounced trends in their individual DT_G and EVI series, these same variables were observed to be universally correlated across each of the groundwater impacted study sites, in a highly significant, rather strong, and universally negative manner. For each polygon, the correlation coefficients describing the DT_G-EVI relationship were found to be the single strongest (-0.55 - -0.91) and most significantly ($0.001 > p > 1x10^{-12}$) correlated environmental variable considered. Across four of the seven polygons (Smith Valley polygons 1 and 2, and Fish Lake Valley polygons 1 and 2), water year PPT was also found to covary with EVI in a moderately strong (0.37-0.59) and somewhat less significant ($0.05 > p > 0.001$) fashion than that of DT_G. Despite this correlation, however, the presence of significant trends in each impacted polygons EVI series, and lack thereof in any of the seven water year PPT time series considered, suggests changes in precipitation are not the driving force of the observed changes in polygon-wide vegetation vigor. Moreover, the aforementioned ability of phreatophytes to preferentially source their water resources explains the somewhat strong water year precipitation-EVI correlation observed for a number of impacted basins.

In the case of Smith Valley, specifically, the basin's long history of Walker River diversion-fed irrigated agriculture may explain the observed covariance between water year PPT and EVI. Dating back to the 1860s, the Walker River, which flows through the heart of Smith Valley provided for the majority of the basins significant irrigation demands through an extensive network of irrigation ditches (Rush & Schroer, 1975). Water infiltrating through the

banks of these unlined ditches recharges the local aquifer, thereby raising the water table and increasing GDE vegetation vigor during wet years (i.e. preferential water sourcing). Historically, infiltration from widespread irrigation ditches and fields significantly raised groundwater levels throughout Smith Valley (Loeltz & Eakin, 1953; Rush & Schroer, 1975). More recently, however, increased reliance on groundwater irrigation during periods of minimal surface water availability has resulted in cyclic periods of aquifer drawdown and recovery (Sharpe et al., 2007).

In addition to the somewhat unique case experienced by Smith Valley, water year and summer precipitation can impact already disturbed GDEs in a variety of ways. Should a GDE become decoupled from groundwater (i.e. DT_G > depth of roots), it will necessarily transition towards shallow soil moisture dependence until it might resecure groundwater access. Shallow soil moisture throughout the Great Basin is typically the result of either precipitation events, or mountain block recharge in the form of snowmelt runoff. Therefore, impacted GDEs become increasingly dependent upon precipitation in order to maintain their structure and function in times of groundwater stress.

That said, results from this study clearly and unequivocally illustrate that the influence of water year PPT is secondary to that of changes in DT_G, which represent the predominant driving force in observed changes to GDE vegetation vigor through space and time. Across all impacted sites, changes in DT_G were found to share significant and pronounced negative correlation through time with spatially averaged observations of GDE vegetation vigor. This was true not only for each of the 6 impacted study polygons underlain by falling water tables, but also by the lone polygon, Boulder Flat 1, characterized by a significantly and consistently rising water table throughout the study record (i.e. falling DT_G), where areas of new, or increasing, groundwater dependence were observed. Moreover, the findings of this study regarding the influence of DT_G on GDE vegetation vigor are in line with a plethora of past studies findings, which also suggest groundwater availability (i.e. depth) as being the predominant constraint on GDE vegetation vigor (Nichols, 1994, 2000; Manning, 1999; Nichols et al., 2000; Elmore et al.,

2006; Cooper et al., 2006; Devitt et al., 2011; Devitt & Bird, 2015). As such, the question becomes not whether or not changes in DT_G impact GDE communities, but rather the manner in which the impacted ecosystems respond to these perturbations.

6.3 GDE response regimes

A number of past studies have suggested the depth and/or rate of groundwater drawdown to be the primary variable constraining GDE vigor and function (Nichols, 1993; 1994; 2000; Manning, 1999; Elmore et al., 2000; 2003; 2006; Naumburg et al., 2005; Cooper et al., 2006; Froend & Sommer, 2009; Pritchett & Manning, 2012). They postulate the rate and duration of changes in DT_G determine whether a given GDE might experience either a linear decline in vegetation vigor or a dramatic transition to an alternative ecohydrological state. Measures of DT_G, do not, however, take into account soil physics, capillary action, shallow soil moisture from precipitation and runoff, and a number of additional factors that have been found to influence the structure and function of Great Basin GDEs (Naumburg et al., 2005; Devitt et al., 2011; Devitt & Bird, 2015). Rather, the results from this study suggest that depending upon the degree of changes to a community's soil moisture content--a result of the rate, depth, and duration of the change in DT_G, and more--a GDE community might exhibit one of two given modes of disturbance response (Scott et al., 1999; Shatfroth et al., 2000).

If the hydrologic disturbance is within a tolerable range, canopy dieback and some mortality will occur in phreatophytic species, resulting in an observable linear cover decline. Linear GDE responses to falling (or rising) water tables are essentially the result of an impacted GDE where DT_G is increasing (or decreasing), but the roots of the community have not become decoupled from their retreating water source (or inundated resulting in anoxia and root mortality). The previously mentioned dramatic root growth rates exhibited by phreatophytes allow these ecosystem engineers to adjust to a changing environment, so long as the rate of drawdown does not exceed their ability to keep up, nor exceed their maximum depth (Naumburg et al., 2005; Canham et al., 2012). Despite some degree of adverse impact, the

functionality of the groundwater dependent ecosystem will not, as a whole, be compromised (Naumburg et al., 2005; Eamus et al., 2006; 2015; Froend & Sommer, 2009; Sommer & Froend, 2010).

Linear cover declines in response to falling water tables were observed in EVI-DT_G time series' for three of seven impacted polygons considered, specifically in the series of Fish Lake Valley polygon 3, San Emidio Desert polygon, and Smith Valley polygon 2 (Figures 16, 19 and 28), which were characterized by water levels falling at rates of 0.27 m $year^{-1}$, 0.09 m $year^{-1}$, and 0.45 m $year^{-1}$, respectively. Each of the above polygons represents a GDE, or assemblage of GDEs, which have experienced disturbance extensive enough to result in a linear cover decline, though not so acute as to induce a nonlinear, threshold, response (Ridolfi et al., 2006; 2007). That being said, however, both their complementary figures and EVI-DT_G time series indicate that while stressed, these communities have likely not become decoupled from their groundwater source. This is an important distinction, as linear declines, unlike threshold responses, generally allow for a high degree of ecosystem recovery following restoration of natural hydrologic function. The scenario where ∂DT_G (i.e. the rate of drawdown) exceeds a given GDEs maximum root growth rate results in a rather starker outcome than the linear scenario described above.

Rapid groundwater declines may result in the complete decoupling of GDEs from the water table, thereby breaching a threshold variable and resulting in the possible subsequent transition to an alternative ecohydrological state (Naumburg et al., 2005; Froend & Sommer, 2009; Devitt et al., 2011; Devitt & Bird, 2015). If an excessive rate of drawdown is sustained for a sufficiently long period, the phreatic surface and capillary fringe will drop below the rooting zone and GDE vegetation will become entirely decoupled from the water table (Naumburg et al., 2005; Devitt & Bird, 2015). If this decoupling results in soil water potentials in GDE rooting zones falling below species and community specific threshold values, extensive xylem cavitation will occur (Hacke et al., 2000). When this threshold is surpassed, GDEs not only lose their

competitive advantage (i.e. consistent water access) over other forms of both endemic and invasive Great Basin floral species, but potentially also experience irrecoverable physical damage resulting in their widespread mortality, thereby opening the window for the potential of highly hysteretic, practically irreversible, community succession (Elmore et al., 2003 2006; naumburg et al., 2005; Ridolfi et al., 2006; 2007; Froend & Sommer, 2009; Pritchett & Manning, 2012; Eamus et al., 2015).

Four of the seven impacted polygons EVI-DT_G time series' considered were observed to depict threshold community responses resulting from GDE-groundwater decoupling. Fish Lake Valley Polygon 1, Fish Lake Valley Polygon 2, and Smith Valley Polygon 1 (Figures 10, 13, and 25) all appear to decline in cover linearly for some time before experiencing a drastic, threshold event. These three polygons had associated well groundwater level decline rates of 0.15 m $year^{-1}$, 0.53 m $year^{-1}$, and 0.42 m $year^{-1}$, respectively. The lone study site characterized by a rising water table, Boulder Flat, was found to respond in a similar if opposite manner, with a threshold event resulting from rising water levels (at a rate of 0.08 m $year^{-1}$) being followed thereafter by linear cover increase (Figure 22).

The EVI and DT_G time series' for Fish Lake Valley polygon 2 represents the most clear case of a threshold response observed in this study (Figure 13). While EVI appears to track DT_G in a linear fashion for a handful of years at the beginning of the record, by ~1995 the two series have diverged completely. To examine this transition, correlation coefficients were re-run for both the early period (1984-1999) and the late (2000-2015), to analyze how the variable driving the ecosystem in question might have changed over time. The early portion returned significant Spearman ($5.0x10^{-4} > p$) and Pearson's ($0.01 > p$) correlation coefficients between only DT_G and EVI, of -0.78 and -0.64, respectively. Conversely, the latter half of the record returned significant ($0.01 > p$) Pearson's and Spearman's ($0.005 > p$) correlations between only EVI and water year precipitation, with magnitudes of 0.59 and 0.67, respectively. These values illustrate that though Fish Lake Valley 2 once functioned as a GDE, changes in DT_G resulted in a threshold response

and functional transition towards precipitation dependence. That said, though the available evidence certainly points in the direction of irreversibility, unless hydrologic and other environmental variables are returned to pre-disturbance values it is impossible to say with complete certainty that hysteric community succession to an alternate ecohydrologic state has occurred for this, as well as all other, sites.

Perhaps the most striking illustration of the functional transition each of these ecosystems experienced may be seen in their respective complementary diagrams. This style of figure illustrates the manner in which a given area's precipitation-vegetation vigor relationship might change through time. This can be most clearly seen in the slope of the best fit line through the EVI-water year PPT scatter, where no slope indicates no relation to water year PPT, a negative slope an inverse relationship (dense, shallow DT_G GDE vulnerable to inundation resulting in root anoxia and mortality) and a positive slope indicates precipitation dependence.

Figures 12, 15, and 24, representing the complementary diagrams for Fish Lake Valley , Fish Lake Valley 2, and Boulder Flat's lone polygon, clearly illustrate negative or nearly flat slopes for their respective periods of groundwater dependence, and increasingly positive slopes with through periods with falling water levels resulting in GDE stress. Additionally, despite the absence of an apparent threshold in the time series, the slopes of best fit for Fish Lake Valley Polygon 3's complementary figure (Figure 18), also indicate the likelihood of a functional transition away from groundwater dependence. These observations suggest the ecosystems in question may likely have experienced a transition in terms of their water dependence, from groundwater dependence towards being precipitation dependent. Moreover, the universal drop in EVI values from periods of groundwater to precipitation, dependence, indicates a drop in primary productivity, likely indicating the loss of ecosystems services associated with GDEs.

Smith Valley's two polygons, along with the lone San Emidio Desert polygon, were found to have relatively unchanged slopes of their best fit lines from the early to the late periods considered. The almost identical slopes indicate that the nature of the precipitation relationship

did not change considerably throughout the study period. Despite the similarity of their slopes, across all three polygons the later period was characterized by nearly universally lower EVI values. These distinctly lower values of EVI indicate the regions in question were, in fact, impacted by changes in DT_G, the polygons simply did not exhibit a threshold response. For both Smith Valley polygons the absence of this dramatic reaction to a falling water table is likely due significant ditch induced aquifer recharge during above average water years providing enough shallow soil moisture to delay a more dramatic, threshold response. for the time being.

The lone polygon considered in San Emidio Desert was found, for both periods, to have an inverse precipitation-vegetation vigor relationship, indicating the continuous functioning of the polygon as a GDE throughout the period of observation. In this case, too, differences in recharge throughout the period may explain this observed change in the EVI magnitude. Once mining operations ceased in 1993, some portion of what was formerly mountain block recharge was diverted towards filling the large excavated mine pit. This change in recharge combined with the change in DT_G (Figure 19), may have resulted in a floristic compositional transition of San Emidio, though the GDE nature was retained.

7.0 Conclusions

The objectives of this study were to both Identify patterns of GDE vegetation vigor change through space and time and to determine the extent to which climate and hydrology might explain those patterns. Through the use of Google's Earth Engine cloud computing platform, and statistical analyses of annual EVI time series, it was determined that DT_G and GDE vegetation vigor, as represented by spatially averaged EVI time series, share a rather strong and quite significant correlation across all impacted study locations.

In the absence of significant anthropogenic perturbation of the hydrologic cycle, this study found GDE communities to be rather resilient to drought and other forms of natural disturbance. Phreatophytes remarkable root growth rates allow them to track rising and falling water tables, so long as the changes in the depth of the phreatic surface aren't too drastic.

Alternatively, study sites characterized by anthropogenically driven significantly changing groundwater levels were universally found to display associated significant changes in their remotely sensed vegetation vigor, suggesting that significant human groundwater abstraction is likely to result in adverse impacts to GDE communities. The type of adverse impacts which a given community was likely to experience, however, proved to be a somewhat more difficult phenomenon to predict. Depending on the severity of the hydrologic impact endured, GDE communities either exhibited linear cover declines, or more drastic threshold transitions. However, groundwater level change alone was not found to explain the observed variance in community response. Instead, it is postulated that antecedent conditions, soil properties, precipitation and more, combine with groundwater conditions to influence GDE vegetation vigor. The role of precipitation and other factors further suggest that soil moisture content at GDE rooting depths may represent a more telling variable regarding community and tissue specific threshold values that once surpassed, result in a non-linear and often irreversible, community transition.

Isolating anthropogenic impacts to GDEs from those arising as a consequence of natural climatic variability is a complicated, multifaceted, and yet highly necessary endeavor. The identification of cause and effect relationships in these dynamic systems is prerequisite to resource manager's ability to make informed decisions that will adequately address the simultaneous the needs of both humans and nature. Across the endorheic Great Basin, balancing the abstraction of groundwater for human use, and the preservation of GDEs and the invaluable services which they perform, requires detailed knowledge regarding multiple modes of disturbance response, historic conditions, specific environmental thresholds, and more (Nichols, 2000; Hacke et al., 2000; Eamus et al., 2006; Hinsby et al., 2008; Kløve et al., 2011; Huntington et al., 2016).Moving forward, adaptive water management frameworks which promote the resilience of GDEs through appropriate regulation of groundwater abstraction, must be implemented. Moreover, it is imperative that GDEs receive renewed interest in both terms of

scientific study, and legislative protection, so that these unique ecosystems and the invaluable services which they perform are not lost forever.

8.0 Figures

8.1 Maps

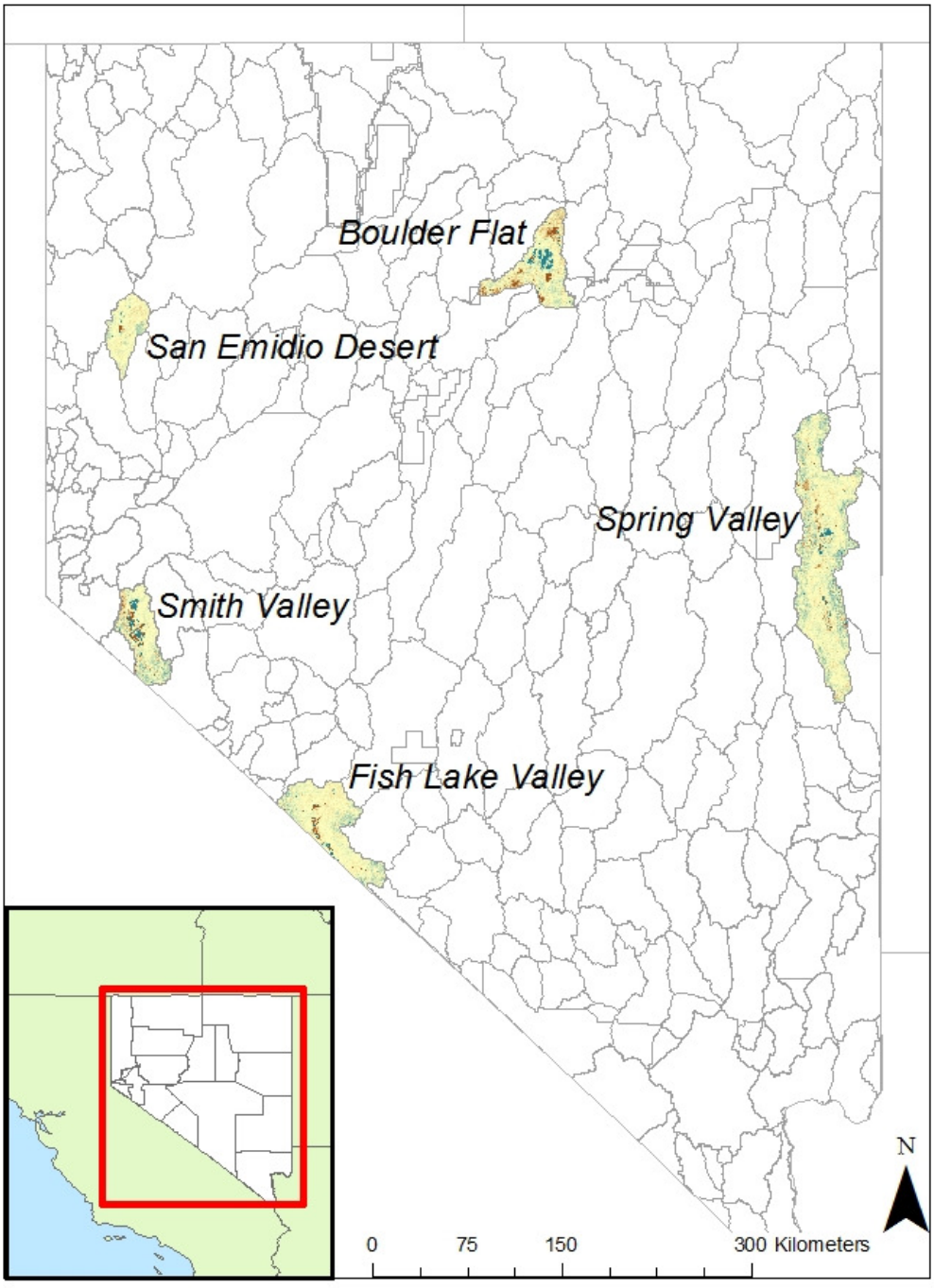

Figure 1: Nevada's hydrologic basins. Study basins are colored by EVI regression slope map.

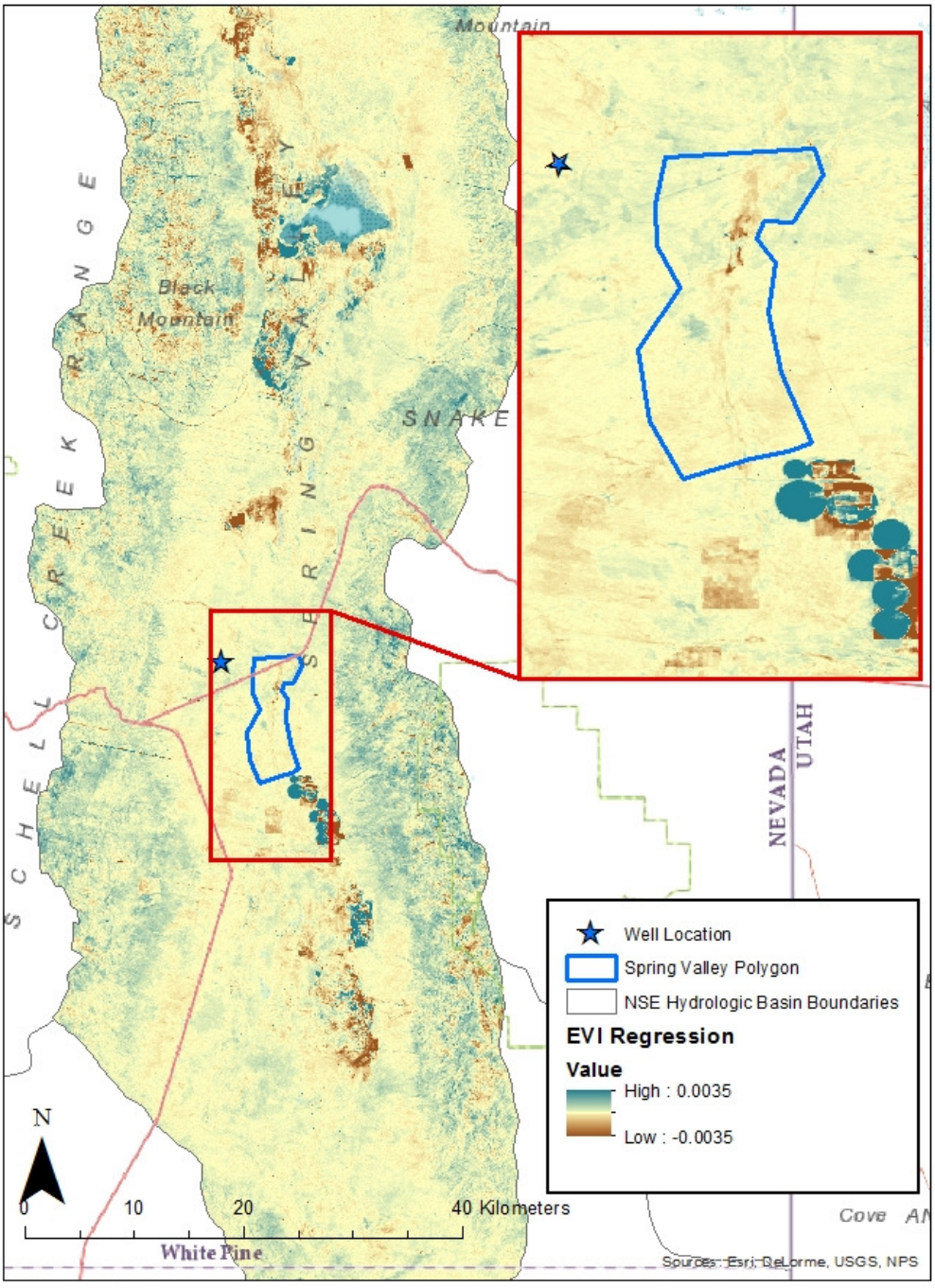

Figure 2: Spring Valley, NV. Color indicates the slope of 32-year summer median value EVI regression.

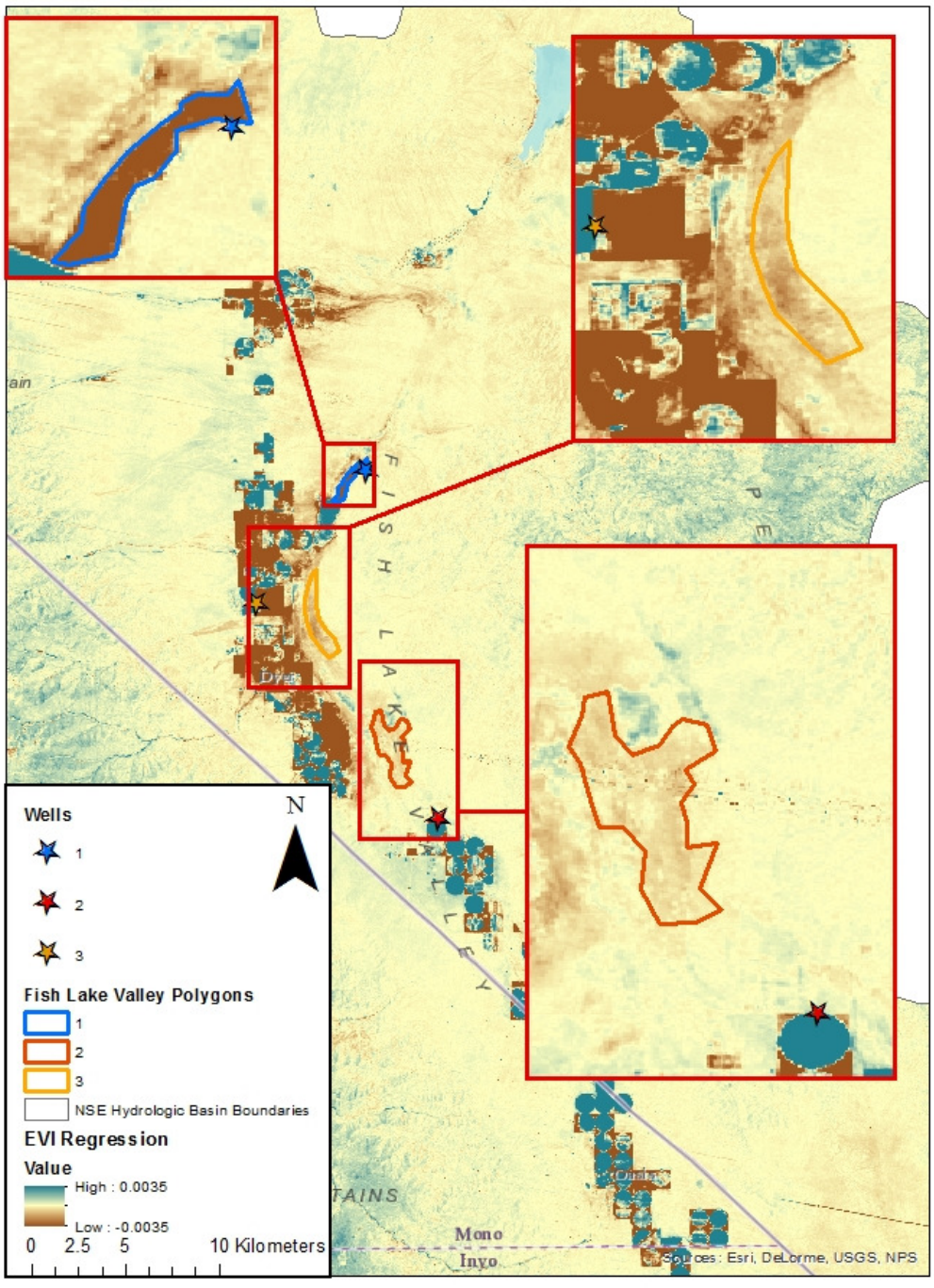

Figure 3: EVI slope map of Fish Lake Valley, NV over 32-year study period.

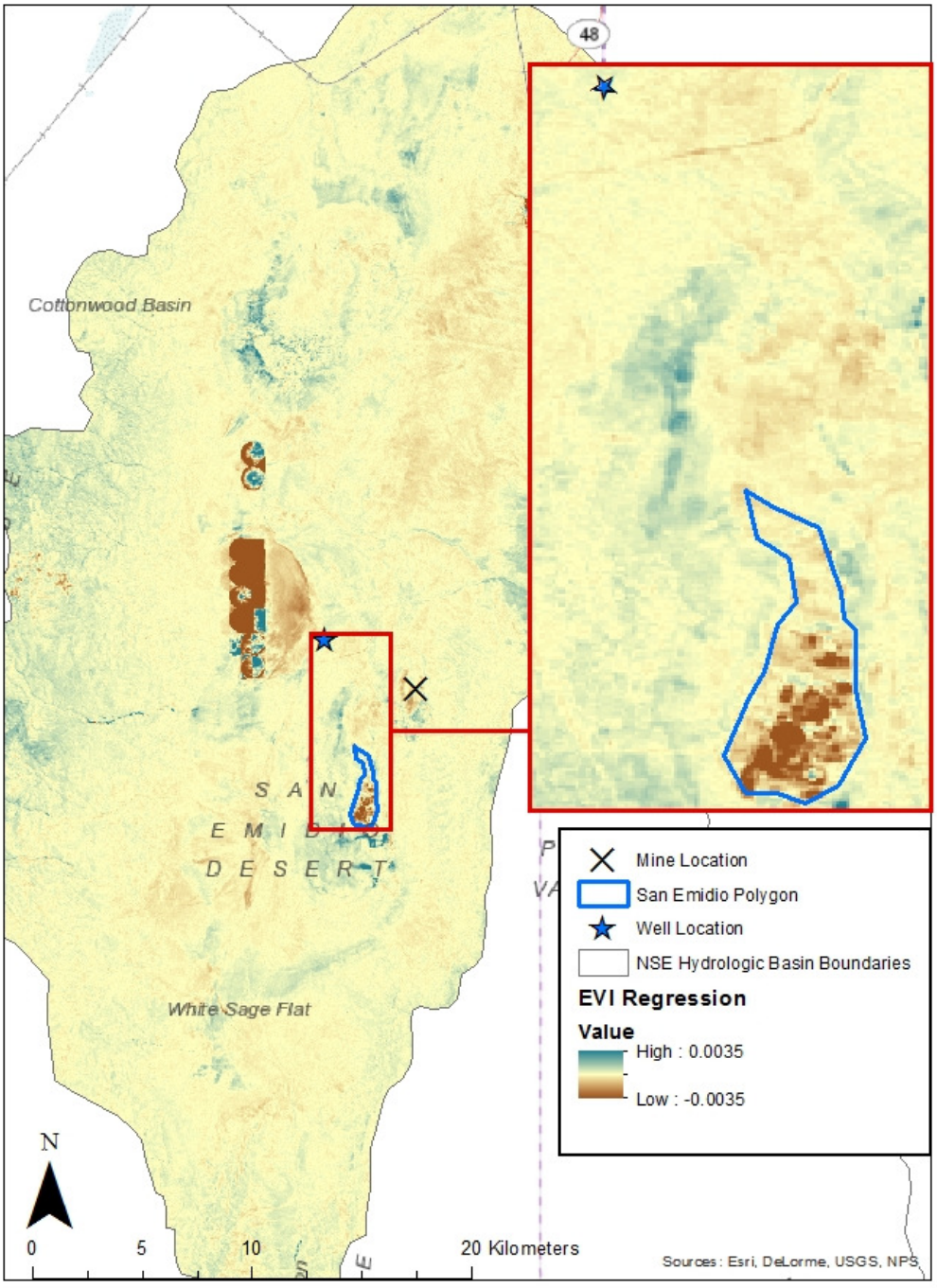

Figure 4: EVI slope map of San Emidio Desert, NV over 32-year study period.

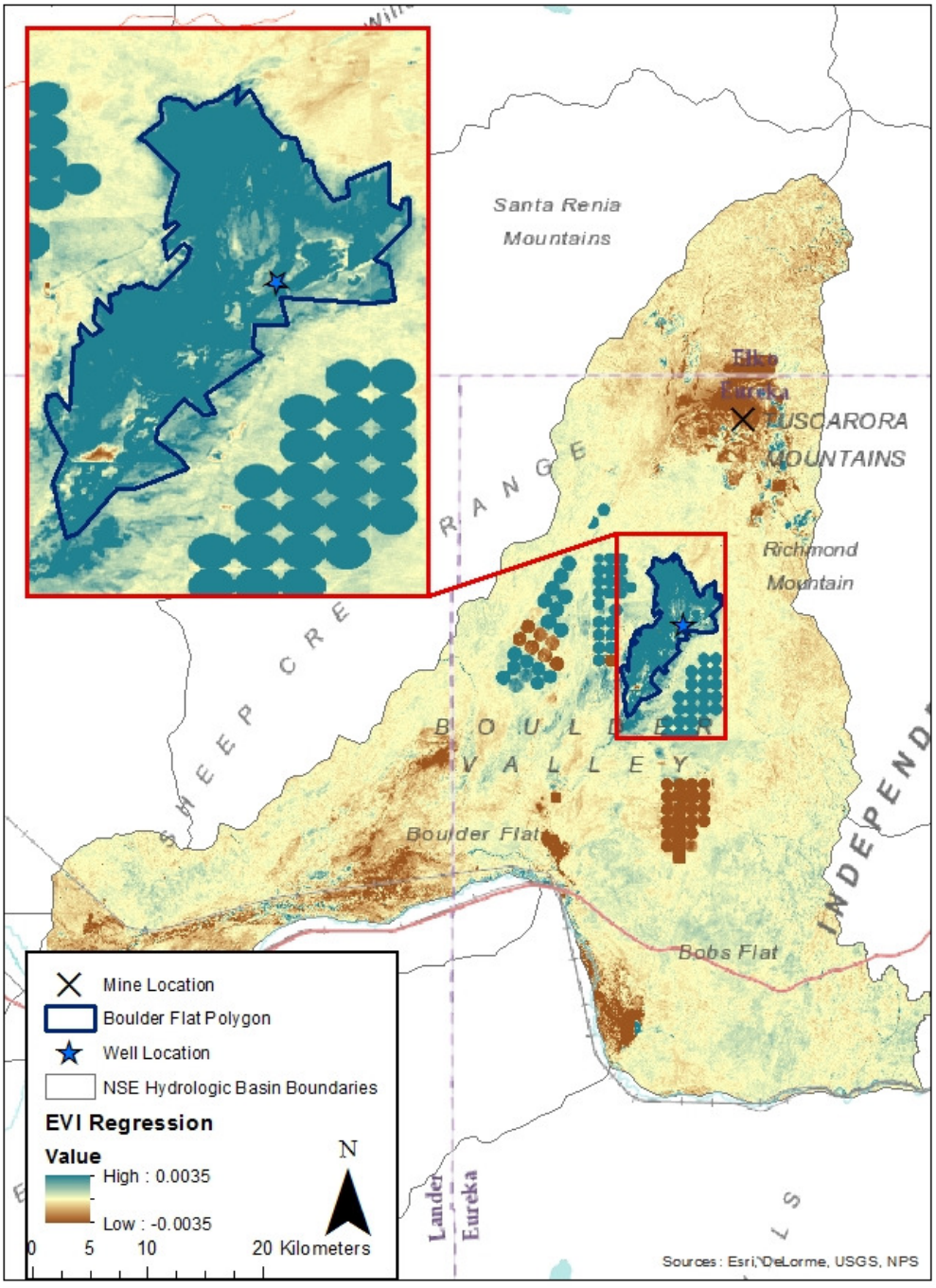

Figure 5: EVI slope map of Boulder Flat hydrographic area, NV over 32-year study period.

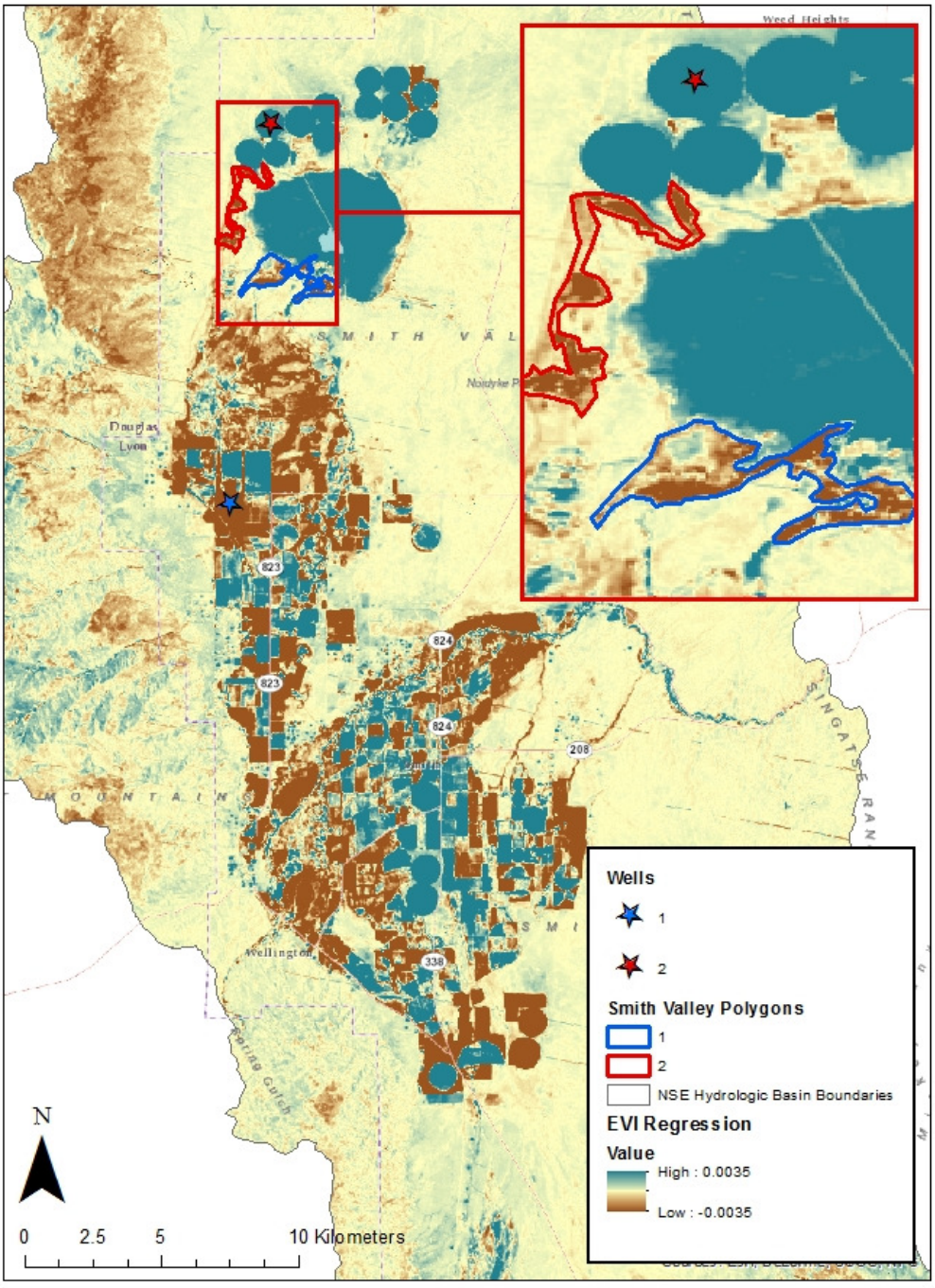

Figure 6: EVI slope map of Smith Valley, NV over 32-year study period.

8.2 Spring Valley

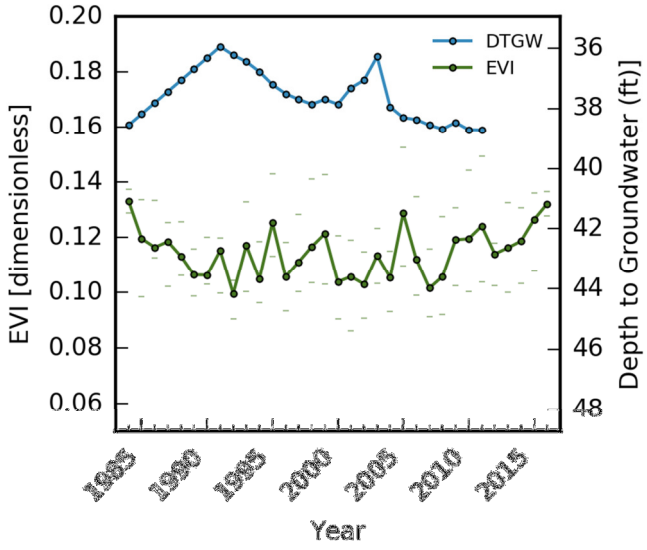

Figure 7: Spring Valley paired 32-year time series of both EVI and DTG (blue). Annual EVI maxima and minima are displayed as semi-transparent ticks above and below the median time series, respectively. The associated well is located 56 feet AMSL above the discharge area.

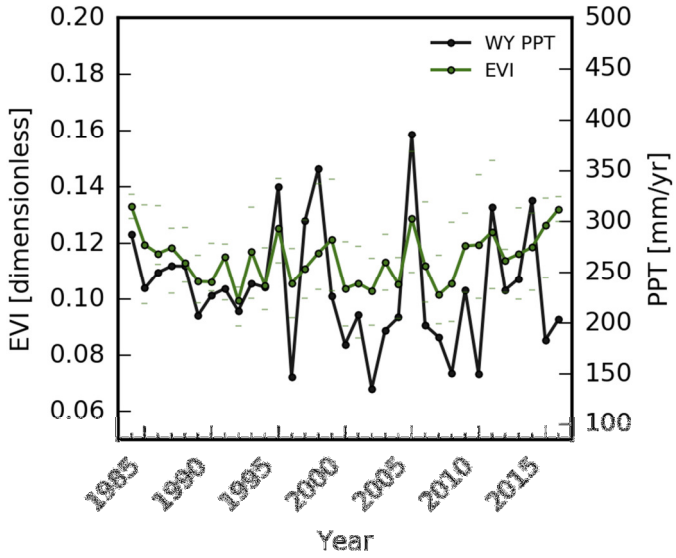

Figure 8: Spring Valley paired 32-year time series of both EVI (green) and water year precipitation (black).

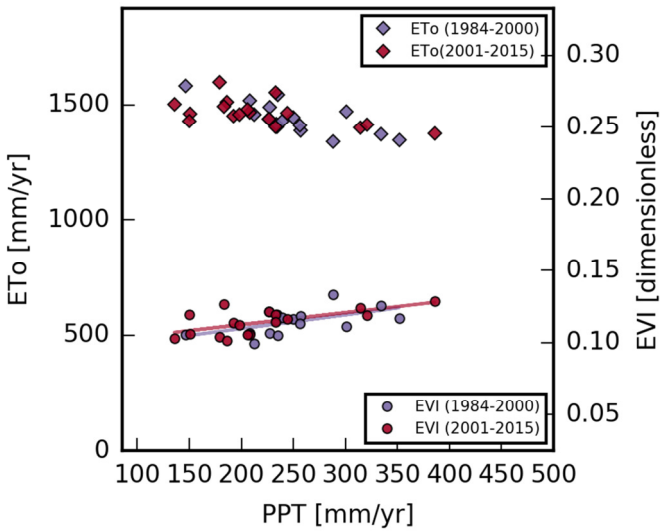

Figure 9: Spring Valley complementary figure. Similar equations of the best fit PPT-EVI scatter lines illustrates stationarity of system over study period.

8.3 Fish Lake Valley polygon 1

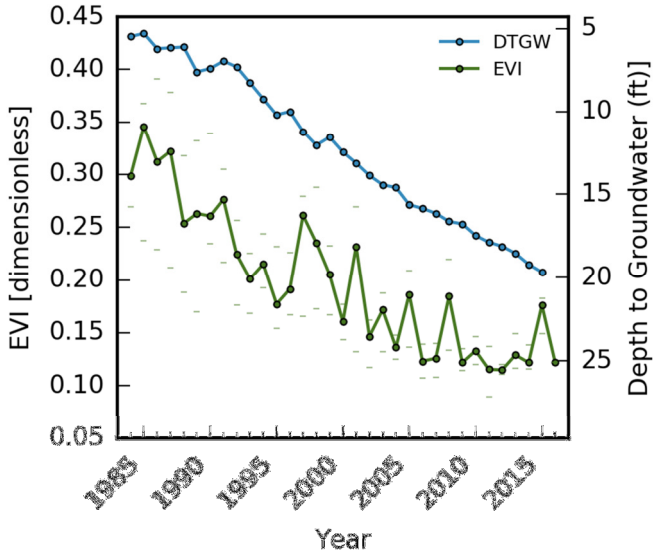

Figure 10: Fish Lake Valley polygon 1 Paired 32-year time series of both EVI (green) and DTG (blue). Annual EVI maxima and minima are displayed as semi-transparent ticks above and below the median time series, respectively. The associated well is located 10 feet AMSL above the centroid of the discharge area.

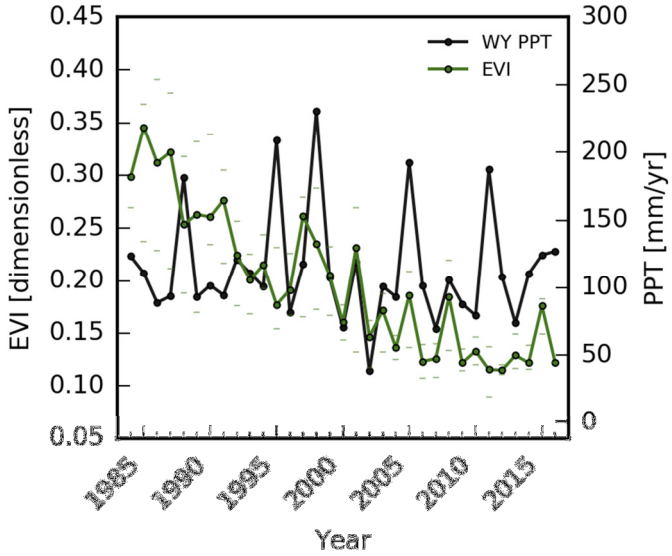

Figure 11: Fish Lake Valley polygon 1 Paired 32-year time series of both EVI (green) and water year precipitation (black).

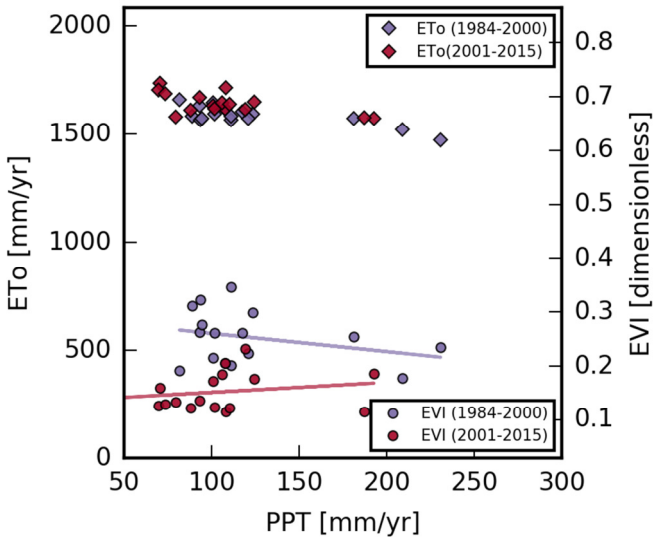

Figure 12: Fish Lake Valley polygon 1 complementary figure. Dramatic change in the slope of the best fit PPT-EVI scatter lines illustrates obvious change in ecosystem function.

8.4 Fish Lake Valley polygon 2

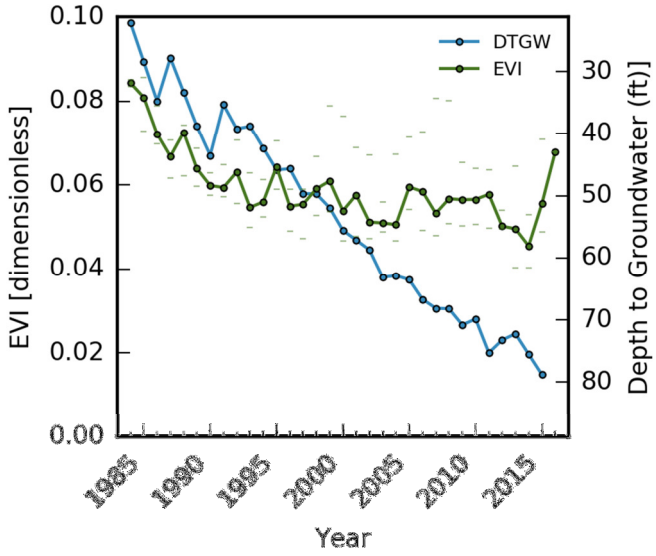

Figure 13: Fish Lake Valley polygon 2 Paired 32-year time series of both EVI (green) and DT_G (blue). Closely tracks DT_G until ~90-95, by 2000 no more tracking and ecosystem appears to have lost all GW dependence. Annual EVI maxima and minima are displayed as semi-transparent ticks above and below the median time series, respectively. The associated well is located 16 feet AMSL above the centroid of the discharge area.

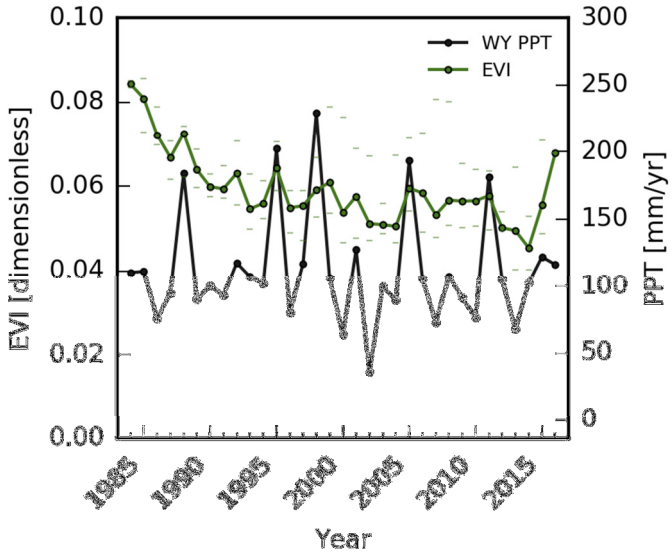

Figure 14: Fish Lake Valley polygon 2 Paired 32-year time series of both EVI (green) and water year precipitation (black). Influential primarily during the latter portion of the record, once region had transitioned away from GW dependence.

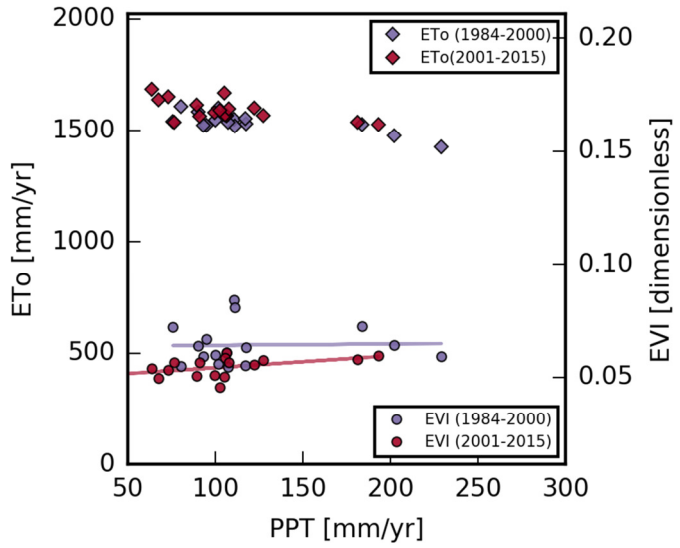

Figure 15: Fish Lake Valley polygon 2 complementary figure. Dramatic change in the slope of the best fit PPT-EVI scatter lines illustrates a distinct transition from ground water dependence to precipitation dependence.

8.5 Fish Lake Valley polygon 3

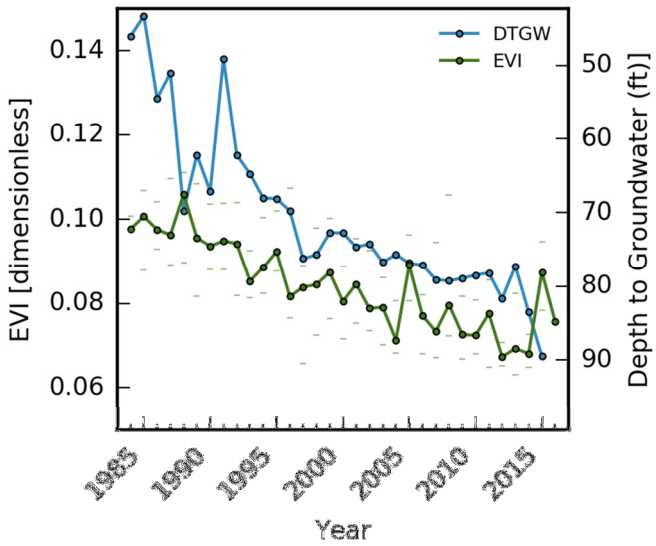

Figure 16: Fish Lake Valley Polygon 3 Paired 32-year time series of both EVI (green) and DT_G (blue). Particular GW depth is too great, but well is decently above observation area. Annual EVI maxima and minima are displayed as semi-transparent ticks above and below the median time series, respectively. The associated well is located 43 feet AMSL above the centroid of the discharge area.

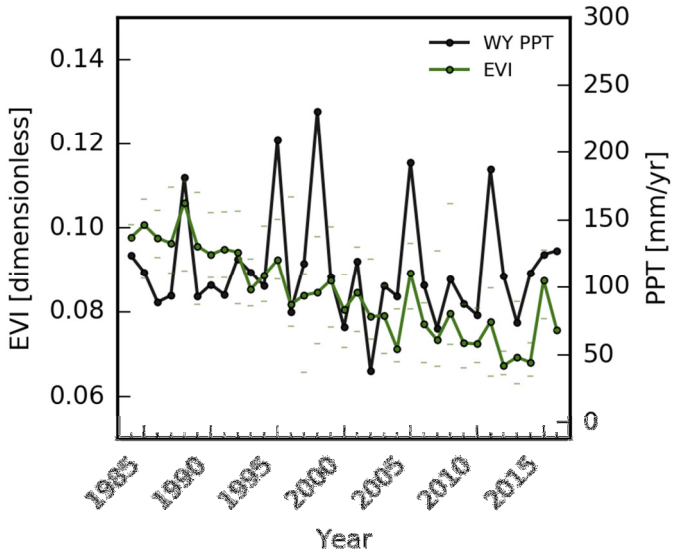

Figure 17: Fish Lake Valley Polygon 3 paired 32-year time series of both EVI (green) and water year precipitation black).

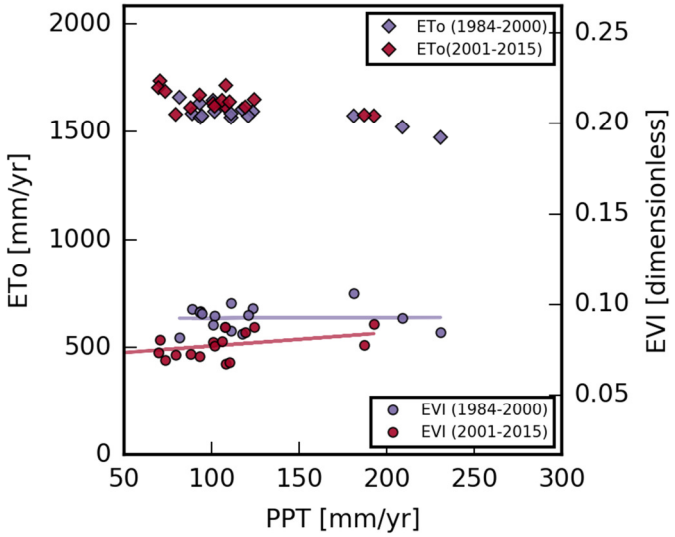

Figure 18: Fish Lake Valley polygon 3 complementary figure. Dramatic change in the slope of the best fit PPT-EVI scatter lines illustrates, once again, a distinct transition from ground water dependence to precipitation dependence.

8.6 San Emidio Desert

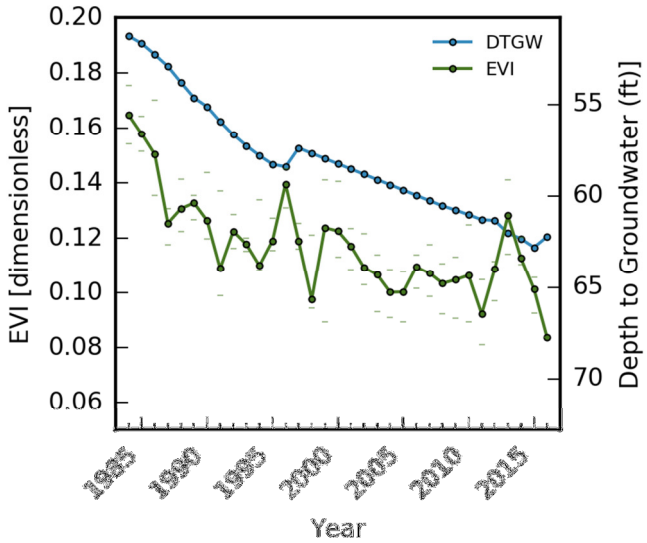

Figure 19: San Emidio Desert Paired 32-year time series of both EVI (green) and DTG (blue). Annual EVI maxima and minima are displayed as semi-transparent ticks above and below the median time series, respectively. The associated well is located 17 feet AMSL below the centroid of the area.

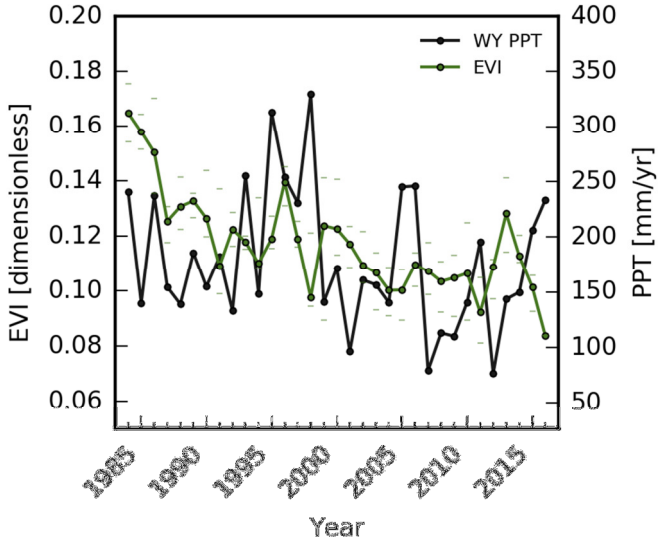

Figure 20: San Emidio Desert paired 32-year time series of both EVI (green) and water year precipitation (black).

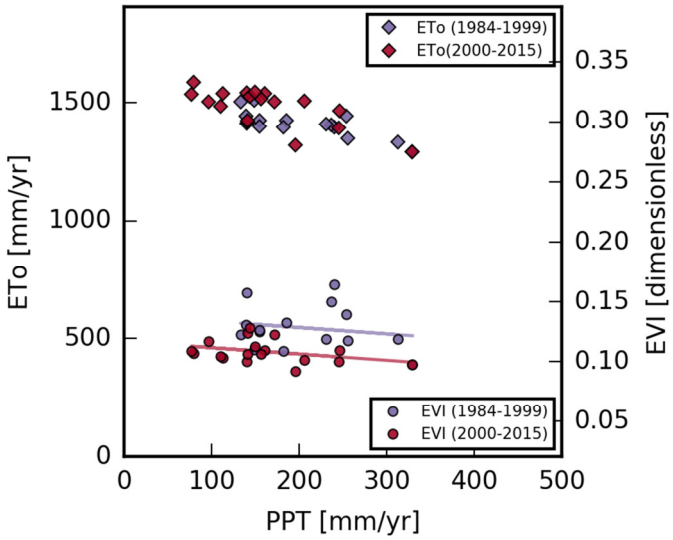

Figure 21: San Emidio Desert complementary figure. A nearly identical negative slope of the best-fit PPT-EVI lines indicates groundwater dependence maintained. Nonetheless, change in EVI magnitude (i.e. y-intercept of best-fit line) suggests lower overall groundwater utilization.

8.7 Boulder Flat

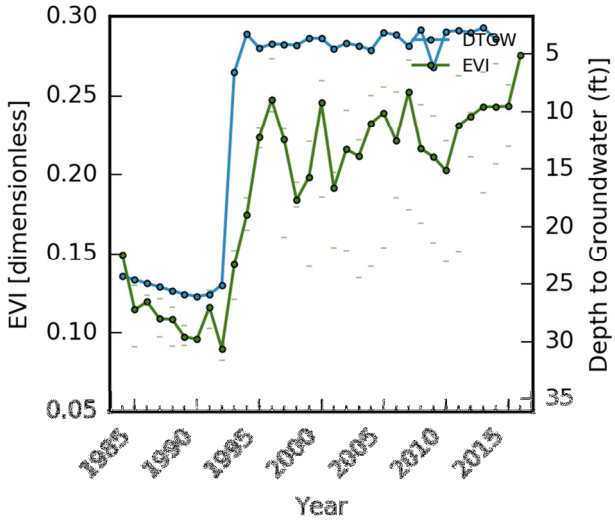

Figure 22: Boulder Flat paired 32-year time series of both EVI (green) and DT_G (blue). EVI closely tracks changes in DT_G throughout the record. Annual EVI maxima and minima are displayed as semi-transparent ticks above and below the median time series, respectively. The associated well is equal in elevation with the centroid of the discharge area.

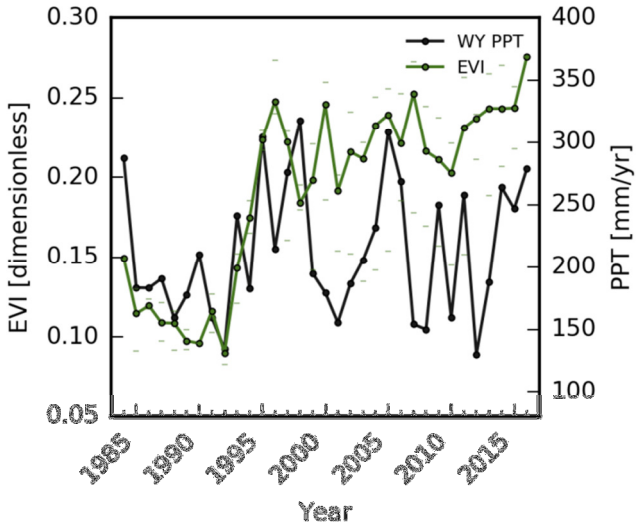

Figure 23: Boulder Flat paired 32-year time series of both EVI (green) and water year precipitation (black).

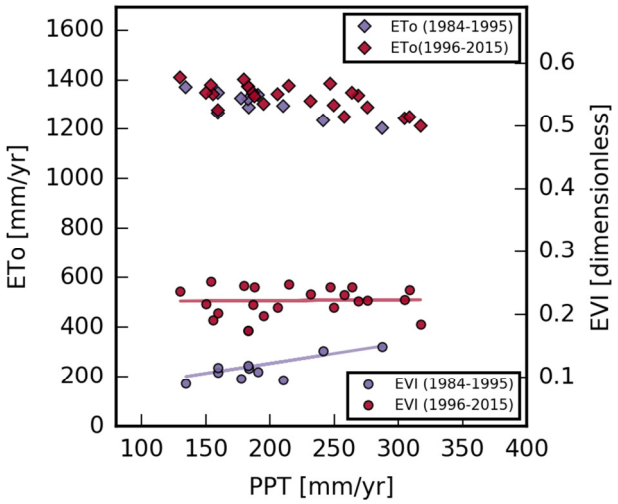

Figure 24: Boulder Flat complementary figure. Dramatic change in the slope of the best fit PPT-EVI scatter lines illustrates the polygons transition from precipitation dependence towards groundwater dependence, as well as the resulting marked increase in EVI.

8.8 Smith Valley polygon 1

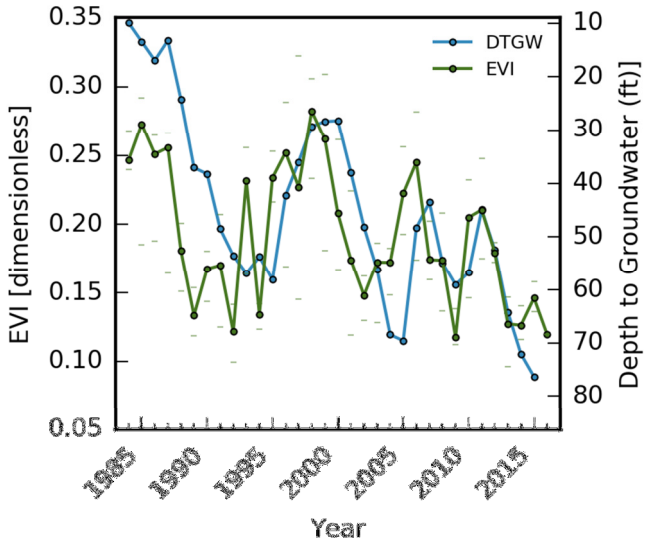

Figure 25: Smith Valley Polygon 1 paired 32-year time series of both EVI (green) and DT_G (blue). Annual EVI maxima and minima are displayed as semi-transparent ticks above and below the median time series, respectively. The associated well is located 66 feet AMSL above the centroid of the discharge area.

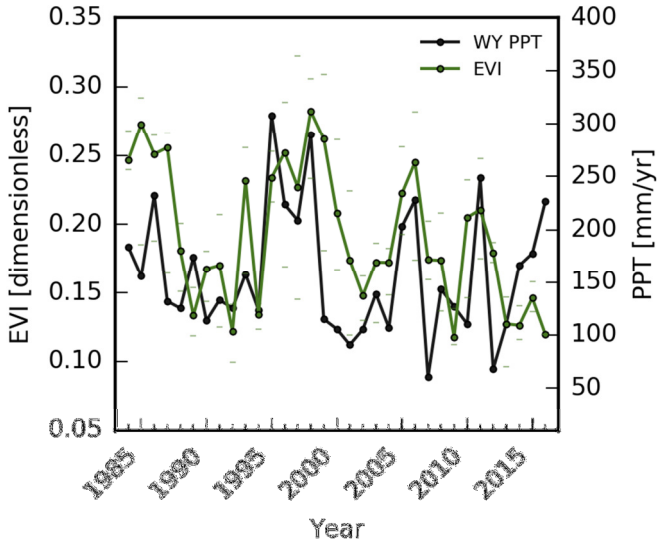

Figure 26: Smith Valley Polygon 1 paired 32-year time series of both EVI (green) and water year precipitation (black).

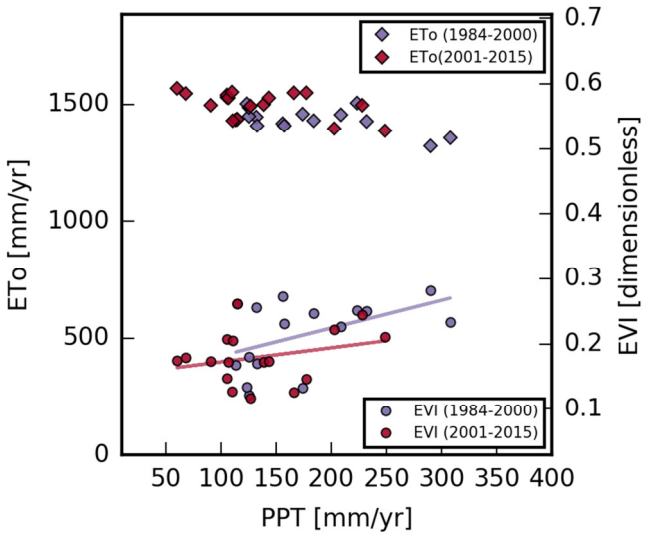

Figure 27: Smith Valley Polygon 1 complementary figure. Best-fit PPT-EVI lines indicate some form of PPT dependence. Nonetheless, change in EVI magnitude (i.e. y-intercept of best-fit line) suggests lower overall groundwater utilization in latter period.

8.9 Smith Valley polygon 2

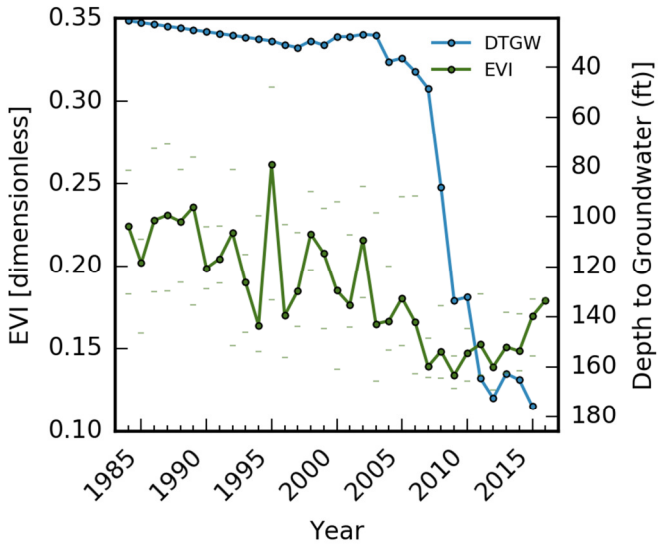

Figure 28: Smith Valley Polygon 1 paired 32-year time series of both EVI (green) and DT_G (blue). EVI impacted from ~1989 onward, much accelerated by accelerated DD ~2003. Annual EVI maxima and minima are displayed as semi-transparent ticks above and below the median time series, respectively. The associated well is located 200 feet AMSL above the centroid of the discharge area.

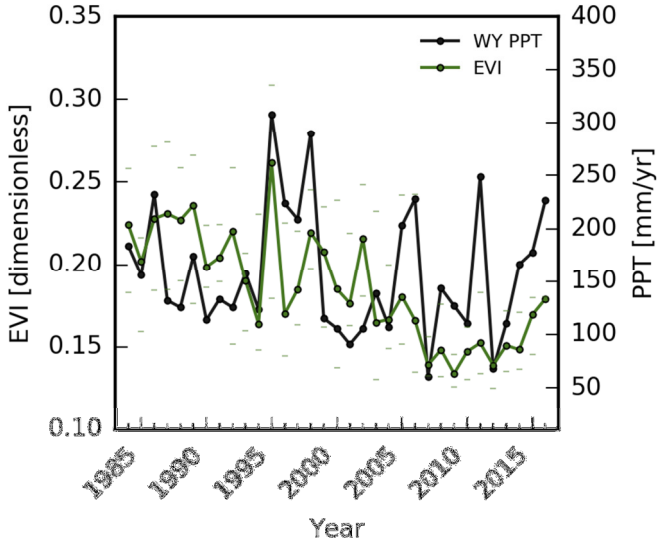

Figure 29: Smith Valley Polygon 2 paired 32-year time series of both EVI (green) and water year precipitation (black).

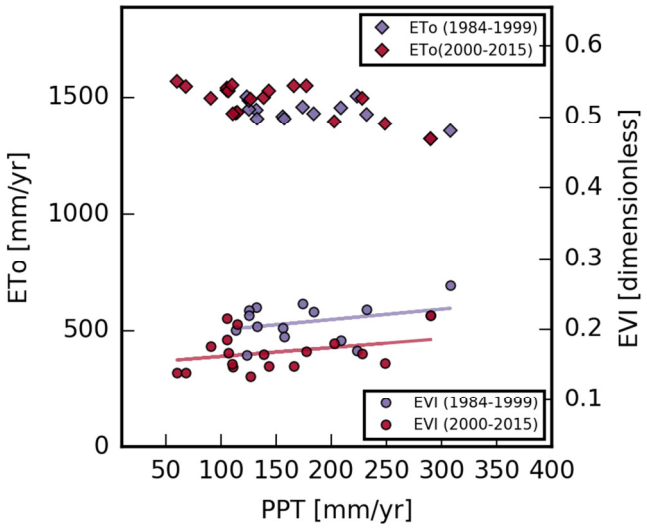

Figure 30:

Smith Valley Polygon 2 complementary figure. Practically unchanged best-fit PPT-EVI line slopes indicates some form of precipitation dependence present throughout record. Despite this, universally lower EVI values throughout the late period suggests lower overall groundwater utilization.

8.10 Field photographs

Figure 31: Dried up spring in Smith Valley. Bare soil occupies what was once a lush GDE. Impacted yet still functional GDEs occupy the area between the former spring and playa visible in the distance. Though a few individuals cling to life, widespread Greasewood and Rabbitbrush mortality is visible in the right-center of the image. Photo was taken at 2:35 pm on 8/26/16 along the southernmost edge of Smith Valley Polygon 1.

Figure 32: Impacted Greasewood-Rabbitbrush flat. Despite extensive water table drawdown, this community has yet to undergo succession to an alternative ecohydrological state. Photo taken along Northwestern edge of Smith Valley Polygon 2 at 2:13 pm 8/26/16.

Figure 33: Apparent Greasewood encroachment on playa. Historically greasewood establishment directly on the playa surface was precluded by periods of shallow groundwater, or even inundation in surface water, resulting in hypoxia and mortality. Consistently lowered groundwater levels more recently, however, have allowed for its establishment upon the margins previously occupied by saltgrass, and as seen here, even propagation onto the playa surface. Photo taken at 3:45 pm, 8/26/16.

Figure 34: Apparent Greasewood encroachment on playa. Historically greasewood establishment directly on the playa surface was precluded by periods of shallow groundwater, or even inundation in surface water, resulting in hypoxia and mortality. Consistently lowered groundwater levels more recently, however, have allowed for its establishment upon the margins previously occupied by saltgrass, and as seen here, even propagation onto the playa surface. Photo taken at 3:55 pm, 8/26/16.

Figure 35: A look back at the Alkali Lake State Wildlife Management Area entrance road. Decreasing groundwater dependence with increasing elevation/distance from playa margin is apparent as decrease in "greenness" of vegetation. Photo taken at 3:05 pm, 8/26/16.

Figure 36: Irrigated agriculture, Smith Valley, Nevada. One of many agriculturally active fields throughout the valley. Water for irrigation comes from both widespread diversion of the Walker River, and from extensive groundwater abstraction. Photo taken at 4:48 pm 8/26/16.

Figure 37: Irrigation ditch, Smith Valley, Nevada. One of many ditches used throughout the valley for widespread diversion of the Walker River for agricultural irrigation. Photo taken at 5:15pm 8/26/16.

Appendix A. Geometric Verification.

Background

To assess the influence the magnitude of a given polygon's area has on the resulting time series', five overlapping polygons of increasing size were drawn in Fish Lake Valley. These polygons were drawn with the aim of capturing only areas of similar EVI regression slope, such that, regardless of their size, each of these polygons might represent a region of common impact. The EVI-slope map of Fish Lake Valley created following a 32-year OLS regression of median summer EVI values (see section 4 for details) was used to guide this process and ensure the regions denoted and subsequently analyzed were indeed representative of regions of common impact. Five overlapping polygons were drawn in this fashion, and their resulting time series analyzed for trend and covariance.

Results

Median EVI values through time of all five of the polygons drawn in order to examine the impacts of polygon size on the resulting time series' are illustrated in figure 8. Despite their respective areas varying by in excess of an order of magnitude, similar Mann-Kendall trends, Sens slopes and relative strengths of correlation with respect to the various environmental variables considered, were observed for all five polygons. Polygons one, two, three, four, and five were found to be 0.081 km^2, 0.49 km^2, 2.7 km^2, and 4.1 km^2, respectively. Smaller polygons were observed to be more prone to drastic swings in EVI values resulting from environmental "noise" like precipitation, human activities and more. Conversely, though large polygons are less prone to sudden changes in EVI values, some aspect of temporal specificity may be lost, as GDE response throughout may not be entirely synchronized, due simply to the size of these larger polygons delaying the propagation environmental process. Due to the overall rather similar behavior of the various polygons, results presented in the following sections were obtained by drawing polygons limited primarily by past reports of species distributions and observations of uniform spatial areas of EVI trend obtained from EVI slope maps.

Across the board, the five geometric verification polygons were found to have decreasing Mann-Kendall EVI trends at the $0.001 > p$ confidence level. Summer PPT, wateryear PPT and summer TWD, however, weren't found to have significant trends in either direction for any of the polygons. Sen's slope estimates and Mann-Kendall test statistic (Z) values for polygons 1, 2, 3, 4 and 5 varied between -8.67×10^{-4} and -1.11×10^{-3}, and -5.11 and -5.77, respectively. Specific values for EVI and environmental trends across individual polygons considered in this portion of the analyses may be found in appendix D.

Across all five polygons EVI was found to have a strong, negative highly significant relationship ($1 \times 10^{-9} > p$) with DT_G, with Pearson's and Spearman's correlation coefficients varying from -0.83 to -0.86, and -0.85 to -0.85, respectively. Water Year precipitation, the next most closely correlated of the time series, were found to have statistically significant ($0.05 > p$) Pearson's coefficients varying between 0.37 and 0.41 for polygons 1-5, and even more significant ($0.01 > p$) and strong Spearman's correlation coefficients varying between 0.44 and 0.49. Specific values of both Pearson's and Spearman's correlation coefficients as well as their respective p-values for geometric verification polygons 1-5 can be found in appendix C.

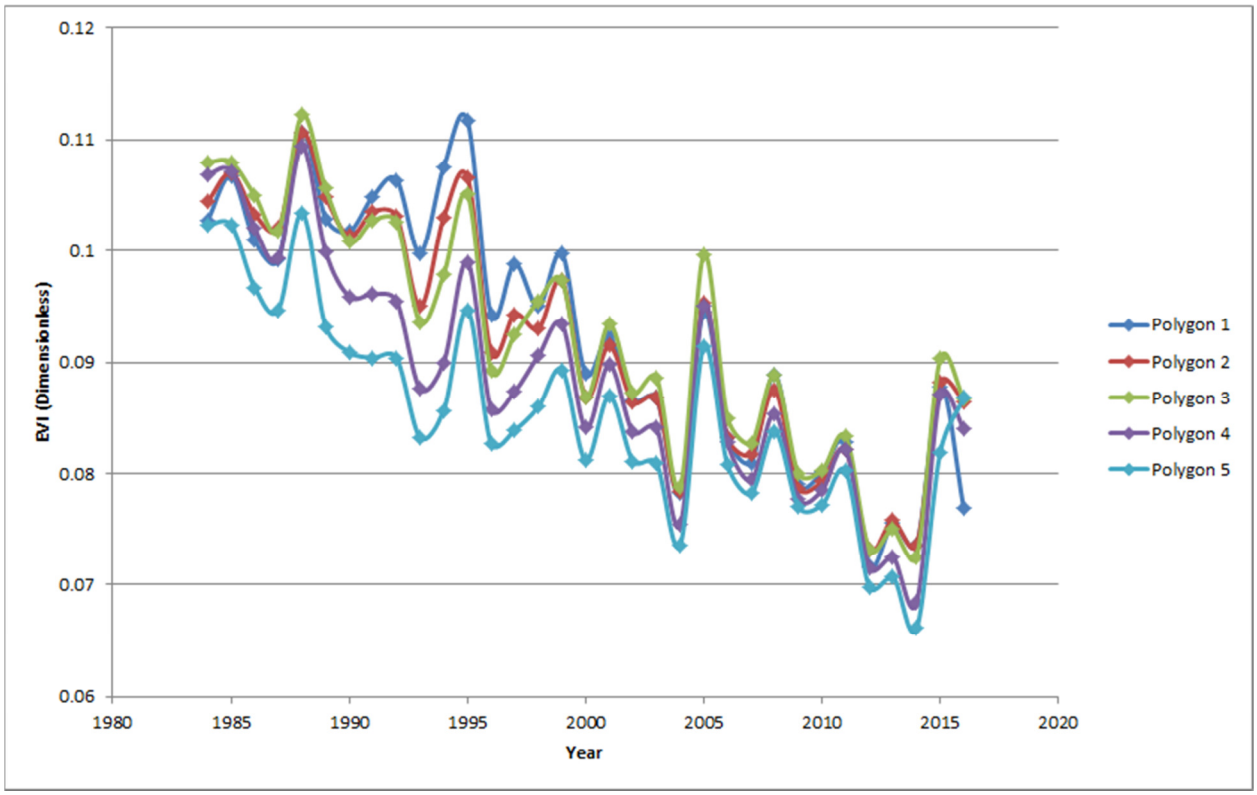

Figure 38: Geometric verification EVI time series for all 5 polygons considered.

Appendix B. Mesquite Valley

Study Site

Mesquite Valley splits the California-Nevada border, with somewhat more than half of the drainages total area of 374 mi^2 lying in Clark County, Nevada (CA DWR, 2004; NSE Summary, 2016). Mesquite Valley is considered hydrologically closed, with an alluvial drainage divide defining the Northern edge, and hydrophobic rock formations underlying the mountain ranges to the West, South and East. No data exist for the perennial yield of the california portion of mesquite valley, the Nevada perennial yield, however, is defined as being 1500 afy (Glancy, 1968). Precipitation throughout the drainage varies from 3 to 20 in $year^{-1}$ in a highly topographically stratified manner, with the highest elevations receiving the greatest totals Glancy, 1968). Depths to the phreatic surface vary throughout Mesquite Valley, with the greatest depths of roughly 130 ft below land surface being observed along the upper portions of alluvial fan, and with the shallowest region existing beneath the valley's playa at depths of less than 5 ft below land surface (Glancy, 1968). Historically, mesquite covered 6,400 acres of the valley at depths of 5-45 feet below land surface, saltbrush covered 6,000 acres at depths of 5-50 feet, and the valley's southerly located playa covered an additional 6,000 acres, and was underlain by water within 4-10 feet of the lands surface. The jointly published USGS and NSE recon report also identified additional 15,000 acres of "scrubby saltbrush of undetermined species" growing upgradient of playa, with DT_G ranging from 35 ft to 60 ft below land surface. Additional studies suggest this region may have been dominated by greasewood (U.S. Coast and Geodetic Survey, 1901; Waring, 1919). Groundwater discharge in hydrographically closed Mesquite valley occurs mainly through pumpage by wells or by evapotranspiration (Waring 1920; DWR 1964). Despite meager groundwater allocations on the Nevada side, significant groundwater abstraction for irrigated agriculture across the California portion of Mesquite Valley's floor combined with 30+ year records of continuously falling groundwater levels throughout basin suggest its overallocation.

Methods

Mesquite Valley represents a somewhat different scenario than either Fish Lake valley or San Emidio Desert, as the continuous and constant drawdown of groundwater throughout the basin is much more mild than the aforementioned basins, and may even be the result of competition within floral communities rather than a consequence of anthropogenic environmental alterations. As such, polygon 1 was drawn with the aim of isolating GDE vegetation of increasing vigor, through time. Whereas polygon 2 was drawn such that its extent captured GDE vegetation whose vigor had decreased through time. Two polygons were drawn for Mesquite Valley, their spatial extents lay entirely within GDE communities described by Glacy and Rush (1968).

See section 4 of main paper for more details on the procedures used.

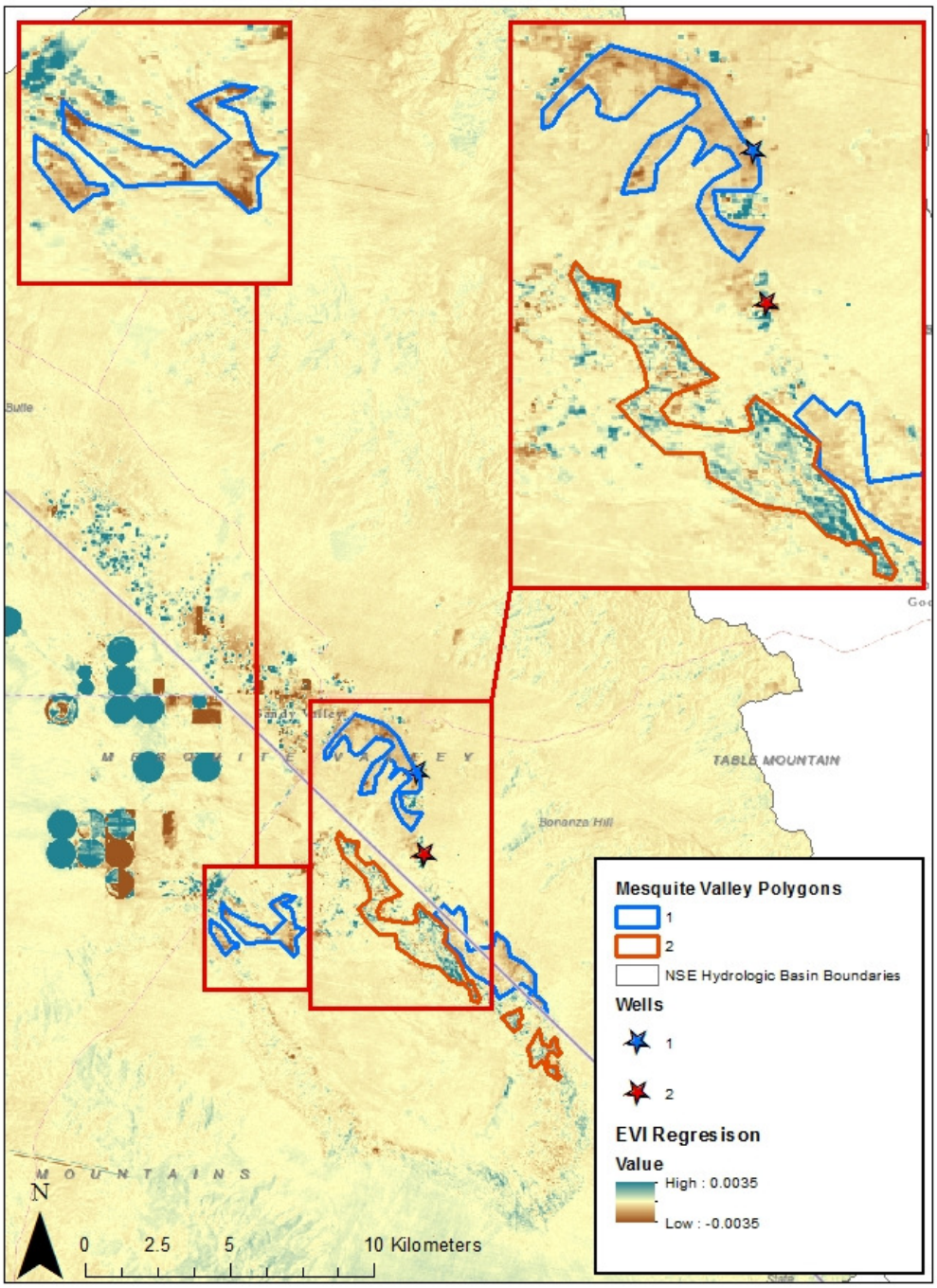

Figure 39: Mesquite Valley 32-year EVI regression slope map, with study polygons highlighted and detailed.

Results

Annual summer median EVI values, in combination with water year PPT and DT_G, are illustrated in figures B2 and B3 for Mesquite Valley polygon 1, and in figures B5, B6 for Mesquite Valley polygon 2. Mann-Kendall trend tests performed on median summer EVI time series for both polygon 1 and polygon 2 were found to be statistically significant at the 0.05 > p and 0.001 > p levels, and with Sen's slope estimates of -5.48×10^{-4} $year^{-1}$ and 1.12×10^{-3} $year^{-1}$, respectively. As the two polygons share a common well, the depth to groundwater time series for both polygons were identical and found to be increasing (i.e. greater depths) in a significant manner (0.001 > p) at a rate of 0.28 ft $year^{-1}$. Basin-wide water year PPT time series for these two polygons were similarly identical (as the two lie in the same basin), and found to be significantly (0.05 > p) decreasing at a rate of -3.33 mm $year^{-1}$. Mann-Kendall trend tests on summer PPT and TWD time series for both polygons 1 and 2 returned no significant trends. Additional information regarding both Sen's slope estimates and Mann-Kendall trend tests, including y-intercept, Z-statistic values, and more, may be found in appendix 3.

Once again, as has been the case for every preceding impacted basin examined, correlation coefficient analyses of both Mesquite Valley polygons suggest DT_G is the variable with the greatest influence over GDE vegetation vigor in the basin. Polygon 1's EVI-DT_G relationship was characterized by moderately strong, negative, statistically significant (0.01 > p) Pearson and Spearman correlation coefficients of -0.55 and -0.46. Polygon 2 boasted much more significant (1×10^{-5} > p) correlations between EVI and DT_G, with strong, positive Pearson's and Spearman's coefficients of 0.72, and 0.74, respectively. The EVI time series of polygon 2 was observed to have no statistically significant correlations with any environmental variable other than DT_G. Polygon 1's EVI time series, however, was found covary in a statistically significant manner (0.005 > p) with water year PPT, with moderately strong, positive Pearson and Spearman's correlation coefficients of 0.51 and 0.52, respectively.

Qualitative examination of polygon 1's EVI time series reveals a close association of DT_G and EVI for the first half or so of the 32-year record, followed in roughly 2004 by an apparent functional transition and loss of this association--not unlike was the case with Fish Lake Valley polygon 2. In light of this observation, correlation statistics for polygon 1 were ran for the period from 1984-2004, in addition to the full record. This limited time window returned more strongly negative and similarly statistically significant (0.005 > p) relationships, despite the unavoidable detrimental impact the shortening of a record has on the p-value returned by both Pearson's and Spearman's correlation coefficients. Pearson's correlation coefficient was found to be -0.63, and Spearman's -0.64, for this shortened record.

Figures B4 and B7 illustrate the quantitative relationship shared by ET and ET_o for Mesquite Valley polygons 1, and 2. In both cases, the slope of the best fit line has increased from the historic (1984-1993) to the recent (1994-2015) periods, indicating a functional shift in the ecosystems comprising these polygons from being almost entirely groundwater dependant to significantly more dependant upon water year PPT totals. Where the complementary relationship changes over time between these two polygons do differ, however, is in the resulting average EVI. For polygon 1 EVI has experienced a marked decrease with this shift to PPT dependance. Conversely, the species occupying polygon 2 appear to have benefitted from decreasing groundwater levels and dependence, as EVI is nearly universally higher in the more recent, PPT dependant, time period.

Mesquite Valley polygon 1

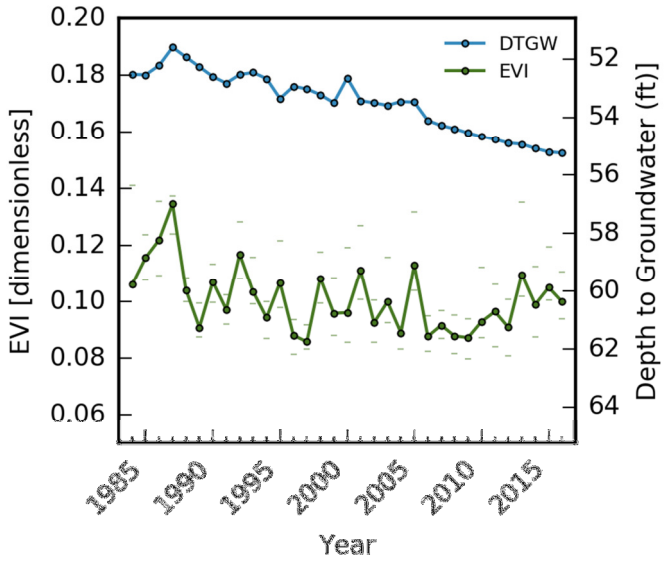

Figure 40: Paired 32-year time series of both EVI (green) and DTG (blue) for Mesquite valley polygon 1.

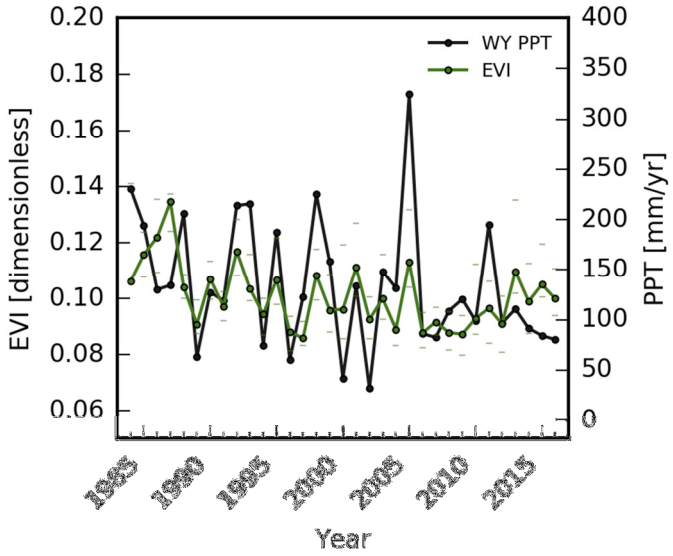

Figure 41: Mesquite valley polygon 1 paired 32-year time series of both EVI (green) and water year precipitation (black).

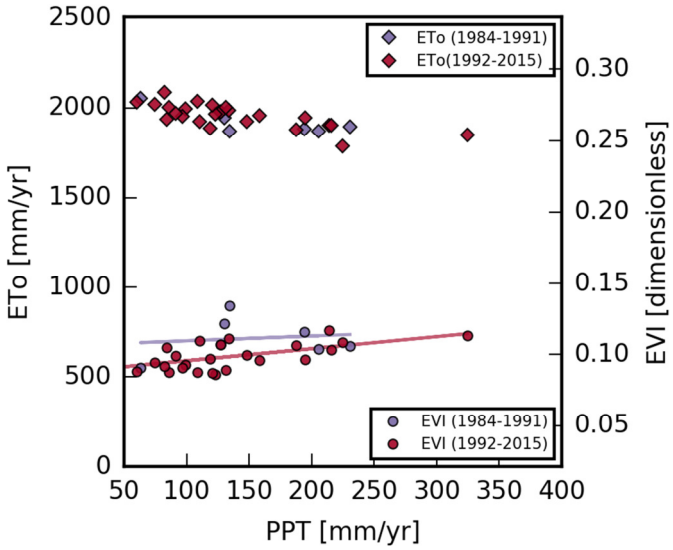

Figure 42: Mesquite Valley polygon 1 complementary figure. Change in the slope of the best fit PPT-EVI scatter lines from near zero to distinctly positive illustrates the ecosystems transition away from ground water dependence and towards greater PPT dependence. Moreover, lower EVI values indicate a drastic drop in primary productivity.

Mesquite Valley Polygon 2

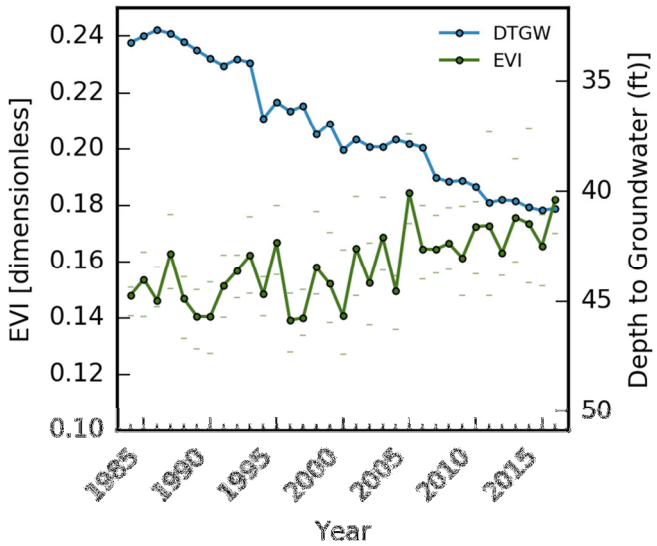

Figure 43: Paired 32-year time series of both EVI (green) and DTG (blue) for Mesquite Valley polygon 2. EVI appears to share an inverse relationship with DTG, indicating increasing DTG likely results in competitive advantage for individuals of this community.

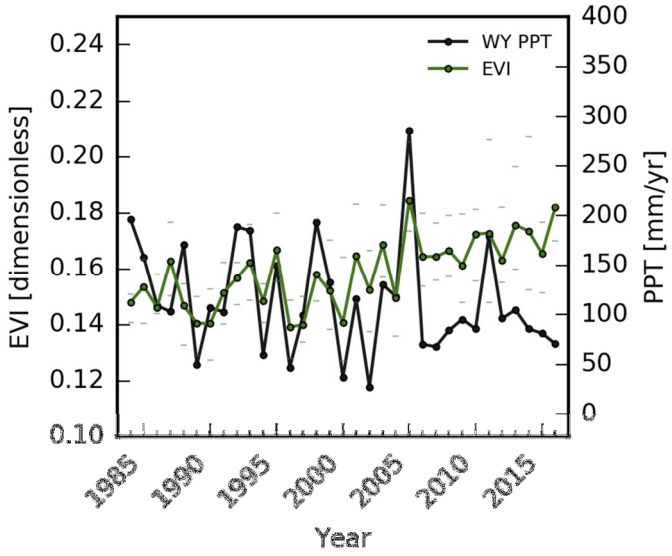

Figure 44: Mesquite Valley polygon 2 paired 32-year time series of both EVI (green) and water year precipitation (black).

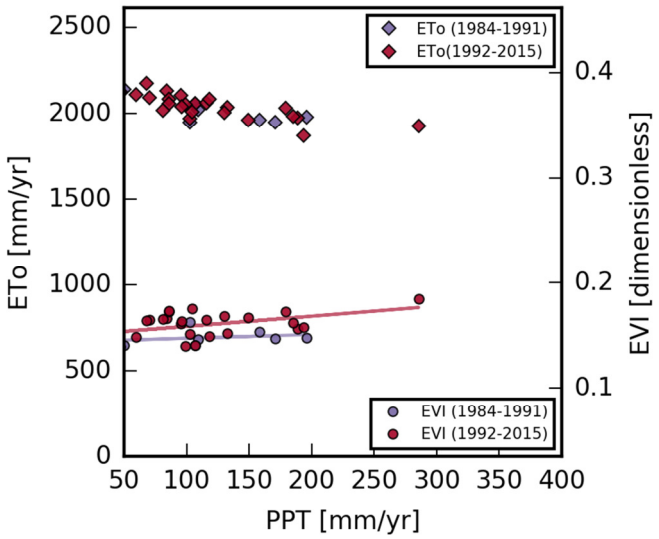

Figure 45: Mesquite Valley polygon 2 complementary figure. Change in the slope of the best fit PPT-EVI scatter lines from near zero to distinctly positive illustrates the ecosystems transition away from ground water dependence and towards greater PPT dependence.

Discussion and Conclusions

Omitted due to the omission of this section from the main report body.

Appendix C. Correlation Coefficient results, including insignificant and otherwise unreported values.

Fish Lake Valley Geometric Verification							
		Pearson's Correlation Coefficent		Spearman's Correlation Coefficent		Kendalls Tau A	
Polygon 1		R	p-value	Rho	p-value	Tau	p-value
	DTGW	-0.83	3.45E-09	-0.86	3.11E-10	-0.66	1.32E-07
	Summer Precip	-0.01	0.953	-0.07	0.723	-0.04	0.721
	Water Year Precip	0.40	0.025	0.44	0.011	0.30	0.015
	Theoretical Water Def	0.11	0.560	0.18	0.337	0.12	0.347
		Pearson's Correlation Coefficent		Spearman's Correlation Coefficent		Kendalls Tau A	
Polygon 2		R	p-value			R	p-value
	DTGW	-0.86	1.78E-10	-0.87	1.12E-10	-0.68	3.74E-08
	Summer Precip	0.05	0.778	0.01	0.963	-0.01	0.948
	Water Year Precip	0.37	0.039	0.45	0.009	0.31	0.014
	Theoretical Water Def	0.14	0.454	0.23	0.197	0.15	0.218
		Pearson's Correlation Coefficent		Spearman's Correlation Coefficent		Kendalls Tau A	
Polygon 3		R	p-value			R	p-value
	DTGW	-0.86	4.16E-10	-0.86	1.73E-10	-0.69	3.30E-08
	Summer Precip	0.10	0.577	0.03	0.887	0.01	0.961
	Water Year Precip	0.41	0.019	0.47	0.006	0.31	0.012
	Theoretical Water Def	0.16	0.378	0.25	0.173	0.16	0.200
		Pearson's Correlation Coefficent		Spearman's Correlation Coefficent		Kendalls Tau A	
Polygon 4		R	p-value			R	p-value
	DTGW	-0.86	2.42E-10	-0.87	9.45E-11	-0.70	1.56E-08
	Summer Precip	0.16	0.392	0.02	0.914	-0.01	0.961
	Water Year Precip	0.40	0.022	0.46	0.008	0.30	0.016
	Theoretical Water Def	0.18	0.317	0.25	0.175	0.15	0.223
		Pearson's Correlation Coefficent		Spearman's Correlation Coefficent		Kendalls Tau A	
Polygon 5		R	p-value			R	p-value
	DTGW	-0.85	5.87E-10	-0.85	1.05E-09	-0.69	3.10E-08

	Summer Precip	0.16	0.380	0.01	0.946	-0.01	0.935
	Water Year Precip	0.41	0.020	0.49	0.004	0.33	0.007
	Theoretical Water Def	0.14	0.441	0.20	0.267	0.13	0.290

Boulder Flat

		Pearson's Correlation Coefficent		Spearman's Correlation Coefficent		Kendalls Tau A	
		R	p-value	Rho	p-value	Tau	p-value
Polygon 1	DTGW	-0.91	1.15E-12	-0.71	7.38E-06	-0.53	3.30E-05
	Summer Precip	0.00	0.996	-0.15	0.425	-0.11	0.376
	Water Year Precip	0.12	0.509	0.15	0.417	0.09	0.496
	Theoretical Water Def	-0.10	0.598	-0.17	0.351	-0.10	0.434

Fish Lake Valley

		Pearson's Correlation Coefficent		Spearman's Correlation Coefficent		Kendalls Tau A	
		R	p-value	Rho	p-value	Tau	p-value
Polygon 1	DTGW	-0.87	1.15E-10	-0.88	3.24E-11	-0.71	1.00E-08
	Summer Precip	0.18	0.327	0.05	0.767	0.04	0.758
	Water Year Precip	0.20	0.261	0.30	0.090	0.20	0.101
	Theoretical Water Def	0.26	0.154	0.28	0.116	0.18	0.140
Polygon 2	Full Record	Pearson's Correlation Coefficent		Spearman's Correlation Coefficent		Kendalls Tau A	
	(1984-2015)	R	p-value	Rho	p-value	Tau	p-value
	DTGW	-0.75	6.05E-07	-0.68	1.84E-05	-0.53	1.69E-05
	Summer Precip	0.38	0.032	0.02	0.930	0.01	0.935
	Water Year Precip	0.36	0.041	0.53	0.002	0.37	0.003
	Theoretical Water Def	0.30	0.101	0.18	0.318	0.14	0.263
Polygon 2		Pearson's Correlation Coefficent		Spearman's Correlation Coefficent		Kendalls Tau A	
	(1984-1999)	R	p-value	Rho	p-value	Tau	p-value
	DTGW	-0.78	3.90E-04	-0.64	7.80E-03	-0.47	1.17E-02
	Summer Precip	0.59	0.015	0.25	0.350	0.18	0.322
	Water Year Precip	0.10	0.715	0.16	0.542	0.10	0.589
	Theoretical Water Def	0.52	0.037	0.25	0.356	0.18	0.322
		Pearson's Correlation Coefficent		Spearman's Correlation Coefficent		Kendalls Tau A	

Polygon 2	(2000-2015)	R	p-value			R	p-value
	DTGW	-0.13	0.62	-0.18	0.52	-0.16	0.39
	Summer Precip	-0.39	0.139	-0.41	0.117	-0.28	0.136
	Water Year Precip	0.59	1.68E-02	0.67	4.67E-03	0.53	4.40E-03
	Theoretical Water Def	-0.34	0.191	-0.43	9.42E-02	-0.28	0.136
		Pearson's Correlation Coefficent		Spearman's Correlation Coefficent		Kendalls Tau A	
Polygon 3		R	p-value			R	p-value
	DTGW	-0.74	1.49E-06	-0.81	2.13E-08	-0.65	2.00E-07
	Summer Precip	0.09	0.610	-0.01	0.938	-0.03	0.820
	Water Year Precip	0.35	0.050	0.40	0.023	0.26	0.035
	Theoretical Water Def	0.23	0.202	0.27	0.130	0.17	0.163

San Emidio Valley

Polygon 1		Pearson's Correlation Coefficent		Spearman's Correlation Coefficent		Kendalls Tau A	
		R	p-value	Rho	p-value	Tau	p-value
	DTGW	-0.76	5.69E-07	-0.65	6.21E-05	-0.49	7.60E-05
	Summer Precip	0.11	0.540	0.25	0.169	0.19	0.136
	Water Year Precip	0.13	0.487	0.14	0.437	0.08	0.517
	Theoretical Water Def	0.18	0.337	0.30	0.100	0.19	0.127

Sandy (Mesquite) Valley

Polygon 1		Pearson's Correlation Coefficent		Spearman's Correlation Coefficent		Kendalls Tau A	
	(1984-2015)	R	p-value	Rho	p-value	Tau	p-value
	DTGW	-0.55	1.10E-03	-0.46	7.95E-03	-0.33	8.61E-03
	Summer Precip	0.13	0.483	0.09	0.618	0.06	0.650
	Water Year Precip	0.51	3.13E-03	0.52	2.50E-03	0.32	1.04E-02
	Theoretical Water Def	0.27	0.128	0.32	0.076	0.18	0.144
Polygon 2		Pearson's Correlation Coefficent		Spearman's Correlation Coefficent		Kendalls Tau A	
	(1984-2015)	R	p-value	Rho	p-value	Tau	p-value
	DTGW	0.72	3.38E-06	0.74	1.36E-06	0.56	5.61E-06
	Summer Precip	0.01	0.946	0.14	0.443	0.12	0.347
	Water Year Precip	0.05	0.792	0.01	0.944	0.02	0.897

	Theoretical Water Def	0.29	0.108	0.28	0.118	0.19	0.120
Polygon 1		Pearson's Correlation Coefficent		Spearman's Correlation Coefficent		Kendalls Tau A	
	(1984-2004)	R	p-value	Rho	p-value	Tau	p-value
	DTGW	-0.63	1.63E-03	-0.64	1.31E-03	-0.48	1.75E-03
	Summer Precip	0.13	0.578	0.23	0.311	0.13	0.414
	Water Year Precip	0.53	1.17E-02	0.57	5.64E-03	0.37	1.65E-02
	Theoretical Water Def	0.26	0.234	0.31	0.159	0.17	0.271
Polygon 2		Pearson's Correlation Coefficent		Spearman's Correlation Coefficent		Kendalls Tau A	
	(1984-2004)	R	p-value	Rho	p-value	Tau	p-value
	DTGW	0.37	9.023E-02	0.33	1.318E-01	0.26	8.542E-02
	Summer Precip	0.01	0.964	0.09	0.684	0.09	0.554
	Water Year Precip	0.53	0.012	0.53	0.012	0.42	0.006
	Theoretical Water Def	0.07	0.760	0.19	0.399	0.13	0.382

Smith Valley

Polygon 1		Pearson's Correlation Coefficent		Spearman's Correlation Coefficent		Kendalls Tau A	
		R	p-value	Rho	p-value	Tau	p-value
	DTGW	-0.66	4.46E-05	-0.78	1.09E-07	-0.58	2.71E-06
	Summer Precip	0.29	0.105	0.29	0.102	0.20	0.108
	Water Year Precip	0.37	3.69E-02	0.32	7.68E-02	0.23	6.66E-02
	Theoretical Water Def	0.34	5.40E-02	0.42	1.64E-02	0.28	2.62E-02
Polygon 2		Pearson's Correlation Coefficent		Spearman's Correlation Coefficent		Kendalls Tau A	
		R	p-value	Rho	p-value	Tau	p-value
	DTGW	-0.59	3.53E-04	-0.58	5.30E-04	-0.39	1.85E-03
	Summer Precip	0.14	0.435	0.01	0.967	0.00	0.974
	Water Year Precip	0.59	3.92E-04	0.50	3.48E-03	0.33	8.61E-03
	Theoretical Water Def	0.16	0.383	0.15	0.415	0.13	0.299

Spring Valley

Polygon 1		Pearson's Correlation Coefficent		Spearman's Correlation Coefficent		Kendalls Tau A	
		R	p-value	Rho	p-value	Tau	p-value
	DTGW	0.35	6.92E-02	0.32	0.102	0.23	9.18E-02
	Summer Precip	0.38	4.90E-02	0.18	0.353	0.13	0.332

	Water Year Precip	0.73	9.35E-06	0.72	1.59E-05	0.53	7.00E-05
	Theoretical Water Def	0.41	3.13E-02	0.32	9.78E-02	0.26	5.50E-02

Appendix D. Mann-Kendall trend test results. Full results including Mann-Kendall test statistics, significance levels, series information and Sen's slope and y-intercept estimates.

Geometrtic Verification All polys (1984-2015)							
	Series Details			Mann-Kendall		Sen's slope estimate	
Time Series Name	First year	Last Year	n	Test Z	Signific.	Q	B
Polygon Summer PPT	1984	2015	32	0.02	N/A	5.36E-03	20.61
Basin-Wide WY PPT	1984	2015	32	-1.51	N/A	-1.24	187.94
Summer TWD (PPT-Eto)	1984	2015	32	-1.18	N/A	-0.67	-608.99
Median Summer EVI Polygon 1	1984	2015	32	-5.11	0.001 > p	-1.11E-03	0.11
Median Summer EVI Polygon 2	1984	2015	32	-5.66	0.001 > p	-1.10E-03	0.11
Median Summer EVI Polygon 3	1984	2015	32	-5.64	0.001 > p	-1.09E-03	0.11
Median Summer EVI Polygon 4	1984	2015	32	-5.77	0.001 > p	-1.04E-03	0.10
Median Summer EVI Polygon 5	1984	2015	32	-5.61	0.001 > p	-8.67E-04	0.10
Depth to Groundwater (ft/year)	1984	2015	32	7.85	0.001 > p	0.53	18.48
Depth to Groundwater (ft/year)	1984	2015	32	7.51	0.001 > p	1.75	26.46
Boulder Flat Polygon1 (1984-2015)							
	Series Details			Mann-Kendall		Sen's slope estimate	
Time Series Name	First year	Last Year	n	Test Z	Signific.	Q	B
Mean Summer EVI	1984	2015	32	4.49	0.001 > p	4.34E-03	0.11
Median Summer EVI	1984	2015	32	4.35	0.001 > p	4.56E-03	0.11
Minimum Summer EVI	1984	2015	32	3.67	0.001 > p	3.14E-03	0.10
Maximum Summer EVI	1984	2015	32	4.56	0.001 > p	5.11E-03	0.12
Polygon Annual ETo	1984	2015	32	1.70	0.1 > p	1.34	1307.70
Polygon WY PPT	1984	2015	32	0.34	N/A	0.37	189.32
Depth to Groundwater	1984	2014	31	-4.18	0.001 > p	-0.26	9.84
Polygon Summer PPT	1984	2015	32	0.60	N/A	0.23	19.55
Basin-Wide WY PPT	1984	2015	32	-0.47	N/A	-0.65	223.59
Summer TWD (PPT-Eto)	1984	2015	32	0.08	N/A	0.11	-575.53
FishLake Polygon1 (1984-2015)							
	Series Details			Mann-Kendall		Sen's slope estimate	
Time Series Name	First year	Last Year	n	Test Z	Signific.	Q	B
Mean Summer EVI	1984	2015	32	-5.95	0.001 > p	-6.25E-03	0.29
Median Summer EVI	1984	2015	32	-5.74	0.001 > p	-6.42E-03	0.30
Minimum Summer EVI	1984	2015	32	-5.82	0.001 > p	-4.28E-03	0.22
Maximum Summer EVI	1984	2015	32	-5.59	0.001 > p	-7.60E-03	0.35
Polygon Annual ETo	1984	2015	32	2.81	0.01 > p	2.56	1571.14

Polygon WY PPT	1984	2015	32	-0.47	N/A	-0.24	109.00
Depth to Groundwater	1984	2015	32	7.67	0.001 > p	0.49	4.78
Polygon Summer PPT	1984	2015	32	0.02	N/A	5.36E-03	20.61
Basin-Wide WY PPT	1984	2015	32	-1.51	N/A	-1.24	187.94
Summer TWD (PPT-Eto)	1984	2015	32	-1.18	N/A	-0.67	-608.99
FishLake Polygon 2 (1984-2015)							
	Series Details			**Mann-Kendall**		**Sen's slope estimate**	
Time Series Name	**First year**	**Last Year**	**n**	**Test Z**	**Signific.**	**Q**	**B**
Mean Summer EVI	1984	2015	32	-4.25	0.001 > p	-5.42E-04	0.07
Median Summer EVI	1984	2015	32	-4.64	0.001 > p	-6.00E-04	0.07
Minimum Summer EVI	1984	2015	32	-4.62	0.001 > p	-6.23E-04	0.06
Maximum Summer EVI	1984	2015	32	-1.88	0.1 > p	-3.75E-04	0.07
Polygon Annual ETo	1984	2015	32	2.71	0.01 > p	2.49	1523.58
Polygon WY PPT	1984	2015	32	-0.44	N/A	-0.17	108.31
Depth to Groundwater	1984	2015	32	7.51	0.001 > p	1.75	26.46
Polygon Summer PPT	1984	2015	32	0.02	N/A	5.36E-03	20.61
Basin-Wide WY PPT	1984	2015	32	-1.51	N/A	-1.24	187.94
Summer TWD (PPT-Eto)	1984	2015	32	-1.18	N/A	-0.67	-608.99
FishLake Polygon 3 (1984-2015)							
	Series Details			**Mann-Kendall**		**Sen's slope estimate**	
Time Series Name	**First year**	**Last Year**	**n**	**Test Z**	**Signific.**	**Q**	**B**
Mean Summer EVI	**1984**	**2015**	**32**	**-5.95**	**0.001 > p**	**-1.03E-03**	**0.10**
Median Summer EVI	1984	2015	32	-5.82	0.001 > p	-1.04E-03	0.10
Minimum Summer EVI	1984	2015	32	-5.74	0.001 > p	-9.19E-04	0.09
Maximum Summer EVI	1984	2015	32	-4.75	0.001 > p	-9.54E-04	0.11
Polygon Annual ETo	1984	2015	32	2.81	0.01 > p	2.56	1571.14
Polygon WY PPT	1984	2015	32	-0.47	N/A	-0.24	109.00
Depth to Groundwater	1984	2015	32	6.60	0.001 > p	0.90	57.70
Polygon Summer PPT	1984	2015	32	0.02	N/A	5.36E-03	20.61
Basin-Wide WY PPT	1984	2015	32	-1.51	N/A	-1.24	187.94
Summer TWD (PPT-Eto)	1984	2015	32	-1.18	N/A	-0.67	-608.99
Sandy Valley Polygon1 (1984-2015)							
	Series Details			**Mann-Kendall**		**Sen's slope estimate**	
Time Series Name	**First year**	**Last Year**	**n**	**Test Z**	**Signific.**	**Q**	**B**
Mean Summer EVI	1984	2015	32	-2.56	0.05 > p	-6.06E-04	0.11
Median Summer EVI	1984	2015	32	-2.48	0.05 > p	-5.48E-04	0.11
Minimum Summer EVI	1984	2015	32	-3.19	0.01 > p	-6.79E-04	0.10
Maximum Summer EVI	1984	2015	32	-2.03	0.05 > p	-5.90E-04	0.12
Polygon Annual ETo	1984	2015	32	1.57	N/A	2.45	1913.53
Polygon WY PPT	1984	2015	32	-2.03	0.05 > p	-2.47	170.16

Depth to Groundwater	1984	2015	32	7.18	0.001 > p	0.28	32.47
Polygon Summer PPT	1984	2015	32	0.02	N/A	1.72E-02	24.84
Basin-Wide WY PPT	1984	2015	32	-2.12	0.05 > p	-3.33	249.00
Summer TWD (PPT-Eto)	1984	2015	32	0.50	N/A	0.70	-737.86
SandyValley Polygon 2 (1984-2015)							
	Series Details			**Mann-Kendall**		**Sen's slope estimate**	
Time Series Name	**First year**	**Last Year**	**n**	**Test Z**	**Signific.**	**Q**	**B**
Mean Summer EVI	1984	2015	32	4.59	0.001 > p	1.12E-03	0.13
Median Summer EVI	1984	2015	32	4.72	0.001 > p	1.12E-03	0.13
Minimum Summer EVI	1984	2015	32	3.84	0.001 > p	8.13E-04	0.12
Maximum Summer EVI	1984	2015	32	4.49	0.001 > p	1.48E-03	0.13
Polygon Annual ETo	1984	2015	32	1.57	N/A	2.45	1913.53
Polygon WY PPT	1984	2015	32	-2.03	0.05 > p	-2.47	170.16
Depth to Groundwater	1984	2015	32	7.18	0.001 > p	0.28	32.47
Polygon Summer PPT	1984	2015	32	0.02	N/A	1.72E-02	24.84
Basin-Wide WY PPT	1984	2015	32	-2.12	0.05 > p	-3.33	249.00
Summer TWD (PPT-Eto)	1984	2015	32	0.50	N/A	0.70	-737.86
San Emidio Desert 1 (1984-2015)							
	Series Details			**Mann-Kendall**		**Sen's slope estimate**	
Time Series Name	**First year**	**Last Year**	**n**	**Test Z**	**Signific.**	**Q**	**B**
Mean Summer EVI	1984	2015	32	-4.56	0.001 > p	-1.27E-03	0.14
Median Summer EVI	1984	2015	32	-4.23	0.001 > p	-1.18E-03	0.13
Minimum Summer EVI	1984	2015	32	-4.70	0.001 > p	-1.47E-03	0.13
Maximum Summer EVI	1984	2015	32	-4.64	0.001 > p	-1.33E-03	0.15
Polygon Annual ETo	1984	2015	32	2.77	0.01 > p	3.87	1402.31
Polygon WY PPT	1984	2015	32	-1.28	N/A	-1.42	185.52
Depth to Groundwater	1984	2015	32	7.70	0.001 > p	0.29	53.58
Depth to Groundwater	1984	2015	32	7.28	0.001 > p	0.31	53.43
Polygon Summer PPT	1984	2015	32	-1.77	0.1 > p	-0.43	21.55
Basin-Wide WY PPT	1984	2015	32	-1.57	N/A	-1.95	244.31
Summer TWD (PPT-Eto)	1984	2015	32	-2.12	0.05 > p	-1.58	-607.65
Smith Valley 1 (1984-2015)							
	Series Details			**Mann-Kendall**		**Sen's slope estimate**	
Time Series Name	**First year**	**Last Year**	**n**	**Test Z**	**Signific.**	**Q**	**B**
Mean Summer EVI	1984	2015	32	-4.91	0.001 > p	-2.69E-03	0.23
Median Summer EVI	1984	2015	32	-4.80	0.001 > p	-2.82E-03	0.23
Minimum Summer EVI	1984	2015	32	-4.17	0.001 > p	-1.75E-03	0.18
Maximum Summer EVI	1984	2015	32	-3.88	0.001 > p	-3.06E-03	0.26
Polygon Annual ETo	1984	2015	32	3.06	0.01 > p	3.89	1429.22
Polygon WY PPT	1984	2015	32	-1.12	N/A	-1.22	157.44
Depth to Groundwater	1984	2015	32	6.60	0.001 > p	1.36	17.08

Polygon Summer PPT	1984	2015	32	-1.22	N/A	-0.34	20.64
Basin-Wide WY PPT	1984	2015	32	-0.83	N/A	-1.22	259.60
Summer TWD (PPT-Eto)	1984	2015	32	-1.77	0.1 > p	-0.99	-572.02
Smith Valley 2 (1984-2015)							
	Series Details			**Mann-Kendall**		**Sen's slope estimate**	
Time Series Name	**First year**	**Last Year**	**n**	**Test Z**	**Signific.**	**Q**	**B**
Mean Summer EVI	1984	2015	32	-1.96	0.05 > p	-2.00E-03	0.23
Median Summer EVI	1984	2015	32	-2.09	0.05 > p	-2.00E-03	0.23
Minimum Summer EVI	1984	2015	32	-1.51	N/A	-1.00E-03	0.17
Maximum Summer EVI	1984	2015	32	-1.93	0.1 > p	-2.00E-03	0.26
Polygon Annual ETo	1984	2015	32	3.00	0.01 > p	3.65	1417.41
Polygon WY PPT	1984	2015	32	-1.28	N/A	-1.42	156.23
Depth to Groundwater	1984	2015	32	4.30	0.001 > p	1.46	20.85
Polygon Summer PPT	1984	2015	32	-1.22	N/A	-0.34	20.64
Basin-Wide WY PPT	1984	2015	32	-0.83	N/A	-1.22	259.60
Summer TWD (PPT-Eto)	1984	2015	32	-1.77	0.1 > p	-0.99	-572.02
Spring Valley 1 (1984-2015)							
	Series Details			**Mann-Kendall**		**Sen's slope estimate**	
Time Series Name	**First year**	**Last Year**	**n**	**Test Z**	**Signific.**	**Q**	**B**
Mean Summer EVI	1984	2015	32	0.06	N/A	1.68E-05	0.11
Median Summer EVI	1984	2015	32	0.23	N/A	4.45E-05	0.11
Minimum Summer EVI	1984	2015	32	-0.24	N/A	-2.50E-05	0.10
Maximum Summer EVI	1984	2015	32	0.62	N/A	1.86E-04	0.12
Polygon Annual ETo	1984	2015	32	1.15	N/A	1.63	1421.31
Polygon WY PPT	1984	2015	32	-1.35	N/A	-1.59	247.69
Depth to Groundwater	1984	2011	28	3.10	0.01 > p	0.07	36.67
Polygon Summer PPT	1984	2015	32	-0.08	N/A	-0.06	45.01
Basin-Wide WY PPT	1984	2015	32	-1.31	N/A	-1.56	313.91
Summer TWD (PPT-Eto)	1984	2015	32	0.28	N/A	0.46	-568.79

Appendix E. Well location and details. Information provided includes associated polygon, data source, and the website URL where the data was accessed.

Latitude	Longitude	Name	Source	Website URL
39.06475	-114.516	Spring Valley	USGS	http://nwis.waterdata.usgs.gov/nwis/gwlevels/?site_no=390352114305401&agency_cd=USGS&amp
40.85377	-116.416	Boulder Flat	NSE	http://water.nv.gov/data/waterlevel/site.cfm?ID=2441
38.86545	-119.399	Smith Valley Polygon 1	NSE	http://water.nv.gov/data/waterlevel/site.cfm?ID=968
38.96222	-119.385	Smith Valley Polygon 2	NSE	http://water.nv.gov/data/waterlevel/site.cfm?ID=973
37.76009	-118.032	Fish Lake Valley Polygon 1	NSE/USGS	http://water.nv.gov/data/waterlevel/site.cfm?ID=1284
37.62809	-117.9	Fish Lake	NSE	http://water.nv.gov/data/waterlevel/site.cfm?ID=1298

	98	Valley Polygon 2		
37.7095	-118.085	Fish Lake Valley Polygon 3	NSE	http://water.nv.gov/data/waterlevel/site.cfm?ID=1295
40.44522	-119.427	San Emidio Desert Polygon	NSE/USGS	http://water.nv.gov/data/waterlevel/site.cfm?ID=295
35.79	-115.586	Mesquite Valley Polygon 1	NSE	http://water.nv.gov/data/waterlevel/site.cfm?ID=1311
35.76915	-115.584	Mesquite Valley Polygon 2	NSE	http://water.nv.gov/data/waterlevel/site.cfm?ID=1313

References cited

Allander, K. K., J. Smith, M. J. Johnson, and R. Pattison (2006), Evapotranspiration (ET) in the Lower Walker River Basin, West-Central Nevada, *Nevada Water Resources Association 2006 Annual Conference. Mesquite, NV. February*, *23*.

Anderies, J. M. (2005), Minimal models and agroecological policy at the regional scale: an application to salinity problems in southeastern Australia, *Regional Environmental Change*, *5*(1), 1-17.

Asbjornsen, H., G. R. Goldsmith, M. S. Alvarado-Barrientos, K. Rebel, F. P. Van Osch, M. Rietkerk, J. Chen, S. Gotsch, C. Tobon, and D. R. Geissert (2011), Ecohydrological advances and applications in plant–water relations research: a review, *Journal of Plant Ecology*, *4*(1-2), 3-22.

ASCE-EWRI (2005), The ASCE standardized reference evapotranspiration equation: ASCE-EWRI Standardization of Reference Evapotranspiration Task Committe Report, ASCE Reston.

Authority, S. N. W. (2011), Spring Valley Hydrologic Monitoring, Management, and Mitigation Plan Status and Data 165 pp.

Bai, J., and P. Perron (1998), Estimating and testing linear models with multiple structural changes, *Econometrica*, 47-78.

Bai, J., and P. Perron (2003), Computation and analysis of multiple structural change models, *Journal of applied econometrics*, *18*(1), 1-22.

Barron, O. V., I. Emelyanova, T. G. Van Niel, D. Pollock, and G. Hodgson (2014), Mapping groundwater-dependent ecosystems using remote sensing measures of vegetation and moisture dynamics, *Hydrological Processes*, *28*(2), 372-385.

Beamer, J. P., J. L. Huntington, C. G. Morton, and G. M. Pohll (2013), Estimating Annual Groundwater Evapotranspiration from Phreatophytes in the Great Basin Using Landsat and Flux Tower Measurements, *Journal of the American Water Resources Association*, *49*(3), 518-533.

Berger, D. L. (2000), Water budget estimates for the 14 hydrographic areas in the middle Humboldt River basin, north-central Nevada, US Geological Survey.

Blaney, H., C. Taylor, H. Nickle, and A. Young (1933), Water loses under natural conditions from wet areas in southern California (Division Water Resources Bulletin 44, 176 p.), *California: Department of Public Works*.

Bredehoeft, J. D. (2002), The water budget myth revisited: why hydrogeologists model, *Ground Water*, *40*(4), 340-345.

Bredehoeft, J. D., S. S. Papadopulos, and H. Cooper (1982), Groundwater: the water budget myth, *Scientific Basis of Water Resource Management*, *51*, 57.

Brutsaert, W., and H. Stricker (1979), An advection-aridity approach to estimate actual regional evapotranspiration, *Water resources research*, *15*(2), 443-450.

Burk, N. I., C. E. Bishop, and M. Lowe (2005), *Wetlands in Tooele Valley, Utah: An Evaluation of Threats Posed by Ground-water Development and Drought*, Utah Geological Survey.

Byrne, R., C. Busby, and R. Heizer (1979), The Altithermal revisited: pollen evidence from the Leonard Rockshelter, *Journal of California and Great Basin Anthropology*, *1*(2), 280-294.

Carroll, R. W. H., G. M. Pohll, C. G. Morton, and J. L. Huntington (2015), Calibrating a Basin-Scale Groundwater Model to Remotely Sensed Estimates of Groundwater Evapotranspiration, *Journal of the American Water Resources Association*, *51*(4), 1114-1127.

Chambers, J. C., and Rocky Mountain Research Station (Fort Collins Colo.) (2011), *Geomorphology, hydrology, and ecology of Great Basin meadow complexes : implications for management and restoration*, iii, 125 pages pp., U.S. Dept. of Agriculture, Forest Service, Rocky Mountain Research Station, Fort Collins, CO.

Chapin, F. S., et al. (2000), Consequences of changing biodiversity, *Nature*, *405*(6783), 234-242.

Chok, N. S. (2010), Pearson's versus Spearman's and Kendall's correlation coefficients for continuous data, University of Pittsburgh.

Cohen, J. (1988), Statistical power analysis for the behavior science, *Lawrance Eribaum Association*.

Cooper, D. J., D. R. D'amico, and M. L. Scott (2003), Physiological and morphological response patterns of Populus deltoides to alluvial groundwater pumping, *Environmental Management*, *31*(2), 0215-0226.

Cooper, D. J., J. S. Sanderson, D. I. Stannard, and D. P. Groeneveld (2006), Effects of long-term water table drawdown on evapotranspiration and vegetation in an arid region phreatophyte community, *Journal of Hydrology*, *325*(1-4), 21-34.

Davis, S. D., F. W. Ewers, J. S. Sperry, K. A. Portwood, M. C. Crocker, and G. C. Adams (2002), Shoot dieback during prolonged drought in Ceanothus (Rhamnaceae) chaparral of California: a possible case of hydraulic failure, *American Journal of Botany*, *89*(5), 820-828.

Deacon, J. E., A. E. Williams, C. D. Williams, and J. E. Williams (2007), Fueling population growth in Las Vegas: How large-scale groundwater withdrawal could burn regional biodiversity, *Bioscience*, *57*(8), 688-698.

DeMeo, G. A., J. Smith, N. A. Damar, and J. Darnell (2008), Quantifying ground-water and surface-water discharge from evapotranspiration processes in 12 hydrographic areas of the Colorado regional ground-water flow system, Nevada, Utah, and Arizona, U. S. Geological Survey.

Devitt, D., and B. Bird (2015), Changes in groundwater oscillations, soil water content and evapotranspiration as the water table declined in an area with deep rooted phreatophytes, *Ecohydrology*.

Devitt, D. A., L. F. Fenstermaker, M. H. Young, B. Conrad, M. Baghzouz, and B. M. Bird (2011), Evapotranspiration of mixed shrub communities in phreatophytic zones of the Great Basin region of Nevada (USA), *Ecohydrology*, *4*(6), 807-822.

Dilts, T. E., P. J. Weisberg, C. M. Dencker, and J. C. Chambers (2015), Functionally relevant climate variables for arid lands: a climatic water deficit approach for modelling desert shrub distributions, *Journal of Biogeography*, *42*(10), 1986-1997.

Donovan, L. A., J. H. Richards, and M. W. Muller (1996), Water relations and leaf chemistry of Chrysothamnus nauseosus ssp. consimilis (Asteraceae) and Sarcobatus vermiculatus (Chenopodiaceae), *American Journal of Botany*, 1637-1646.

Eamus, D., and R. Froend (2006), Groundwater-dependent ecosystems: the where, what and why of GDEs, *Australian Journal of Botany*, *54*(2), 91-96.

Eamus, D., R. Froend, R. Loomes, G. Hose, and B. Murray (2006), A functional methodology for determining the groundwater regime needed to maintain the health of groundwater-dependent vegetation, *Australian Journal of Botany*, *54*(2), 97-114.

Eamus, D., S. Zolfaghar, R. Villalobos-Vega, J. Cleverly, and A. Huete (2015), Groundwater-dependent ecosystems: recent insights, new techniques and an ecosystem-scale threshold response, *Hydrol. Earth Syst. Sci. Discuss*, *12*(5), 4677-4754.

Eaton, G. P. (1982), The Basin and Range province: Origin and tectonic significance, *Annual Review of Earth and Planetary Sciences*, *10*, 409.

Elmore, A., J. Kaste, G. Okin, and M. Fantle (2008), Groundwater influences on atmospheric dust generation in deserts, *Journal of Arid Environments*, *72*(10), 1753-1765.

Elmore, A. J., J. F. Mustard, and S. J. Manning (2003), Regional patterns of plant community response to changes in water: Owens Valley, California, *Ecological Applications*, *13*(2), 443-460.

Elmore, A. J., J. F. Mustard, S. J. Manning, and D. B. Lobell (2000), Quantifying vegetation change in semiarid environments: precision and accuracy of spectral mixture analysis and the normalized difference vegetation index, *Remote sensing of environment*, *73*(1), 87-102.

Elmore, A. J., S. J. Manning, J. F. Mustard, and J. M. Craine (2006), Decline in alkali meadow vegetation cover in California: the effects of groundwater extraction and drought, *Journal of Applied Ecology*, *43*(4), 770-779.

Elvidge, C. D., and R. J. P. Lyon (1985), INFLUENCE OF ROCK SOIL SPECTRAL VARIATION ON THE ASSESSMENT OF GREEN BIOMASS, *Remote Sensing of Environment*, *17*(3), 265-279.

Engineer, N. S., edited.

Engineer, T. O. o. t. N. S. (1988), Ruling no. 3569, in *IN THE MATTER OF APPLICATIONS 51773, 51774, 51775, 51816, 51881, 51882 and 51929 FILED TO APPROPRIATE WATER FROM THE SAN EMIDIO DESERT GROUNDWATER BASIN, WASHOE COUNTY, NEVADA.*, edited, Nevada State Enineer, water.nv.gov.

Fenneman, N. M. (1928), Physiographic divisions of the United States, *Annals of the Association of American Geographers*, *18*(4), 261-353.

Fenneman, N. M. (1966), Physiography of the western United States.

Fernandez-Illescas, C. P., A. Porporato, F. Laio, and I. Rodriguez-Iturbe (2001), The ecohydrological role of soil texture in a water-limited ecosystem, *Water Resources Research*, *37*(12), 2863-2872.

Froend, R., and B. Sommer (2010), Phreatophytic vegetation response to climatic and abstraction-induced groundwater drawdown: Examples of long-term spatial and temporal variability in community response, *Ecological Engineering*, *36*(9), 1191-1200.

Garcia, C. A., J. M. Huntington, S. G. Buto, M. T. Moreo, J. L. Smith, and B. J. Andraski (2014), Groundwater discharge by evapotranspiration, Dixie Valley, west-central Nevada, March 2009-September 2011*Rep. 2330-7102*, US Geological Survey.

Gatewood, J. S., T. Robinson, B. Colby, J. Hem, and L. Halpenny (1950), Use of water by bottom-land vegetation in lower Safford Valley, Arizona, *US Geological Survey Water-Supply Paper*, *1103*, 210.

Gitelson, A. A., and M. N. Merzlyak (1997), Remote estimation of chlorophyll content in higher plant leaves, *International Journal of Remote Sensing*, *18*(12), 2691-2697.

Gitelson, A. A., Y. Peng, and K. F. Huemmrich (2014), Relationship between fraction of radiation absorbed by photosynthesizing maize and soybean canopies and NDVI from remotely sensed data taken at close range and from MODIS 250m resolution data, *Remote Sensing of Environment*, *147*, 108-120.

Glancy, P. A., and R. EUGENE (1968), Water-Resources Appraisal of Smoke Creek-San Emidio Desert Area, Nevada and California.

Glazer, A. N., and G. E. Likens (2012), The Water Table: The Shifting Foundation of Life on Land, *Ambio*, *41*(7), 657-669.

Glenn, E. P., P. L. Nagler, and A. R. Huete (2010), Vegetation index methods for estimating evapotranspiration by remote sensing, *Surveys in Geophysics*, *31*(6), 531-555.

Groeneveld, D. P. (2008), Remotely-sensed groundwater evapotranspiration from alkali scrub affected by declining water table, *Journal of hydrology*, *358*(3), 294-303.

Groeneveld, D. P., W. M. Baugh, J. S. Sanderson, and D. J. Cooper (2007), Annual groundwater evapotranspiration mapped from single satellite scenes, *Journal of Hydrology*, *344*(1), 146-156.

Hacke, U. G., J. S. Sperry, and J. Pittermann (2000), Drought experience and cavitation resistance in six shrubs from the Great Basin, Utah, *Basic and Applied Ecology*, *1*(1), 31-41.

Harrill, J. R., J. S. Gates, and J. M. Thomas (1988), Major ground-water flow systems in the Great Basin region of Nevada, Utah, and adjacent states.

Harrill, J. R., D. E. Prudic, and Geological Survey (U.S.) (1998), *Aquifer systems in the Great Basin region of Nevada, Utah, and adjacent states : summary report*, vi, 66 pages pp., U.S. G.P.O. ;

For sale by U.S. Geological Survey, Branch of Information Services, Washington

Denver, CO.

Harrill, J. R., A. Welch, D. Prudic, J. Thomas, R. Carman, R. Plume, J. Gates, and J. Mason (1983), Aquifer systems in the Great Basin region of Nevada, Utah, and adjacent states; a study plan*Rep. 2331-1258*, US Geological Survey.

Harrington, R., A. Steinwand, P. Hubbard, D. Martin, J. Stroh, and D. Or (2003), Evapotranspiration from groundwater dependent plant communities: comparison of micrometeorological and vegetation-based measurements, *Draft Cooperative Study Progress Report prepared by the County of Inyo Water Department and Los Angeles Department of Water and Power. 79pp. and appendices*.

Hershey, R. L., V. M. Heilweil, P. Gardner, B. F. Lyles, S. Earman, J. M. Thomas, and K. W. Lundmark (2007), *Ground-water chemistry interpretations supporting the Basin and Range Regional Carbonate-rock Aquifer System (BARCAS) Study, eastern Nevada and western Utah*, Desert Research Institute.

Hinsby, K., M. T. C. de Melo, and M. Dahl (2008), European case studies supporting the derivation of natural background levels and groundwater threshold values for the protection of dependent ecosystems and human health, *Science of the Total Environment*, *401*(1), 1-20.

Hobbins, M. T., J. A. Ramírez, and T. C. Brown (2004), Trends in pan evaporation and actual evapotranspiration across the conterminous US: Paradoxical or complementary?, *Geophysical Research Letters*, *31*(13).

Homer, C. G., R. D. Ramsey, T. C. Edwards, and A. Falconer (1997), Landscape cover-type modeling using a multi-scene thematic mapper mosaic, *Photogrammetric Engineering and Remote Sensing*, *63*(1), 59-67.

Homer, C. G., G. Xian, C. L. Aldridge, D. K. Meyer, T. R. Loveland, and M. S. O'Donnell (2015), Forecasting sagebrush ecosystem components and greater sage-grouse habitat for 2050: Learning from past climate patterns and Landsat imagery to predict the future, *Ecological Indicators*, *55*, 131-145.

Horton, G. A., and Nevada. Division of Water Planning. (1998), *Water words dictionary*, Eighth edition. ed., 2 volumes pp., Division of Water Planning, Carson City, Nev.

Horton, J. L., T. E. Kolb, and S. C. Hart (2001), Physiological response to groundwater depth varies among species and with river flow regulation, *Ecological Applications*, *11*(4), 1046-1059.

Huntington, J., K. McGwire, C. Morton, K. Snyder, S. Peterson, T. Erickson, R. Niswonger, R. Carroll, G. Smith, and R. Allen (2016), Assessing the role of climate and resource management on groundwater dependent ecosystem changes in arid environments with the Landsat archive, *Remote Sensing of Environment*.

Huntington, J. L., J. Szilagyi, S. W. Tyler, and G. M. Pohll (2011), Evaluating the complementary relationship for estimating evapotranspiration from arid shrublands, *Water Resources Research*, *47*(5).

Huntington, J. L., C. G. Morton, M. Bromley, R. Liebert, and K. Paudel (2014), Landsat Evapotranspiration from
Phreatophyte and Irrigated Areas,
Boulder Flat, Humboldt River Basin,
Nevada, Prepared for
Barrick Gold Corporation.

Irish, R. R. (2000), Landsat 7 automatic cloud cover assessment, paper presented at AeroSense 2000, International Society for Optics and Photonics.

Jackson, R. B., E. G. Jobbágy, and M. D. Nosetto (2009), Ecohydrology in a human-dominated landscape, *Ecohydrology*, *2*(3), 383-389.

Jaksa, W. T., V. Sridhar, J. L. Huntington, and M. Khanal (2013), Evaluation of the complementary relationship using Noah Land Surface Model and North American Regional Reanalysis (NARR) data to estimate evapotranspiration in semiarid ecosystems, *Journal of Hydrometeorology*, *14*(1), 345-359.

Klove, B., et al. (2011), Groundwater dependent ecosystems. Part I: Hydroecological status and trends, *Environmental Science & Policy*, *14*(7), 770-781.

Laymon, C., D. Quattrochi, E. Malek, L. Hipps, J. Boettinger, and G. McCurdy (1998), Remotely-sensed regional-scale evapotranspiration of a semi-arid Great Basin desert and its relationship to geomorphology, soils, and vegetation, *Geomorphology*, *21*(3-4), 329-349.

Le Maitre, D. C., D. F. Scott, and C. Colvin (1999), Review of information on interactions between vegetation and groundwater.

Leffler, A. J., L. E. England, and J. Naito (2000), Vulnerability of Fremont cottonwood (Populus fremontii Wats.) individuals to xylem cavitation, *Western North American Naturalist*, 204-210.

Loeltz, O. J., and T. E. Eakin (1953), *Geology and Water Resources of Smith Valley, Lyon and Douglas Counties, Nevada*, US Government Printing Office.

Mann, H. B. (1945), Nonparametric tests against trend, *Econometrica: Journal of the Econometric Society*, 245-259.

Manning, S. J. (1998), The effects of water table decline on groundwater-dependent Great Basin plant communities in the Owens Valley, California, paper presented at McArthur, E. Durant; Ostler, W. Kent; Wambolt, Carl L., comps. Proceedings: shrubland ecotones.

Mathie, A. M., T. L. Welborn, D. D. Susong, and M. L. Tumbusch (2011), *Phreatophytic Land-Cover Map of the Northern and Central Great Basin Ecoregion: California, Idaho, Nevada, Utah, Oregon, and Wyoming*, US Department of the Interior, US Geological Survey.

Maurer, D. K. (2006), *Rates of evapotranspiration, recharge from precipitation beneath selected areas of native vegetation, and streamflow gain and loss in Carson Valley, Douglas County, Nevada, and Alpine County, California*, US Department of the Interior, US Geological Survey.

McLendon, T., P. J. Hubbard, and D. W. Martin (2008), Partitioning the use of precipitation- and groundwater-derived moisture by vegetation in an arid ecosystem in California, *Journal of Arid Environments*, *72*(6), 986-1001.

Mensing, S., J. Smith, K. B. Norman, and M. Allan (2008), Extended drought in the Great Basin of western North America in the last two millennia reconstructed from pollen records, *Quaternary International*, *188*(1), 79-89.

Mensing, S. A. (2001), Late-glacial and early Holocene vegetation and climate change near Owens Lake, eastern California, *Quaternary Research*, *55*(1), 57-65.

Mensing, S. A., L. V. Benson, M. Kashgarian, and S. Lund (2004), A Holocene pollen record of persistent droughts from Pyramid Lake, Nevada, USA, *Quaternary Research*, *62*(1), 29-38.

Mitchell, K. E., D. Lohmann, P. R. Houser, E. F. Wood, J. C. Schaake, A. Robock, B. A. Cosgrove, J. Sheffield, Q. Duan, and L. Luo (2004), The multi-institution North American Land Data Assimilation System (NLDAS): Utilizing multiple GCIP products and partners in a continental distributed hydrological modeling system, *Journal of Geophysical Research: Atmospheres*, *109*(D7).

Moreo, M. T., R. J. Laczniak, and D. I. Stannard (2007), *Evapotranspiration Rate Measurements of Vegetation Typical of Ground-Water Discharge Areas in the Basin and Range Carbonate-Rock Aquifer System, White Pine County, Nevada, and Adjacent Areas in Nevada and Utah, September 2005-August 2006*, US Geological Survey.

Munch, Z., and J. Conrad (2007), Remote sensing and GIS based determination of groundwater dependent ecosystems in the Western Cape, South Africa, *Hydrogeology Journal*, *15*(1), 19-28.

Murray, B. R., G. C. Hose, D. Eamus, and D. Licari (2006), Valuation of groundwater-dependent ecosystems: a functional methodology incorporating ecosystem services, *Australian Journal of Botany*, *54*(2), 221-229.

Naumburg, E., R. Mata-Gonzalez, R. G. Hunter, T. McLendon, and D. W. Martin (2005), Phreatophytic vegetation and groundwater fluctuations: A review of current research and application of ecosystem response modeling with an emphasis on Great Basin vegetation, *Environmental Management*, *35*(6), 726-740.

Nguyen, U., E. P. Glenn, P. L. Nagler, and R. L. Scott (2015), Long-term decrease in satellite vegetation indices in response to environmental variables in an iconic desert riparian ecosystem: the Upper San Pedro, Arizona, United States, *Ecohydrology*, *8*(4), 610-625.

Nichols, W. D. (1993), ESTIMATING DISCHARGE OF SHALLOW GROUNDWATER BY TRANSPIRATION FROM GREASEWOOD IN THE NORTHERN GREAT-BASIN, *Water Resources Research*, *29*(8), 2771-2778.

Nichols, W. D. (1994), GROUNDWATER DISCHARGE BY PHREATOPHYTE SHRUBS IN THE GREAT-BASIN AS RELATED TO DEPTH TO GROUNDWATER, *Water Resources Research*, *30*(12), 3265-3274.

Nichols, W. D. (2000), *Regional ground-water evapotranspiration and ground-water budgets, Great Basin, Nevada*.

Orellana, F., P. Verma, S. P. Loheide, and E. Daly (2012), Monitoring and modeling water-vegetation interactions in groundwater-dependent ecosystems, *Reviews of Geophysics*, *50*(3).

Patten, D. T., L. Rouse, and J. C. Stromberg (2008), Isolated spring wetlands in the Great Basin and Mojave Deserts, USA: potential response of vegetation to groundwater withdrawal, *Environmental Management*, *41*(3), 398-413.

Plume, R. W. (2005), *Changes in ground-water levels in the Carlin Trend area, north-central Nevada, 1989-2003*, US Department of the Interior, US Geological Survey.

Plume, R. W., and D. A. Ponce (1999), Hydrogeologic framework and ground-water levels, 1982 and 1996, middle Humboldt River basin, north-central Nevada.

Price, K. P., D. A. Pyke, and L. Mendes (1992), Shrub dieback in a semiarid ecosystem: the integration of remote sensing and geographic information systems for detecting vegetation change, *Photogrammetric Engineering and Remote Sensing*, *58*(4), 455-463.

Pringle, C. M. (2000), Threats to US public lands from cumulative hydrologic alterations outside of their boundaries, *Ecological Applications*, *10*(4), 971-989.

Pringle, C. M. (2001), Hydrologic connectivity and the management of biological reserves: A global perspective, *Ecological Applications*, *11*(4), 981-998.

Pritchett, D., and S. J. Manning (2012), Response of an intermountain groundwater-dependent ecosystem to water table drawdown, *Western North American Naturalist*, *72*(1), 48-59.

Reiner, S. R., R. J. Laczniak, G. A. DeMeo, J. L. Smith, P. E. Elliott, W. E. Nylund, and C. J. Fridrich (2002), Ground-water discharge determined from measurements of evapotranspiration, other available hydrologic components, and shallow water-level changes, Oasis Valley, Nye County, Nevada, United States Geological Survey-Nevada, Las Vegas, NV (US).

Resources, N. D. o. W. (2016a), Boulder Flat Hydrographic Area Summary, edited by N. S. E. s. Office, http://water.nv.gov/data/underground/printableSummary.cfm?basin=061.

Resources, N. D. o. W. (2016b), Spring Valley Hydrographic Area Summary, edited by N. S. E. s. Office, http://water.nv.gov/data/underground/printableSummary.cfm?basin=184.

Resources, N. D. o. W. (2016c), Smith Valley Hydrographic Area Summary, edited by N. S. E. s. Office, http://water.nv.gov/data/underground/printableSummary.cfm?basin=107.

Resources, N. D. o. W. (2016d), San Emidio Desert Hydrographic Area Summary, edited by N. S. E. s. Office, http://water.nv.gov/data/underground/printableSummary.cfm?basin=022.

Resources, N. D. o. W. (2016e), Fish Lake Valley Hydrographic Area Summary, edited, http://water.nv.gov/data/underground/printableSummary.cfm?basin=117.

Ridolfi, L., P. D'Odorico, and F. Laio (2006), Effect of vegetation-water table feedbacks on the stability and resilience of plant ecosystems, *Water Resources Research*, *42*(1).

Ridolfi, L., P. D'Odorico, and F. Laio (2006), Effect of vegetation–water table feedbacks on the stability and resilience of plant ecosystems, *Water Resources Research*, *42*(1).

Ridolfi, L., P. D'Odorico, and F. Laio (2007), Vegetation dynamics induced by phreatophyte–aquifer interactions, *Journal of theoretical biology*, *248*(2), 301-310.

Robertson, J. H. (1983), Greasewood (Sarcobatus vermiculatus (Hook.) Torr.), *Phytologia*, *54*(5), 309-324.

Robinson, T. W. (1958), *Phreatophytes*, US Government Printing Office.

Robinson, T. W., and A. O. Waananen (1970), Evapotranspiration by woody phreatophytes in the Humboldt River valley near Winnemucca, Nevada, with a section on soil-moisture determinations*Rep. 2330-7102*.

Rood, S. B., S. Patiño, K. Coombs, and M. T. Tyree (2000), Branch sacrifice: cavitation-associated drought adaptation of riparian cottonwoods, *Trees*, *14*(5), 248-257.

Rush, F. E. (1973), Water-Resources Appraisal of Fish Lake Valley, Nevada and California.

Rush, F. E., and S. Kazmi (1965), *Water resources appraisal of Spring Valley, White Pine and Lincoln Counties, Nevada*, State of Nevada Department of Conservation and Natural Resources.

Rush, F. E., and C. Schroer (1975), Geohydrology of Smith Valley, Nevada, with special reference to the water-use period, 1953-72*Rep. 2331-1258*, US Geological Survey].

RUSH, F. E. E. (1965), WATER RESOURCES–RECONNAISSANCE SERIES.

Salmi, T. (2002), *Detecting trends of annual values of atmospheric pollutants by the Mann-Kendall test and Sen's slope estimates-the Excel template application MAKESENS*, Ilmatieteen laitos.

Scott, M. L., P. B. Shafroth, and G. T. Auble (1999), Responses of riparian cottonwoods to alluvial water table declines, *Environmental Management*, *23*(3), 347-358.

Shafroth, P. B., J. C. Stromberg, and D. T. Patten (2000), Woody riparian vegetation response to different alluvial water table regimes, *Western North American Naturalist*, 66-76.

Sharpe, S. E., M. E. Cablk, and J. M. Thomas (2007), *The Walker Basin, Nevada and California: physical environment, hydrology, and biology*, Desert Research Institute.

Shiklomanov, I. A., and J. C. Rodda (2003), *World water resources at the beginning of the twenty-first century*, xiv, 435 pages pp., Cambridge University Press, Cambridge, U.K. ; New York.

Shreve, F. (1942), The desert vegetation of North America, *The Botanical Review*, *8*(4), 195-246.

Smith, J., R. J. Laczniak, M. T. Moreo, and T. L. Welborn (2007), Mapping Evapotranspiration Units in the Basin and Range Carbonate-Rock Aquifer System, White Pine County, Nevada, and Adjacent Areas in Nevada and Utah, U. S. Geological Survey.

Smith, M. O., S. L. Ustin, J. B. Adams, and A. R. Gillespie (1990), VEGETATION IN DESERTS .1. A REGIONAL MEASURE OF ABUNDANCE FROM MULTISPECTRAL IMAGES, *Remote Sensing of Environment*, *31*(1), 1-26.

Smith, M. O., S. L. Ustin, J. B. Adams, and A. R. Gillespie (1990), Vegetation in deserts: I. A regional measure of abundance from multispectral images, *Remote sensing of Environment*, *31*(1), 1-26.

Sommer, B., and R. Froend (2011), Resilience of phreatophytic vegetation to groundwater drawdown: is recovery possible under a drying climate?, *Ecohydrology*, *4*(1), 67-82.

Sperry, J. S., and U. Hacke (2002), Desert shrub water relations with respect to soil characteristics and plant functional type, *Functional Ecology*, *16*(3), 367-378.

Sperry, J. S., and U. G. Hacke (2002), Desert shrub water relations with respect to soil characteristics and plant functional type, *Functional Ecology*, *16*(3), 367-378.

Sperry, J. S., U. Hacke, R. Oren, and J. Comstock (2002), Water deficits and hydraulic limits to leaf water supply, *Plant, Cell & Environment*, *25*(2), 251-263.

Steinwand, A. L., R. F. Harrington, and D. Or (2006), Water balance for Great Basin phreatophytes derived from eddy covariance, soil water, and water table measurements, *Journal of Hydrology*, *329*(3-4), 595-605.

Stephenson, N. (1998), Actual evapotranspiration and deficit: biologically meaningful correlates of vegetation distribution across spatial scales, *Journal of Biogeography*, *25*(5), 855-870.

Stephenson, N. L. (1990), Climatic control of vegetation distribution: the role of the water balance, *American Naturalist*, 649-670.

Tasumi, M., R. G. Allen, and R. Trezza (2008), At-surface reflectance and albedo from satellite for operational calculation of land surface energy balance, *Journal of Hydrologic Engineering*, *13*(2), 51-63.

Theis, C. V. (1940), The source of water derived from wells, *Civil Engineering*, *10*(5), 277-280.

Thiros, S. A., and A. Susan (2003), *Quality and sources of shallow ground water in areas of recent residential development in Salt Lake Valley, Salt Lake County, Utah*, US Department of the Interior, US Geological Survey.

Thomas, J. M., A. H. Welch, and M. D. Dettinger (1996), *Geochemistry and isotope hydrology of representative aquifers in the Great Basin region of Nevada, Utah, and adjacent states*, US Geological Survey.

Trezza, R., and R. Allen (2013), Report on developing albedo weighting coefficients and surface reflectance coefficients for the Landsat 8 operational land imager, *Report by the University of Idaho Kimberly Research and Extension Center, Kimberly, Idaho*, 15.

Wigand, P. E., and P. J. Mehringer Jr (1985), Pollen and seed analyses, *The Archaeology of Hidden Cave, Nevada. Anthropological Papers of the American Museum of Natural History*, *61*(1), 18-124.

Yang, X., P. L. Smith, T. Yu, and H. Gao (2011), Estimating evapotranspiration from terrestrial groundwater-dependent ecosystems using Landsat images, *International Journal of Digital Earth*, *4*(2), 154-170.

Zhan, G.Listerud, B. Jones, M.A., (2011) *Transactions of the society of Mining, Metallurgy, and Engineering*(330), 519-525.

Zhu, Z., and C. E. Woodcock (2014), Continuous change detection and classification of land cover using all available Landsat data, *Remote sensing of Environment*, *144*, 152-171.

Zhu, Z., C. E. Woodcock, and P. Olofsson (2012), Continuous monitoring of forest disturbance using all available Landsat imagery, *Remote Sensing of Environment*, *122*, 75-91.

Zhu, Z., S. Wang, and C. E. Woodcock (2015), Improvement and expansion of the Fmask algorithm: Cloud, cloud shadow, and snow detection for Landsats 4–7, 8, and Sentinel 2 images, *Remote Sensing of Environment*, *159*, 269-277.